University of Sussex

Design and performance assessment of correlation filters for the detection of objects in high clutter thermal imagery

By

Ahmad Alkandri

SUBMITTED FOR THE DEGREE OF DOCTOR OF PHILOSOPHY AT THE UNIVERSITY OF SUSSEX

School of Engineering and Informatics University of Sussex

Brighton , UK

Declaration

I hereby declare that this thesis has not been and will not be, submitted in whole or in part to another University for the award of any other degree.

Signature: Ahmad Alkandri

Dated:

Acknowledgment

I would like to thank Allah the Almighty for giving me the strength and power to do my PhD and I hope that I will use this knowledge that I have gained to help humanity which will lead me towards Allah's blessing in this life and the life after.

I also thank my father and mother for all the support and blessing words that led me to such success. Fatima my wife, best loving caring person in my life, thank you so much for supporting me in every aspect. You are always there for me when I needed you, from the bottom of my heart thank you. Lolwah, Omar, Othman and the happening addition of the newborn baby Abdullah thank you for putting up with me in my busy life and short temper sometimes, I love you all from the bottom of my heart.

To all my supervisors, Dr. Rupert Young, Prof. Chris Chatwin and Dr. Philip Birch thank you for all the advice, support and help that you gave me during my studies, which resulted in me successfully completing my thesis.

I am grateful to the Kuwaiti Defence Minister Sheikh Khalid Al-Sabah for his kind support and directions. The previous Chief of the Kuwaiti Naval Force Major General Ahmad Al-Mulla, thank you for selecting me to continue my studies. Lieutenant General Mohammed Al-Khuder, thank you for your support, effort and help. For you all, my fellow officers, friends and family who supported me in many ways may Allah the almighty bless you all.

I am also grateful for my friend Dr. Akber Gardezi, the man with a great heart for everyone. Dr. Nagachetan Bangalore the respected gentleman and great friend, thank you is not enough to express my feeling towards you and your wife and family.

Abstract

The research reported in this thesis has examined means of enhancing the performance of the Optimal Trade-off Maximum Average Correlation Height (OT-MACH) filter for target detection in Forward Looking Infra-Red (FLIR) imagery acquired from a helicopter and border security FLIR camera in northern Kuwait. The data acquired with these FLIR sensors allows real-world evaluation of the comparative performance of the various filters that have been developed in the thesis. The results obtained have been quantified using well known performance measures such as Peak to Side-lobe Ratio (PSR) and Total Detection Error (TDE). The initial focus was to study the effect of modifying the OT-MACH parameters on the correlation metrics. A new optimisation technique has been presented, which computes statistically the filter alpha parameter associated with controlling the response of the filter to clutter noise. A further modification of the OT-MACH filter performance using the Difference of Gaussian bandpass filter (named the D-MACH filter) as a pre-processing stage has been described. The D-MACH has been applied to several test images containing single and multiple targets in the scene. Enhanced performance of the modified filter is demonstrated with improved metrics being obtained with less false side peaks in the correlation plane, especially when multiple targets are present in the test images.

A further pre-processing technique was investigated using the Rayleigh distribution as a pre-processing filter (named the R-MACH filter). The R-MACH filter has been applied to multiple target types with tests conducted across various image data sets. The filter demonstrated an improvement over the Difference of Gaussian filter in terms of

reducing the number of parameters needing to be tuned whilst producing further enhanced correlation plane metrics.

Finally, recommendations for future work has been made to improve the use of the OT-MACH filter in target detection and identification. A novel training image representation is proposed for further investigation, which will minimise the computational intensity of using the MACH filter for unconstrained object recognition.

Table of Contents

List of Figures

List of Tables

List of publications resulting from thesis work

1. Alkandri, Ahmad, Akber Gardezi, Philip Birch, Rupert Young, and Chris Chatwin. "Parameter optimization of the optimal trade-off maximum average correlation height filter (OT-MACH) for FLIR imaging in high clutter environments." *In SPIE Defense, Security, and Sensing, pp. 805508-805508. International Society for Optics and Photonics, 2011.*

2. Alkandri, Ahmad, Akber Gardezi, Nagachetan Bangalore, Philip Birch, Rupert Young, and Chris Chatwin. "Automatic parameter adjustment of difference of Gaussian (DoG) filter to improve OT-MACH filter performance for target recognition applications." *In SPIE Security+ Defence, pp. 81850M-81850M. International Society for Optics and Photonics, 2011.*

3. Alkandri, Ahmad, Nagachetan Bangalore, Akber Gardezi, Philip Birch, Rupert Young, and Chris Chatwin. "Improving OT-MACH filter performance for target recognition applications with the use of a Rayleigh distribution filter." *In SPIE Defense, Security, and Sensing, pp. 83980D-83980D. International Society for Optics and Photonics, 2012.*

4. Alkandri, Ahmad, Nagachetan Bangalore, Akber Gardezi, Philip Birch, Rupert Young, and Chris Chatwin. "Human detection using OT-MACH filter in cluttered FLIR imagery." *In Southeastcon, 2013 Proceedings of IEEE, pp. 1-7. IEEE, 2013.*

5. Gardezi, Akber, Ahmed Alkandri, Philip Birch, Rupert Young, and Chris Chatwin. "A space variant maximum average correlation height (MACH) filter for object recognition in real time thermal images for security applications." *In Security+ Defence, pp. 78380N-78380N. International Society for Optics and Photonics, 2010.*

6. Gardezi, A., Alkandri, A., Birch, P., Qureshi, T., Young, R., Chatwin, C., "An implementation and performance evaluation of a space variant OT-MACH filter for a security detection application using FLIR sensor," *Applied Imagery Pattern Recognition Workshop (AIPR), 2010 IEEE 39th* , pp.1-7, 13-15 ,Washington D.C. USA Oct. 2010.

7. Gardezi, Akber, Ahmad Al-Kandri, Philip Birch, Rupert Young, and Chris Chatwin. "Enhancement of the speed of space-variant correlation filter implementations by using low-pass pre-filtering for kernel placement and applications to real-time security monitoring." *In SPIE Defense, Security, and Sensing, pp. 805509-805509. International Society for Optics and Photonics, 2011.*

8. Gardezi, Akber, Nagachetan Bangalore, Ahmed Al-Kandri, Philip Birch, Rupert Young, and Chris Chatwin. "Application of speed-enhanced spatial domain correlation filters for real-time security monitoring." *In SPIE Security+ Defence, pp. 81890R-81890R. International Society for Optics and Photonics, 2011.*

List of Symbols and Acronyms

2D	Two dimension
3D	Three dimension
ACH	Average correlation height
AHH	Area at half peak height
AICH	All-Image Correlation Height
ASE	Average Squared Error
ASM	Average Similarity Matrix
ATC	Air Traffic Control line
ATR	Automatic Target Recognition
BPR	Biometric pattern recognition
C	Additive noise
CAD	Computer aided design
COPI	Correlation output peak Intensity
CPR	Correlation Pattern Recognition
D_x	Diagonal average power spectral density
D-MACH	Different of Gaussian modified OT-MACH
DFT	Discrete Fourier transform
DIP	Digital image processing
DoG	Different of Gaussian
DSP	Digital signal processing
EMACH	Extended Maximum Average Correlation Height

FFT	Fast Fourier transform
FLIR	Forward Looking Infrared
GPS	Global positioning system
I	Intensity matrix
IFF	Identification, Friend or Foe
IFFT	Inverse Fast Fourier transform
InSb	Indium Antimonide
LoG	Laplacian of Gaussian
LWIR	Long wave infrared
m_x^*	Average of training vector
MACH	Maximum Average Correlation Height
MCT	Mercury Cadmium Telluride
MWIR	Mid-wave infrared
M_x	The mean of the summation of all training image spectra
NPHH	Number of peaks at half the maximum peak height
NVESD	US Army Night Vision and Electronic Sensor Directorate
OCR	Optical character recognition
OT-MACH	Optimal trade-off maximum average correlation height
PCE	Peak-to-correlation energy
PSR	Peak-to-sidelobe ratio
PWHH	Peak width at half of the peak height
R-MACH	Rayleigh distribution modified OT-MACH
ROI	Regional of interest
RV	Random variables

r	Radial co-ordinate
R_{total}	Total number of run
$R_{detection}$	Number of detection count in the run
SBAR	Satellite based aerial recognition
SDF	Synthetic discrimination function
S_x	Similarity matrix
TDE	Total detection error
X_i	i^{th} training image
α	OT-MACH Parameter
β	OT-MACH Parameter
γ	OT-MACH Parameter
μ	Mean
σ	Standard deviation

Chapter 1

Introduction

Chapter 1 Introduction

1.1 Background

Image processing techniques have been widely used in different fields and domains. Such fields nowadays are unlimited and have become an everyday experience for even a non-technical person. Applications include what we see in hospitals or at the dentist, for example, where x-rays and CT scans play an important part of the diagnosis procedure. An important field that we will be focusing on in this thesis is the defence and security usage of image processing technology.

There are several natural pattern recognition operations carried out by humans and other animals on a daily basis. A classical example is the ability of a person to recognise a face. In most cases of natural pattern recognition, the capability is a function of the brain's ability in which the recognisable pattern is imprinted in the memory and compared with the sensed reality in order to carry out the recognition.

One of the main drives in image processing is to mimic Nature's ability to perform pattern recognition using the image as a classifiable pattern. Out of all image processing techniques, correlation pattern recognition is the research area chosen for detailed investigation in this thesis. Correlation pattern recognition techniques are used in the detection, tracking, recognition, identification and localisation of defined objects and targets [1]–[11].

1.2 Pattern recognition

The encyclopaedia Britannia defines Pattern Recognition as:

"The imposition of identity on input data, such as speech, images, or a stream of text, by the recognition and delineation of patterns it contains and their relationships. Stages in pattern recognition may involve measurement of the object to identify distinguishing attributes, extraction of features for the defining attributes, and comparison with known patterns to determine a match or mismatch. Pattern recognition has extensive application in astronomy, medicine, robotics and remote sensing by satellites"

Bow and Sing [12] give the definition: "Pattern recognition can broadly be defined as a process to generate a meaningful description of data and a deeper understanding of a problem through manipulation of a large set of primitive and quantifying data"

The main goal in pattern recognition is thus to make an observation and generate a classification from this. The observation can be anything which can be classified as a signal. A signal may comprise any information such as speech data, video sequences, images or multi-dimensional signals. One of the main applications of pattern recognition is in the Automatic Target Recognition (ATR) field that is predominantly used in the defence and security sectors which is the main focus in this thesis. The aim of ATR is to classify the input observation into either a natural or man-made object. The classification can go further to higher levels to classify objects such as cars, tanks, trucks, ships, aircraft and many more.

There are several pattern recognition paradigms, in one of which the use of training data is made as opposed to feature detection and subsequent pattern classification. The use of

images of a specified object as training data has become an important technique used when performing real-time recognition of targets or patterns [12]–[16].

Correlation methods in pattern recognition have been applied to many useful applications such as: character recognition, speech recognition, image based object recognition, medical anomaly recognition and analysis, satellite imagery interpretation, on-land object detection, target acquisition and many more [12].

1.3 Correlation pattern recognition

Correlation is an accurate and general method that can be used in multiple applications such as, but not limited to, automatic target recognition (ATR), optical character recognition (OCR), Biometric pattern recognition (BPR) and Satellite based aerial recognition (SBAR). The use, design and analysis of correlation based pattern recognition requires a background of linear systems theory, random variables and processes, matrix and vector methods, detection and estimation theory, digital signal processing (DSP), digital image processing (DIP) and optical processing. Correlation as a technique arises from probability theory wherein two random variables (RV), but in our case two patterns or signals, are correlated or compared so as to determine their degree of similarity. In pattern recognition, the correlation result is used to determine how similar or dissimilar a test object is from a training pattern set [12], [17].

Digital correlation is the most commonly used technique in modern pattern recognition systems. The target image and the reference pattern (generated from training image sets) are usually represented in the form of discrete two dimensional arrays. These

image arrays are derived from an optical sensing device after converting the analogue data to digital data. The correlation function can be computed by one of two methods, namely, directly in the spatial domain or via the spatial frequency domain obtained by discrete Fourier transformation.

The direct correlation computation can be performed using a digitized input scene *r[m,n]* with a digitized target image defined as *s[m,n]*. The two digitised functions are shifted and summed to obtain a direct correlation output *c[m,n]*. The resultant correlation *c[m,n]* can thus be expressed as follows:

$$c[m,n] = \sum_{k=1}^{Ns} \sum_{l=1}^{Nr} s[k,l]r[k-m,l-n] \qquad \textbf{Eq. 1.1}$$

*s[k,l]*and *r[k,l]* are zero when *k* and *l* lie outside the support for the images. The resultant correlation output of c*[m,n]* is of size $(N_s + N_r)^2$ where the complete computation requires $(N_s N_r)^2$ multiplications. Thus the direct correlation computation is cumbersome due to the requirement for repeated floating point or multi-bit fixed-point multiplications between the images.

Digital correlation carried out via the spatial frequency domain is predominantly implemented using the fast Fourier transform (FFT) method. The use of FFT is more efficient as compared to the direct computation method. The desired correlation can be performed using the following steps [18]–[20]:

a. Compute *S[k,l]* and *R[k,l]*, the *N x N* two dimensional discrete Fourier transforms of the target image *s[m,n]* and the training image set *r[m,n]*.

b. Multiply *S[k,l]* by $R^*[k,l]$ to obtain *C[k,l]*, where the $R^*[k,l]$ is the complex conjugate of *R[k,l]*, the training image set discrete Fourier spectrum.
c. Perform an *N x N* inverse two-dimensional discrete Fourier transform of *C[k,l]* to obtain the correlation output *c[m,n]* [12], [21]–[26].

Whatever the method of computation, if the target signal is the same as the training signal the result is called an auto-correlation and if the target signal is different from the training signal the result is called a cross-correlation [12], [22], [27], [28].

In correlation pattern recognition (CPR) the main aim is to assign a target object to one of a set of multiple classes. This capability of correlation pattern recognition is clearly very useful in defence and security operations such as surveillance, intelligence and subsequent decision cycles.

Figure 1.1 shows a block diagram of the major generic steps involved in data driven, bottom-up image pattern recognition [12].

Figure 1.1 Image pattern recognition process

In such a pattern recognition scheme, a training set of images are processed with a selected method to extract the pre-determined features and segmented into classifiable pattern classes. This can then be used to obtain classification of subsequent test patterns input to the system.

Correlation pattern recognition adds a top-down process template matching process to these stages and provides a powerful means of using training images to implement a classifier [29].

Correlation based classification methods differ from alternative classification systems such as probabilistic methods. Probabilistic methods tend to classify objects based on various extracted feature sets. The main disadvantage of probabilistic methods is the need for extensive testing and performance evaluations due to the wide range of expected patterns. Correlation based methods on the other hand do not require extensive testing since the target can be represented as a single known set of patterns derived from the object to be classified.

Much information can be extracted from an image. Different image types give different information that can be extracted as, for example, in colour images, grey scale images and thermal images. Throughout this thesis, the main focus has been on thermal imaging due to its ability to give important and prominent information about the target objects of interest in almost all weather conditions and at night.

1.4 Forward looking infra-red (FLIR)

Infrared is one of the bands of the used in the thermal camera consistes of three basic ranges, namely far infrared, min wave the near infrared. the far infrared or also called as long wave infrared (LWIR) cameras, operate at 8 to 12 μm and can be used to visualise heat sources such as hot engine parts or human body heat from a few kilometres range.

Longer range viewing is often difficult with LWIR due to the infrared light being absorbed, scattered and refracted by air and water vapour.

Mid-wave infrared (MWIR) cameras operate in the 3 to 5 µm range of the spectrum. The MWIR frequencies are less affected by water vapour absorptions than are those used in the LWIR. A drawback of IR cameras is the requirement for the use of expensive sensor arrays and cooling systems such as cryogenic cooling modules.

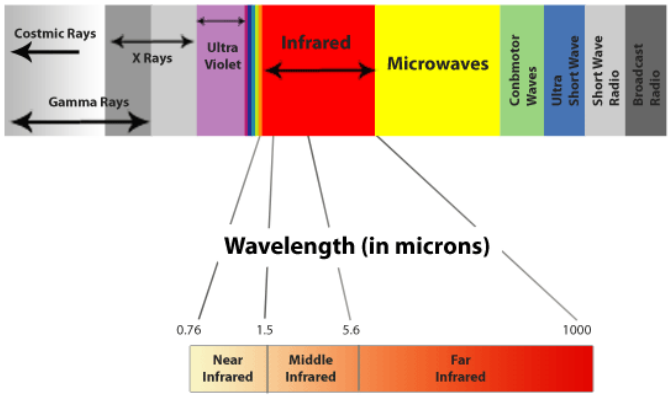

Figure 1.2 Full electromagnetic spectrum with infra-red range highlighted

FLIR systems detect the emitted infrared radiation from heated objects in the scene, which is then used to form a 2-D thermal image. Shown in Figure 1.2, are the three infrared wavelengths starting from near, middle and ending with the far infrared. A typical thermal camera system can be described in terms of a breakdown of modules as shown in Figure 1.3.

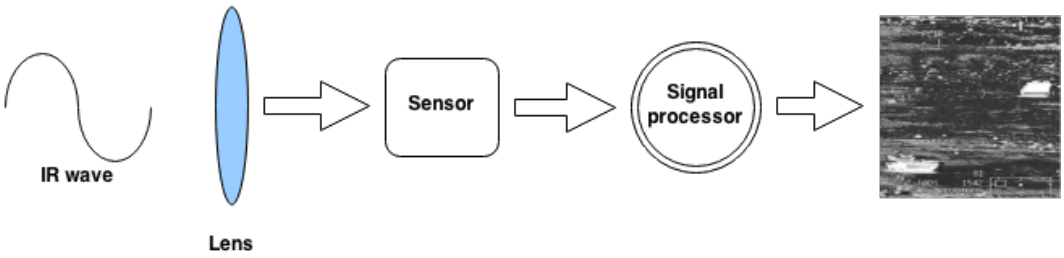

Figure 1.3 Basic thermal camera system

The infrared waves that lie between 0.76 and 100 microns are passed through a lens, which for the longer wavelengths must be fabricated from germanium. The thermal radiation is thus imaged onto a thermal detector array which is made of Indium Antimonide (InSb) or Mercury Cadmium Telluride (MCT) as in the HRC ranger FLIR camera used to obtain some of the images employed in the thesis research. After A/D conversion, the sensor output passes through a series of signal processing stages as shown in Figure 1.3. An example of the FLIR image output using a long range HRC camera is also shown in Figure 1.3 as the resultant image from the signal processing module.

For the work of this thesis, video and still images have been acquired using various platforms and real-world targets in order to provide realistic data for the assessment of the detection and recognition capabilities of the filters examined. The videos have been acquired in both day and night conditions to simulate the effect of solar heating on the target vehicles.

The advantages of the FLIR imaging system for military use is clear: it can be used in all-weather conditions; it is very difficult to detect the FLIR system as it is fully passive; and there is difficulty to hide or camouflage the heat emitted from the target objects.

1.5 FLIR in defence and security applications

In the last 50 years, defence and security research has contributed much to image processing technologies [30]–[44]. One of the main focuses has been the pattern recognition and target identification support system. The use of imaging support systems and technologies gives useful information that can be used in targeting, navigation, decision-making and surveillance etc. In this section, several examples will be discussed to illustrate the way in which thermal imaging can be used in defence and security applications.

(a)

(b) (c)

Figure 1.4 FLIR image samples (a) Road at night time using normal camera and FLIR (b) Coastguard patrol boat FLIR image (c) Apache helicopter FLIR image.

In Figure 1.4(a) a comparison is made between a FLIR camera and a normal, visible wavelength, camera where, with the latter, only the road lit by the car lights can be seen. The FLIR image shows a deer that was not visible with the normal camera. Navigation is a hazardous operation, especially at night where the human eye or a visible wavelength camera cannot operate due to the low lighting conditions.

Figure 1.4(b) and 1.4(c), show the hot parts of the target objects such as the engine and exhaust. The information gathered could be used, for instance, to determine if the engine is running or for approximately how long it has been idle.

(a) (b)

Figure 1.5 (a) British warrior armour with engine on (b) T90 tank static with engine off

During the data collection, the author has directed the movement of five different vehicles and arranged for the starting of their engines for 30 minutes to give a realistic targeting scenario. An Apache helicopter hovered around those targets and videoed the scene as directed in order to provide views from different orientations of the vehicles.

Figure 1.5(a) shows a British warrior armour vehicle with a hot body due to the heat produced by the engine. Figure 1.5(b) shows an old T90 tank on a display stand with no engine. It is very clear that the FLIR imaging gives vital information about the vehicle or target state. From this information, an experienced operator can reliably estimate the target type and time of operation. However, the lack of experienced operators requires researches to devise an advisory system that gives automatic identification and targeting information. The existing systems now in operation give an advisory and prioritise a

target according to the threat imposed characterised by, for instance, distance, speed and angle of attack.

1.6 Detection, recognition and identification theory

In the 1950's, John Johnson, a scientist at the United States Army Night Vision and Electronic Sensor Directorate (NVESD) developed an observation analysis theory where he stages and quantifies the visual surveillance approach which has become known as Johnson's criteria [45]. Detection, recognition and identification are the classification cycle used now in almost every defence and security organisation.

Figure 1.6 FLIR image with target detection in the scene

Figure 1.7 FLIR image with recognised targets

(a) (b)

Figure 1.8 FLIR image with identified targets (a) Human and car targets (b) walking male target

Figures 1.6 to 1.8 show good examples of the visual classification cycle. An example of target detection can be seen in Figure 1.6 were only two target blobs can be seen and we cannot gather any more information about the target type or identity. Figure 1.7 shows better target details that can lead to the recognition of the targets as a human and a car. Figure 1.8 clearly shows enough detail and target information that make the identification more certain. Figure 1.8(a) shows a male beside a four wheeled drive car

and with the appropriate operator knowledge this can be identified to be a Nissan Patrol made between 1997 – 2009. Figure 1.8(b) shows a male aged in his 20's or 30's with a hot drink in his hand and a watch on his right wrist. Although this detailed information may seem to be not needed, in real life scenarios the smallest amount of information can be very important in making an operational decision.

1.7 Correlation filter development

As previously discussed, correlation is a signal processing method of measuring similarity between two input signals. The signal can result from images or other waveforms; the correlation gives a quantitative measure of the match between the two signals. There are two types of correlation: auto-correlation and cross-correlation. When two identical input functions are correlated with each other it is known as auto-correlation, whereas, when two dissimilar functions are correlated the operation is called cross-correlation. Equation 1.2 below shows discrete cross-correlation of two different functions, *f* and *g*, implemented in the spatial domain.

$$c_{(m,n)} = \sum_i \sum_j f_{(i,j)} g_{(i+m,j+n)} \qquad \textbf{Eq. 1.2}$$

The most basic form of correlation filter is the matched filter. There are a few drawbacks to basic correlation filters for pattern recognition:

a. The correlation pattern recognition filters have very large bandwidth, thus leading to the impracticality of using these methods for classifying similar targets for real time applications.
b. The sensor noise and background clutter is often neglected in the design of simple correlation based filters.
c. The filter has some scale or rotation invariance but less than that of an appropriately multiplexed filter.

The main intention behind correlation pattern recognition research is to overcome these limitations by modifying the filter function to accommodate for the limitations of the matched filter. Hester and Casasent made a major contribution to the field in 1980 with the formulation of the synthetic discriminant function (SDF) that allows multiple training image sets to be included in a single filter design [46]. A variety of synthetic discriminant function (SDF) based filters have been proposed since then to accommodate various kinds of arbitrary distortions in the filter training images caused by changes in the viewing angle, scale and rotation of the target object [47]–[53].

The main issues to be considered and overcome in designing improved correlation filters are that the filter should be invariant to distortions, supress clutter noise and be able to obtain a distinguishable correlation peak for classification purposes.

It was reported in the early research literature concerned with the design of correlation filters that the SDF filters failed to adequately meet any of the above design requirements [54]. Optimisation and hence improvements to overcome the known negative characteristics of the SDF which involved rigorous developments in the area of

minimum variance synthetic discriminant functions were made by Kumar in 1986 [55]. Kumar reported that the minimum variance synthetic discriminant function (MVSDF) filters need to be considered as optimum filters that are tolerant to the effects of additive Gaussian white noise on classification results.

The major drawback of implementing the MVSDF, and subsequent improvements, included the inversion of a large covariance matrix and this involved intensive computations. The computational intensity and the lack of tolerance to clutter noise (that does not have a white power spectrum) provided major challenges to improving the performance of the filters.

A variation to the SDF family that received good attention in the pattern recognition and automatic target recognition community is the minimum average correlation energy (MACE) filter proposed and developed by Mahalanobis *et al* [56]. The MACE filter proved to be capable of generating detectable correlation peaks by suppressing image based clutter. However, it remained too sensitive to image distortions thus challenging the ATR community to continue to innovate in the field of correlation pattern recognition filters [57].

Mahalanobis *et al* [58] went on to propose the maximum average correlation height (MACH) filter to overcome the hard constraints involved in the SDF based filter designs which require the correlation peak heights to be pre-specified with constant value [58], [59]. The hard constraint requirement is unnecessary as it limits the number of possible SDF results and in any case is unlikely to be effective since there is a low probability of correlating the filter function with a target test image in exactly the same orientation as that of any of the views included in the training set.

The MACH filter theory thus provides a better filter solution by removing the peak-height constraint from the SDF based design pattern recognition filters. The MACH filter design includes the minimisation of an average similarity measure (ASM) that leads to a compact set of correlation planes that resemble each other and exhibit the least possible variation. This approach of statistically correlating the filter function makes it more robust as compared to the pattern recognition filters previously designed. Many improvements have since been made in the literature to the MACH filter design to accommodate various application requirements. Shaug and Chen, used a Mexican hat approach to overcome distortion [11].Others authors such as Lui and Luo, have introduced the Action MACH [60][73] to address motion activity.

The main motivation of the work in this thesis involves modifying the frequency domain optimal trade-off (OT-MACH) filter design, by employing various band-pass filtering techniques to assist in obtaining more accurate target detection and recognition results [59]. Analyses have been carried out of the OT-MACH performance measures to improve upon its performance. The results and subsequent discussion of such improvements to the OT-MACH filter are reported in this thesis to provide possible enhancements to the solution of difficult target detection and classification problems.

1.8 Achievements

The Optimal Trade-off Maximum Average Correlation Height (OT-MACH) filter has been tested and improved in this thesis. Testing was focused initially on the setting of

the filter parameters to try to optimise performance. It has been found that the β parameter is the main drive for the overall OT-MACH filter behaviour. Further investigation and tests were conducted and concluded that the noise parameter in the OT-MACH transfer function can be automatically computed using the statistics of the input image intensities. This technique simplifies the filter design and decreases the computational processing power needed to compute the OT-MACH transfer function. Further, an additional bandpass filter has been incorporated into the OT-MACH filter based on the Difference of Gaussian (DoG) filter. This additional filter acts as a pre-processer and has been shown to result in improvements on the discrimination ability of the overall composite filter. Moreover, a method of automating selection of the DoG filter standard deviation setting has been proposed. In subsequent chapters, an alternative pre-processing filter has been introduced, namely the Rayleigh distribution filter. The incorporation of the Rayleigh filter into the OT-MACH filter resulted better detection accuracy when the filter was applied to highly cluttered backgrounds and difficult target detection scenarios such as human detection in thermal infra-red imagery. This new pre-processing filter led to very promising target identification results when incorporated into a two stage process of detection/segmentation and identification. Finally, some novel ideas for representing the filter training set images are outlined in a concluding section on future work.

1.9 Thesis chapter organisation

The thesis is divided into several chapters that discuss the problems of performance enhancement of correlation pattern recognition filters, in particular, by improving the

OT-MACH filter and its usability as a target detection filter. Chapter 2 of the thesis deals with the generic derivation and related considerations regarding the OT-MACH filter. Chapter 2 goes on to discuss the performance measures used to quantify the performance of the OT-MACH filter. Chapter 3 describes parameter optimisation methodologies for minimising the computational intensity involved in designing and using the OT-MACH filter. Chapter 4 describes the improvements to the OT-MACH filter performance implemented by pre-processing the original filter with a Difference of Gaussian (DoG) bandpass filter. Results are presented to demonstrate the improvements to the filter metrics and accuracy of target detection obtained when using the bandpass DoG filter. Chapter 5 discusses the Rayleigh distribution filter based OT-MACH filter (R-MACH) and demonstrates that the R-MACH filter further reduces the multiple parameter tuning issues involved in using the OT-MACH filter for target detection purposes. A novel method of using a two stage R-MACH filter sequence for not only the detection but also in the identification of targets is introduced. The results obtained with this method are then discussed and evaluated. Finally, Chapter 6 presents conclusions drawn from the results achieved in the thesis along with a discussion of possible future research to further improve the use of correlation pattern recognition filters for target detection and identification in realistic scenarios.

Chapter 2

Pattern Recognition Correlation Filters

Chapter 2 Pattern Recognition Correlation Filters

2.1 Chapter organisation

The chapter begins with a brief introduction to correlation filters and discusses their features and advantages in the pattern recognition domain. It then presents the OT-MACH filter and its derivation in section 2.3. A parametric study concerning the OT-MACH filter function design parameters presented in section 2.4. A through discussion of filter training is conducted in section 2.5. Section 2.5 also provides an introduction to training image summation and a discussion of the effect of illumination differences between real and 3D data. The chapter progresses with a discussion of correlation response issues due to background clutter and rotational distortions in section 2.6. Various performance matrices and quantification measures of the correlation plane are presented in section 2.7. The chapter then gives a brief discussion of target constraint assumptions in section 2.8. Several conclusions have been drawn and discussed in detail in section 2.9.

2.2 Introduction

Correlation filters have been extensively used in the world of defence and security [6], [31], [62], [77]–[86]. Their ability to discriminate objects or targets from a cluttered background makes correlation filters a very powerful tool that can be used in demanding real time applications. Correlation filters are very well known for their

ability to provide shift-invariance and distortion tolerance, which makes their use attractive for pattern recognition applications.

In 1994, Mahalanobis *et al* [58] introduced an unconstrained correlation filter named the Maximum Average Correlation Height (MACH) filter [58]. The MACH filter is one of the most effective filter design algorithms since it permits the control of three important features in pattern recognition:

a. Correlation peak localisation.
b. Distortion tolerance.
c. Suppression of noise/clutter.

There have been several derivatives of the MACH filter during the past years. In 1997, Mahalanobis and co-workers introduced the optimal trade-off maximum average correlation height filter OT-MACH [59], in which statistical analysis of the OT-MACH filter showed it to be the optimal filter for target detection with high background clutter. However, Alkanhal *et al.* [63] have discussed the high false alarm rate in the correlation results generated by background clutter when using the OT-MACH filter. A new matrix has been introduced in Alkanhal named the All-Image Correlation Height (AICH) to replace the Average Similarity Matrix (ASM) in the filter design. These improvements lead to the Extended-MACH (EMACH) that shows a reduction in false alarms caused by side peaks in the correlation plane.

A filter bank needed to detect a dynamic object with in plane, out-of-plane and scale distortion is a demanding task. Goyal *et al* [65] introduced a wavelet modified OT-

MACH to overcome the computational difficulties. By looking at the research conducted on improving the OT-MACH performance, the potential areas of research into OT-MACH filter design can be broken down into three main areas as shown in Figure 2.1 below, each of which the research reported in this thesis addresses in turn.

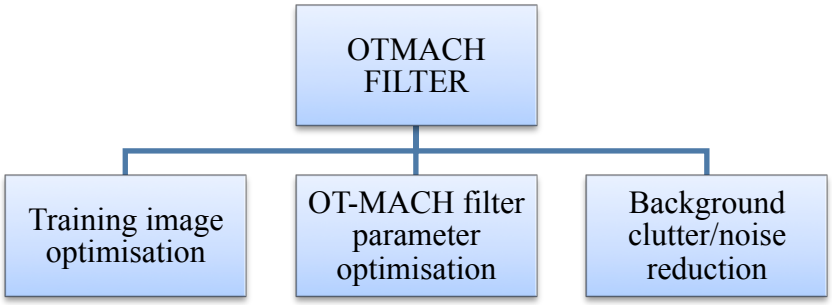

Figure 2.1 OT-MACH areas of research interest

2.3 OT-MACH filter derivation

Extensive research has been carried out on correlation filters over the past forty years [10], [49], [58], [81], [85], [87]–[97]. Their unique ability in discriminating objects from a highly cluttered backgrounds has made them one of the main techniques used in difficult pattern recognition problems encountered in defence and security applications.

Correlation pattern matching or recognition provides a mechanism for comparing two image signals. It has the benefit of being shift-invariant so it can also provide tracking at no extra computational cost. The relation below describes the one dimensional basic correlation operation:

$$c(x,y) = \int_{-\infty}^{\infty}\int_{-\infty}^{\infty} f(x,y)g^{*}(x+a,y+b)dadb \qquad \textbf{Eq. 2.1}$$

where e is a dummy variable and the function, $c(x,y)$, gives a measure of the similarity of the functions $f(x,y)$ and $g(x,y)$. The function $f(x,y)$ is referred to as the input signal and the function $g(x,y)$ as the target signal. However, when dealing with discrete images, as outlined in Chapter 1, it is more common to express the integral in the form of a discrete two-dimensional summation:

$$C_{(m,n)} = \sum_i \sum_j f_{(i,j)} g^*_{(i+m,j+n)} \qquad \textbf{Eq. 2.2}$$

where i and j are the 2-D pixel co-ordinates. For larger images this can be computationally intensive and in order to reduce latency, the computation can be carried out via the Fourier domain, which can be expressed:

$$c(x,y) = F^{-1}(F[f(x,y)].F[g^*(x,y)]) \qquad \textbf{Eq. 2.3}$$

where the $F(.)$ indicates a Fourier transform operation and the $F^{-1}(.)$ denotes the inverse Fourier transform, of the functions contained within the brackets. In a discrete image, Equation 2.3 is therefore computed by two forward fast Fourier transforms (FFTs), a complex multiply between the spectrum of the input image and the conjugate spectrum of the reference image, and then an inverse fast Fourier transform (IFFT). Since it is convenient for the answer to be real, the modulus squared of $c(x,y)$ is used by convention.

The component $F[g^*(x,y)]$ in Equation 2.3 can be regarded as a filter function. This is the most basic form of the correlation filter and is also known as the matched filter. It

has been frequently observed that the correlation filter has some disadvantages and limitations [91]. These have been overcome by modifying the filter function for better target discrimination, scale and rotation invariance and also to cope with clutter noise [91]. The synthetic discriminate function filter concept was proposed in an attempt to overcome these difficulties [48], [49]. This had some limitations due to the hard constraints imposed on the correlation peak values by the design method.

The maximum average correlation height filter (MACH) was subsequently proposed by Mahalanobis *et al*. [58]. The MACH filter allows a better filter solution by removing the peak-height constraint from the various SDF based design techniques [47]. The filter design includes the minimisation of an average similarity measure (ASM) that leads to a compact set of correlation planes that resemble each other and exhibit the least possible variation [2]. This statistical approach to the correlation filter design process makes the filter more robust as compared to other designs based on SDFs with hard constraints [98]. The MACH filter maximises the relative height of the average correlation peak with respect to the expected distortions.

In order to understand the OT-MACH filter it is useful to review its derivation as made in [12]. It is assumed that the training set consists of N true-class images and M images from the false-class. Each of these images contain p pixels, where $p = u$ x v (size of the image). The i^{th} training image is denoted by $X_i\ (u,v)$ and is represented in the frequency domain by a p x 1 vector X_i , obtained by lexicographically reordering its 2-D FFT. The filter transfer function is denoted by a p x 1 vector h.

The correlation of the i^{th} training image with the filter function can then be expressed in the frequency domain as:

$$c_i = X_i h \qquad \textbf{Eq. 2.4}$$

where X_i is a p x p diagonal matrix containing the elements of training image spectra. Equation (2.4) denotes the FFT of the i^{th} correlation output. The Average Squared Error (ASE) is then defined as a measure that quantifies the deviation of the correlation plane with respect to an ideal shape factor $\boldsymbol{f}$. ASE can be expressed as:

$$ASE = \frac{1}{N}\sum_{i=1}^{N}(X_i - M_x)^*(X_i - M_x) \qquad \textbf{Eq. 2.5}$$

where X_i is the diagonal matrix of the training images, M_x is the average of X_i and * indicates the conjugate transpose of the vector.

$$\nabla_f(ASE) = \frac{2}{N}\sum_{i=1}^{N}\left(X_i - p_x\right) = 0 \qquad \textbf{Eq. 2.6}$$

This determines the minimum value of the function and so yields [12]:

$$f_{Optimum} = \bar{c} = \overline{X_i} h \qquad \textbf{Eq. 2.7}$$

where the bars indicate the mean values are taken. Substituting the optimum shape factor expression in Equation (2.7) the average similarity measure (ASM) of the training-set correlation planes is obtained. This is defined as follows:

$$ASM = \frac{1}{N}\sum_{i=1}^{N}\left(X_i - \overline{X}\right)^{*}\left(X_i - \overline{X}\right) \quad \textbf{Eq. 2.8}$$

$$= h^{*} S_x h \quad \textbf{Eq. 2.9}$$

where,

$$S_x = \frac{1}{N}\sum_{i=1}^{N}\left(X_i - M_x\right)^{*}\left(X_i - M_x\right) \quad \textbf{Eq. 2.10}$$

The MACH filter is designed so that it not only minimises the ASM and the correlation energy of the false class images but also maximises the on-axis peak of the average training-set correlation plane.

The intensity of the on-axis peak of the average training set correlation plane can be expressed as:

$$\left|\bar{c}(0,0)\right|^2 = h^{*} M_x M_x^{*} h \quad \textbf{Eq. 2.11}$$

The average correlation energy (ACE) of the false-class images is given as:

$$ACE = \frac{1}{N}\sum_{i=1}^{n} h^{*} X_i X_i^{*} h \quad \textbf{Eq. 2.12}$$

$$= h^{*}\left(\frac{1}{N}\sum_{i=1}^{N} X_i X_i^{*}\right) h \quad \textbf{Eq. 2.13}$$

$$= h^{*} D_x h \quad \textbf{Eq. 2.14}$$

where, in Equation (2.12), X_i is the diagonal matrix containing the elements of the 2-D FFT of the i^{th} false class image arranged in a vector form, and

$$D_x = \frac{1}{N}\sum_{i=1}^{N} X_i X^* \qquad \textbf{Eq. 2.15}$$

The average correlation height (ACH) is defined as:

$$W = \frac{1}{N}\sum \left|h^T X_i\right| = \left|h\overline{X}\right| \qquad \textbf{Eq. 2.16}$$

The OT-MACH then seeks to minimise the energy function:

$$E(h) = \alpha(ONV) + \beta(ACE) + \gamma(ASM) - \delta(ACH) \qquad \textbf{Eq. 2.17}$$

$$= \alpha h^+ Ch + \beta h^+ D_x h + \gamma h^+ S_x h - \delta\left|h^T m_x^*\right| \qquad \textbf{Eq. 2.18}$$

where α, β, δ, and γ are variables whose sum equals one, *ONV* is the output noise variance, *ACE* is the average correlation energy, *ASM* is the average similarity measure, and *ACH* is the average correlation height. In Equation 2.18, *C* is related to the power spectral density matrix of the additive noise, D_x is the diagonal average power spectral density of the training images and S_x is the denotes the similarity matrix of the training images. The ACE now refers to the true class of the training images. Rearranging this gives us [2]:

$$h = \frac{m_x^*}{\alpha C + \beta D_x + \gamma S_x} \qquad \textbf{Eq. 2.19}$$

where, α, β and γ are non-negative OT parameters, m_x is the frequency domain average of the training vector. Since the correct information for the additive noise value is not available at all times, a statistical method has been implemented to automatically set this value [99], so allowing the parameter α to be removed from the transfer function. *Dx* is the diagonal average power spectral density of the training images and *Sx* denotes a similarity matrix of the training images as given by Equations (2.8) and (2.10), above.

The different values of β and γ control the OT-MACH filter's behaviour to match different application requirements. For the work presented in this thesis, , OT-MACH parameters β and γ have been set to unity in order to analyse and test the behaviour of a fixed parameter OT-MACH filter modified only with a variable band-pass pre-processing filter.

A sub-set of the training images can be used to compute the OT-MACH filter transfer function as expressed by Equation (2.18). Correlation planes obtained by correlating the filter function with an in-class image can be represented as a correlation mesh plot, an example being shown in Figure 2.2.

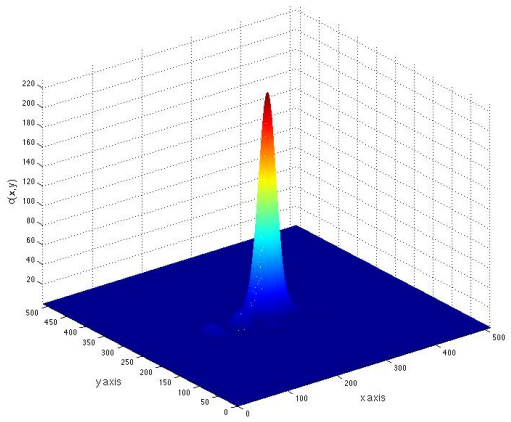

Figure 2.2 Correlation plot for an in-class target image correlated with the OT-MACH filter function

However, the idealised response shown in Figure 2.2 quickly deteriorates when the input object does not exactly match one of the stored templates or there is significant background clutter in the scene. To try and improve the performance of the OT-MACH filter, we have applied band pass pre-processing filters to the OT-MACH filter in order to explicitly force a band pass response and eliminate both low and high spatial frequency components that disrupt the filter response [74].

2.4 OT-MACH filter parameter study

From the derivation summarised in the last section, it can be seen there are three parameters in the OT-MACH filter frequency domain transfer function, symbolised as α, β and γ:

$$h = \frac{m_x^*}{\alpha C + \beta D_x + \gamma S_x} \qquad \textbf{Eq. 2.20}$$

These are the three OT-MACH parameters used to control the OT-MACH filter to produce the desired output. The parameter alpha (α) controls the additive noise added to the filter to reduce the output noise variance [59]. The beta parameter (β) controls the diagonal average power spectral density of the training images and the gamma parameter (γ) controls the similarity matrix of the training images, which is defined in Equation 2.10.

In Equation 2.10, the term N denotes the total number of training images considered for the filter design, the terms X_i and M_x denote the Fourier transform of the i^{th} training image and the mean of the summation of all training image spectra, respectively. It can be seen by looking at the OT-MACH transfer function in Equation (2.20) that there are three main drivers of the filter design. The additive noise incorporated into the filter, the training image complex spectra that generate the similarity matrix and the power spectral density terms. These terms collectively control the filter performance in target detection scenarios.

It is also very important to take in to account the human interaction with the filter in real time scenarios were the logical adjustment and fine tuning of the parameters are required for a successful result.

2.5 Filter training image study

There are multiple aspects that need to be focused on when looking at training image optimisation for robust filter design as discussed in the following sections.

2.5.1 Training image summation blurring

There is a limitation on the number of training images that can be used in the filter design. It has been determined for the application with FLIR images and the test data collected that the number of training images used in the OT-MACH filter can vary from just a single image to a maximum of around 8-10 images depending on the target image complexity. The correct number of training images in the filter design is vital, since this also affects the correlation peak quality and discrimination ability from a cluttered background. If the number of images exceeds about ten in the filter, then a result will be generated in which most of the features of the training image information will be lost. On the other hand, too few number of training images will lack the information needed to train the filter and will result in poor recognition and false alarms, especially in video sequences where the object is changing orientation with respect to the camera.

Several training images are added with a double precision in order to compute a rotationally multiplexed reference image before utilising the training images in the filter design. A few examples of rotationally multiplexed reference images are shown in Figure 2.3(a), (b) and (c).

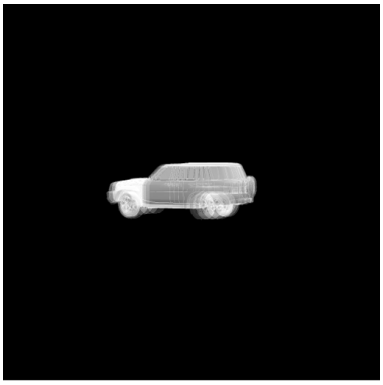

(a)

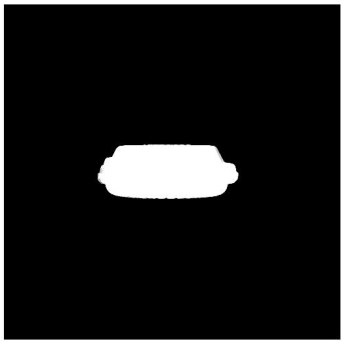

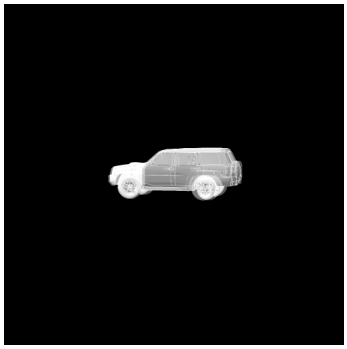

(b) (c)

Figure 2.3 (a) 5 training images multiplexed together. (b) 15 training images multiplexed. (c) Two training images multiplexed.

Figure 2.3(a) shows an acceptable number of training images rotationally multiplexed and it is clear that the image features are preserved. Figure 2.3(b) illustrates the over-trained filter image, were most of the information lost is due to over multiplexing of the images and so loos of detail. Finally, Figure 2.3(c) shows two images in the training set, which also has about the minimum information required for a successful training of the OT-MACH filter.

The effect of the number of training images can also be seen in the correlation plane. Figure 2.4 shows the correlation result of an OT-MACH filter trained with 1, 5 and 15 training images, respectively.

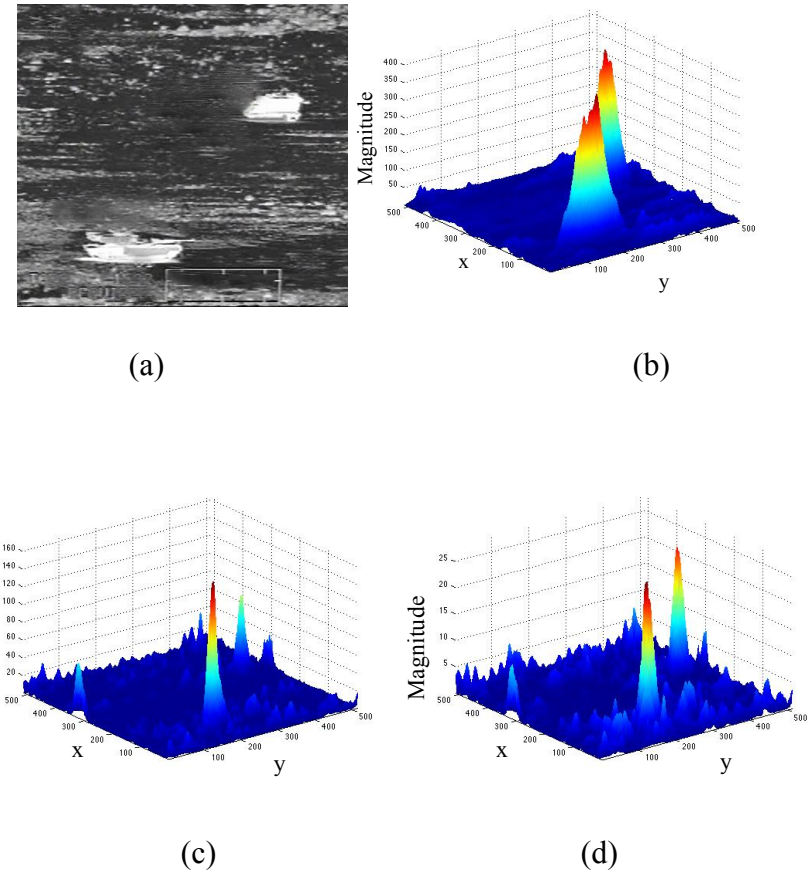

Figure 2.4 (a) Input image with M1A2 tank and M113 personal carrier (b) Correlation result for OT-MACH with 1 training image. (c) Correlation result for OT-MACH with 5 training images. (d) Correlation result for OT-MACH with 15 training images

Figure 2.4(b) shows the correlation result of an OT-MACH trained with only one M1A2 tank training image. There are two peaks present in the correlation plane for both the true and false targets. As discussed, there is not enough information in the training images to allow the OT-MACH to detect the true target. Figure 2.4(c) shows the acceptable training image number, i.e. five, which results in the sharper and higher peak

at the true target location at the bottom of the input image (Figure 2.4(a)), in this case the Abrams M1A2. Figure 2.4(d) shows a result of the correlation with an OT-MACH over-trained with 15 training images and is clearly showing two very high and similar peaks of both true and false targets.

2.5.2 Illumination effect using real and 3D data

When using FLIR imagery it is very important to take into consideration the illumination of the target compared to the background. The heat signature emitter from the target, which generates a grey scale pattern, was measured and used to superimpose it on the 3D models that have been designed. Figure 2.5 below shows the two types of training images both before and after the superimposing of the FLIR texture.

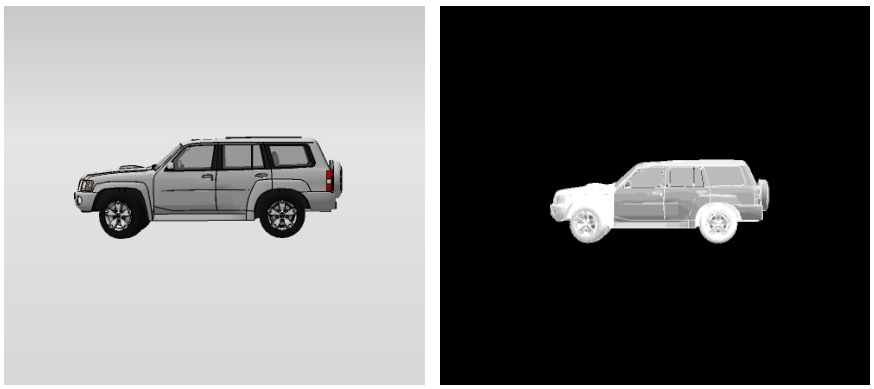

(a) (b)

Figure 2.5 3D Nissan patrol cars (a) without FLIR texture and (b) with FLIR texture.

The OT-MACH filter was trained with two-dimensional projected views of the 3D CAD models using several out-of-plane rotations (0° to 360°) of the selected targets.

As an example dataset we employed 2D representations of a 3D model of a Nissan Patrol vehicle to train the OT-MACH filter. The training images are rendered for

different rotation angles (between 0 to 360 degrees) as shown in Figure 2.6. The OT-MACH filter will then be trained with 5-10 training images as determined to be suitable for this particular application. Multiple OT-MACH filters needed to be trained to cover the overall rotations of the target present in the real time dynamic scenarios.

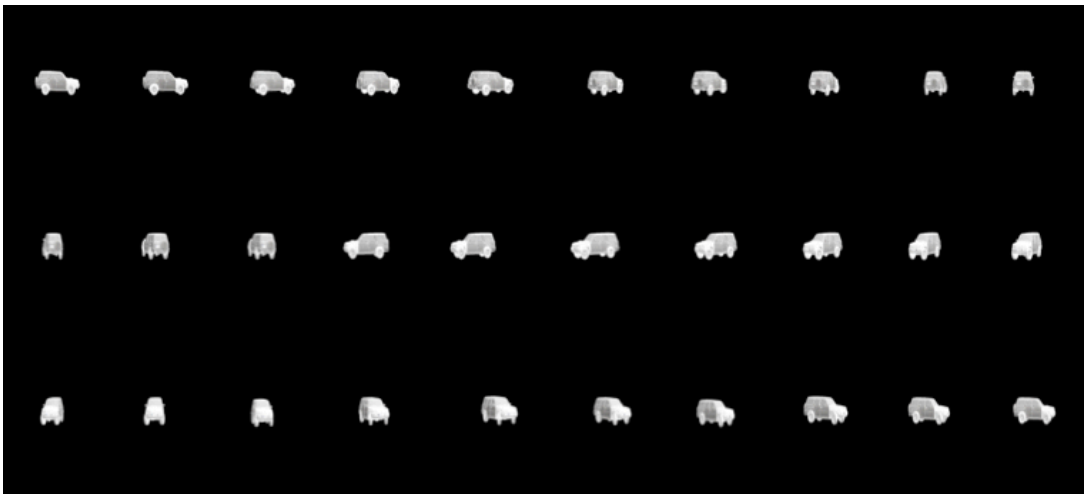

Figure 2.6 An example of a Nissan Patrol training dataset (angle of rotation between 0 and 360 degrees)

The use of two-dimensional views of the 3D model of the target as training images allows the OT-MACH filter to efficiently detect real targets due to the presence of enhanced and complete edges in comparison to training images derived directly from a FLIR camera. Figures 2.7(a) and (b) shown below depict the real training image and a 2D representation of the target derived from a 3D model.

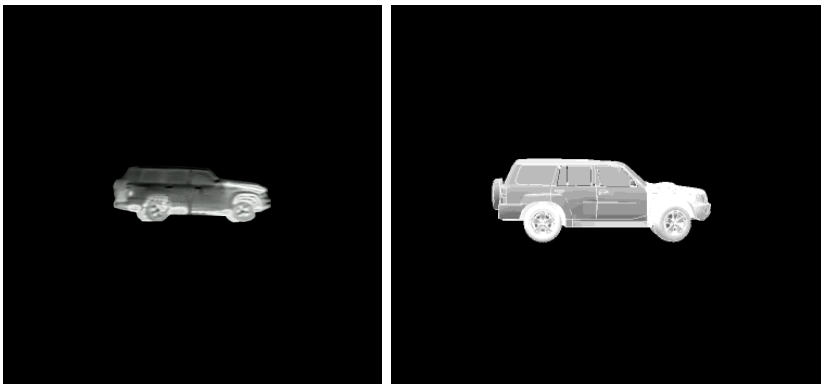

(a) (b)

Figure 2.7 Nissan Patrol training images (a) Real training image, (b) 3D training image

The ability to render the 3D models to match the FLIR signature of the target objects makes it possible to efficiently correlate against the FLIR data. In contrast, the degradation of the edges that is present in the actual target data makes it less effective as a source of training images to detect targets in varied conditions. The ultimate solution would be to be able to design and render the 3D models of any target description, which can be used in any desired detection scenario.

The training sets have been made for several types of military and civilian vehicles. The texture of the models has been modified to match the FLIR texture in order to improve the recognition capability to the OT-MACH filter with FLIR imagery. Tests have been conducted on five different vehicles, as listed below:

a. M1A2 Abrams tank
b. British Warrior armoured vehicle
c. M113 armoured personnel carrier
d. Military truck
e. Nissan patrol car
f. Military HUMVEE

Figure 2.8 below shows an examples of a single training image from different training sets used for the different targets employed in the research conducted.

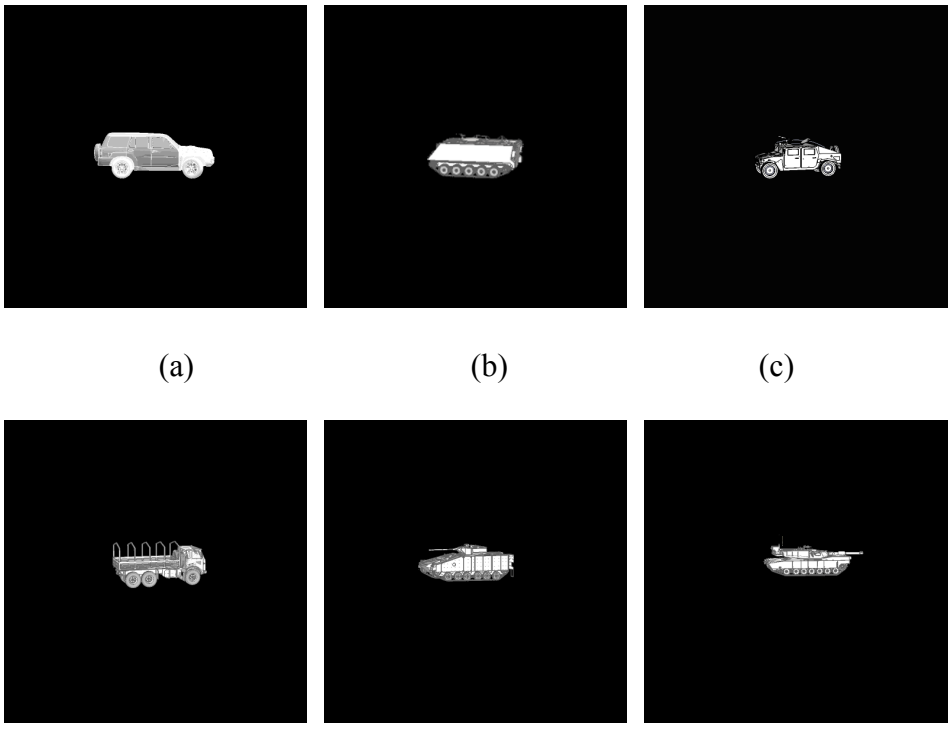

(a) (b) (c)

(d) (e) (f)

Figure 2.8 Multiple target Training images, (a) Nissan Patrol car, (b) M113 troop carrier, (c) military HUMVEE, (d) military Truck, (e) British warrior armour and (f) M1A2 tank.

2.6 Correlation response disruption due to background clutter noise and rotational distortion

There has been a considerable amount of research focused on finding an effective method to reduce the deleterious effects of background clutter and rotational distortion on the correlation result [65], [69], [89], [90], [93], [100]. The improvements were

introduced to boost the discrimination ability for the required target against other objects and also to reduce the false alarms generated. Statistical, mathematical and pre-processing stages have been applied to the OT-MACH filter design to enhance target detection in cluttered backgrounds.

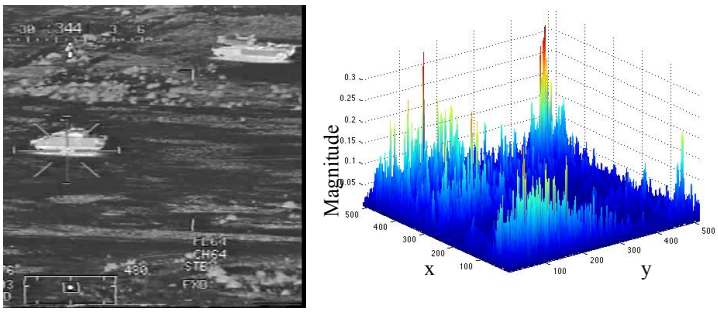

(a)

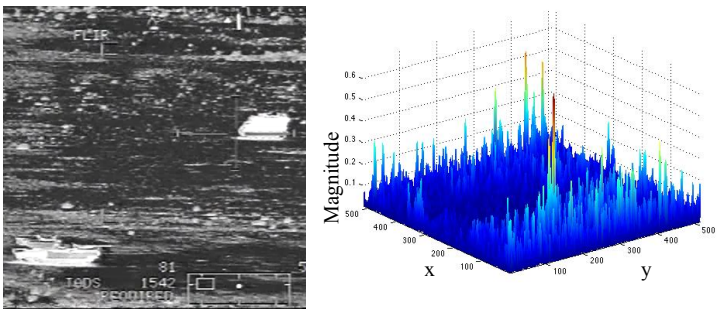

(b)

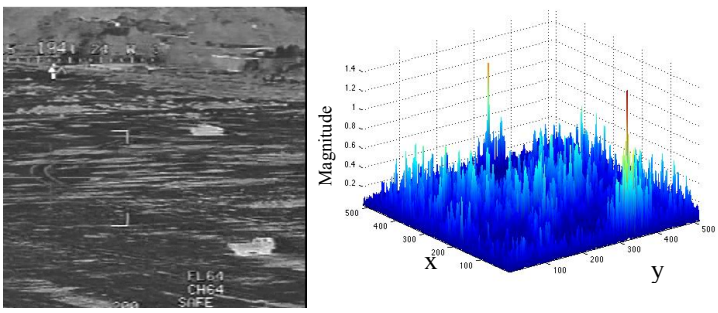

(c)

Figure 2.9 Correlation result with high background clutter with multiple targets in the scene (a) British warrior armoured vehicle and M1A2 tank (b) M1A2 tank with M113 personal carrier (c) British warrior armoured vehicle and military truck

Figure 2.9 shows some examples of the Apache data set where high clutter is present. It is clearly evident that the clutter has a significant effect on the target discrimination when using the OT-MACH filter. Thus the need of a technique to reduce the background noise disruption in the correlation process is vital.

Rotational distortion is also one of the technical difficulties in pattern recognition scenarios. In-plane and out-of-plane rotational distortion reduction techniques are very much needed, especially for real-time target detection and tracking. The OT-MACH filter can accommodate to a certain extent minor distortion due its inherent capability of distortion tolerance. A filter bank approach has been used to accommodate large changes in the target orientation in addition to the individual filter multiplexing of training images described in Section 2.5.1. A few hundred OT-MACH filters are each trained with several training images in different rotational view ranges to cover all aspects of the target view. However, such an extensive process of applying many correlations to each frame in real-time scenarios will clearly require very high computational power.

2.7 Performance metrics and quantification of correlation response

Several correlation performance metrics have been discussed in the literature to quantify and compare different filter designs. Kumar and Hassebrook [101] originally presented a now commonly employed approach to evaluate correlation filter performance. In addition to the correlation performance metrics introduced by Kumar and Hassebrook,

others have been presented to quantify the correlation result realistically and accurately. The metrics are as follows:

a. Peak-to-sidelobe ratio (PSR).
b. Peak-to-correlation energy (PCE).
c. Area at half peak height (AHH).
d. Number of peaks at half the maximum peak height (NPHH).
e. Total detection error (TDE).

2.7.1 Peak-to-sidelobe ratio

The peak-to-sidelobe ratio (PSR) is a measure of the correlation peak quality. The peak height is compared to the surrounding sidelobe peak values and the PSR is given as:

$$PSR = \frac{Peak - \mu}{\sigma_c} \qquad \textbf{Eq. 2.21}$$

where μ is the mean and σ_c is the standard deviation of the correlation plane pixel intensities in a defined region around the peak. This is taken to be within a 5 x 5 pixel masked region and, together with the surrounding sidelobe region of a defined size, is used to compute the PSR. It is a common measure used to describe the peak quality and the degree of match between the target and the input image. Its application to a typical correlation response is illustrated in Figure 2.10.

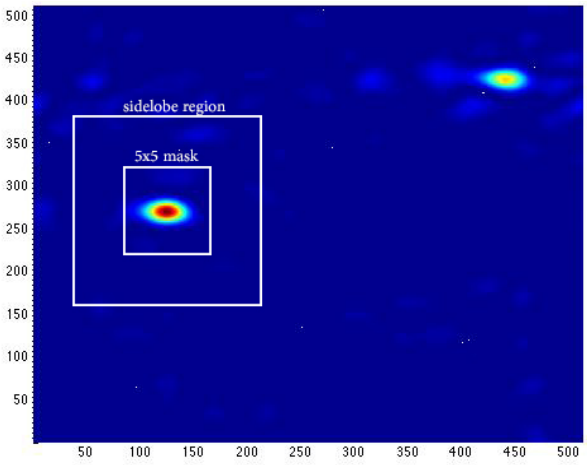

Figure 2.10 Peak-to-sidelobe ratio estimation

2.7.2 Peak-to-correlation energy

The peak-to-correlation energy (PCE) measures the correlation peak sharpness and is given as [101]:

$$PCE = \frac{\left[COPI - \left|\overline{C(x,y)}\right|^2\right]}{\left(\sum \frac{\left[\left|C(x,y)\right|^2 - \left|\overline{C(x,y)}\right|^2\right]^2}{N_x N_y - 1}\right)^{\frac{1}{2}}} \qquad \textbf{Eq. 2.22}$$

where N_x and N_y are the x and y dimensions of the correlation plane and COPI is the correlation output peak intensity i.e.:

$$COPI = \max\left|C(x,y)\right|^2 \qquad \textbf{Eq. 2.23}$$

where $C(x,y)$ is the correlation peak magnitude. The PCE measurement compares the peak correlation energy to the overall correlation plane energy. Higher PCE values

indicate a better correlation peak output and thus a better detection of the true target objects. This measure is predominantly used for single target object scenarios [102] due to the fact that the measure is based on one single correlation peak in the correlation plane.

2.7.3 Area at half peak height (AHH)

Traditionally, peak width at half of the peak height (PWHH) is a well-known measurement of peak quality (to give an indication of peak localisation). For a 2D correlation peak, PWHH will not result in a consistently accurate measurement of the peak width since the correlation peak is not uniform in both dimensions. The examples below in Figures 2.11(a) and (b), show a correlation peak and its cross-section at half the peak height.

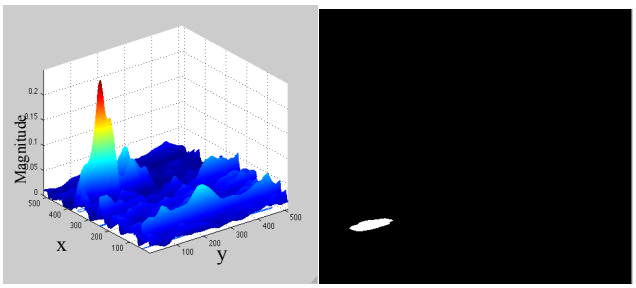

(a) (b)

Figure 2.11 An example peak with a cross-section at half the peak height. (a) Correlation peak. (b) Peak cross section

From these images it is clear that the peak is oval in shape. Thus the width measurement would be different if measured along the *x*-axis and the *y*-axis. A more useful measure would be the peak area at half the peak height (AHH) which will reflect a consistent

measurement for any peak width shape. The area will be a scalar whose value corresponds, for example, to the total number of pixels in the white area of the thresholded binary image shown in Figure 2.11.

2.7.4 Number of peaks at half the maximum peak height (NPHH)

A further measurement will be employed that indicates the number of peaks at half the maximum peak height (i.e. at half of the detection peak height). This will indicate how well the filter detects the true target versus the false targets or clutter. It also gives an indication of the peak quality when the peaks start to become scattered as the amount of clutter noise exceeds an acceptable value, as shown below in Figure 2.12(a).

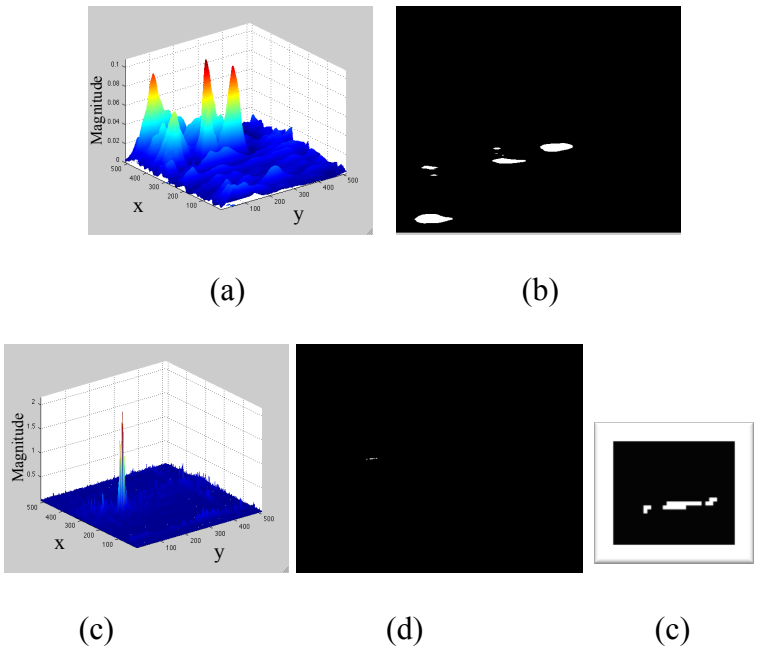

Figure 2.12 (a) and (b) Correlation plane with a detection peak and some false alarm peaks. (c) and (d) An apparently isolated correlation peak that is actually three peaks located closely together

Although the peak in Figure 2.12(c) appears localised, upon close examination of the peak structure we find that, due to a non-optimal setting of the filter parameter values, the peak is in fact fractionated which will lead to false detections.

2.7.5 Total detection error (TDE)

The total detection error gives a measure of the OT-MACH filter performance when the OT-MACH parameters are changed along with the additional other filter parameters that are added to the OT-MACH filter as described below. The TDE is used to calculate how many times a single peak is present in the correlation plane, so representing a successful detection. The TDE is given as:

$$TDE = \left| \frac{R_{total} - R_{detection}}{R_{total}} \right| \times 100 \qquad \textbf{Eq. 2.24}$$

where the total run, R_{total}, is calculated as the number of increments over which the OT-MACH β and γ parameter values are varied in the range of 0 and 1, while testing for detection of the target in a particular scenario. $R_{detection}$ is the number of detections counted in the run. The TDE is thus calculated as the number of failed detections divided by the total number of runs performed which indicates the overall performance of the correlation process and can be used to find the best parameter range generating the least false detections.

2.8 Target constraint assumptions

In this thesis, the focus has been toward a specific application of the use of FLIR imagery in defence and security applications. The research has been focused on the improvement of the OT-MACH filter performance using multiple methods and techniques. There have been some assumptions during data collection and testing. The research has been conducted only on the FLIR imagery data acquired from the Kuwait Armed Forces using multiple sensors. The FLIR images were at high resolutions and the target heat signature was between medium heat (18^{o}C) and high heat (45^{o}C). Target scale and out-of-plane rotations were approximately fixed during the testing. Minor changes to scale and out-of-plane rotation were accepted and accommodated by the OT-MACH filter distortion tolerance capability. Target occlusion was also assumed to be no more that 10 - 20 percent in any scenario. A quality measure has been introduced to refine the quantification process. The resultant correlation peak of the true target can only be counted as a true detection peak if there are no other peaks in the correlation plane that exceed 50% of the detection peak height. Introducing such a criterion should give a better, more accurate and reliable result. Figure 2.13(a) shows a detection peak with no other side peaks or false alarms in the correlation plane. Figure 2.13(b) shows a discarded target detection example due to the presence of other peaks whose height exceeds 50% of the detection peak.

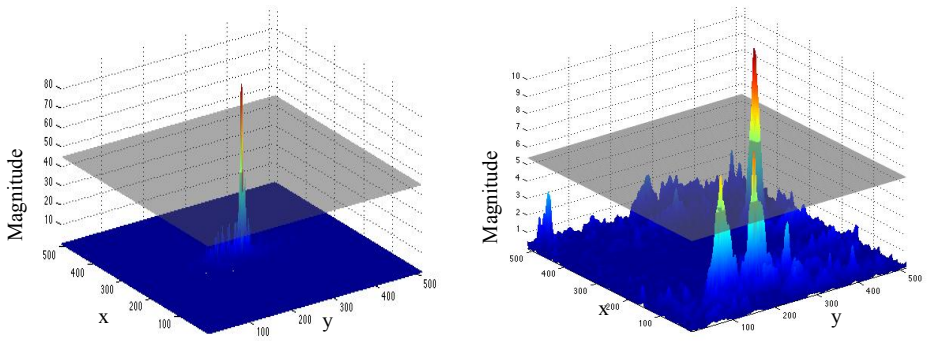

(a) (b)

Figure 2.13 (a) An acceptable correlation result. (b) Non-acceptable correlation result.

2.9 Summary

This chapter has introduced the Optimal Trade-off Maximum Correlation Height (OT-MACH) filter design considerations in detail. As described in Section 2.3, there is an important need for optimising the filter to assist in target detection in various environmental conditions. The OT-MACH optimisation problems discussed in Section 2.4 illustrate the importance of the various parameters of the filter transfer function. An optimisation study of these parameters has been undertaken and is described in detail in Chapter 3.

One of the important filter design research criteria, namely the selection of the number of training images in the dataset used to create the filter transfer function, is discussed in detail in Section 2.5. It is concluded that there is an optimum number of training images that can be used to construct a near to ideal filter. Out-of-plane rotational multiplexing of the training images in order to attain computational efficiency is also detailed, along with conclusions regarding the number of training images possible in a single filter. Illumination effects when using real and 3D training data have been discussed, along

with considerations concerning the mapping of FLIR data texture information onto the CAD target model to improve the accuracy of the model and allow improved target detection. Section 2.6 discusses background clutter noise reduction and rotational distortion effects in the design of the OT-MACH filter. Section 2.7 has described the classical performance metrics for correlation filter performance assessment such as PSR and PCE. Furthermore, new performance metrics are also introduced, namely: Area of peak at half-height (AHH); Number of peaks at half maximum height (NPHH) and Total detection error (TDE), which are discussed in detail as additional performance metrics to support quantification of the filter performance. The chapter is concluded with discussion of the target constraints used in the work discussed in this thesis.

Chapter 3

OT-MACH filter parameter optimisation

Chapter 3 OT-MACH filter parameter optimisation

3.1 Chapter organisation

The chapter starts with an illustration of the OT-MACH parameters and their role in controlling the filter behaviour. The section 3.3 addresses the optimisation of the OT-MACH filter in detail. Section 3.3 also discusses various test results whilst keeping the OT-MACH filter parameters at unity. The noise term contained in the filter function is optimised using multiple statistical measures discussed in section 3.4. The proposed modification of the OT-MACH filter is justified and evaluated using several results, which are presented in section 3.5. The chapter is concluded in section 3.6.

3.2 Introduction

The optimisation of the OT-MACH filter α, β and γ parameters has been investigated over the last decade by a number of research groups [2], [3], [12], [58], [62], [66], [74], [98]. The main focus of the effort was to improve the performance of the OT-MACH filter correlation result by finding a suitable value for these parameters. Each of the parameters controls part of the OT-MACH transfer function in order to adjust the filter according the desired result. The alpha (α) parameter controls the output noise variance, the beta (β) parameter controls the average correlation energy and the gamma (γ) parameter controls the average similarity matrix. When setting the beta parameter to a low value the OT-MACH filter will have a better peak sharpness but will have increased sensitivity to intra-class target object distortions. Changing the value of the alpha parameter will result in an increase of the robustness of the filter to distortions and

to noise but it will reduce the correlation peak sharpness. In order to obtain the desired OT-MACH behaviour, the parameters must be balanced in such a manner that allows the correct compromise between distortion tolerance, discrimination ability and noise robustness of the filter [12].

3.3 OT-MACH filter parameter optimisation method

In this section, the behaviour of the OT-MACH filter has been tested while changing the controlling parameters. The OT-MACH parameters are changed one at a time while the others are kept at unity. The parameter values have been pre-selected to 14 values within the range 0 to 1 and the resultant OT-MACH filter behaviour recorded. The test was carried out on three different images from a real-world scenario video sequence. The OT-MACH filter was trained each time with suitably rendered CAD training images to discriminate the target result from the cluttered background. Figure 3.1 below shows the four target images and a sample of the training images that were used in this test.

(a)

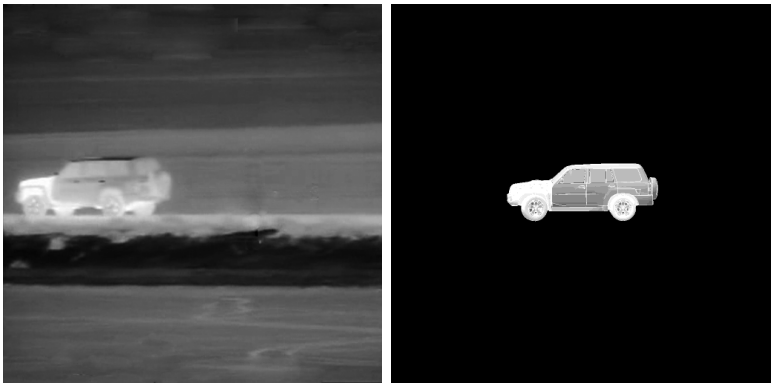

(b)

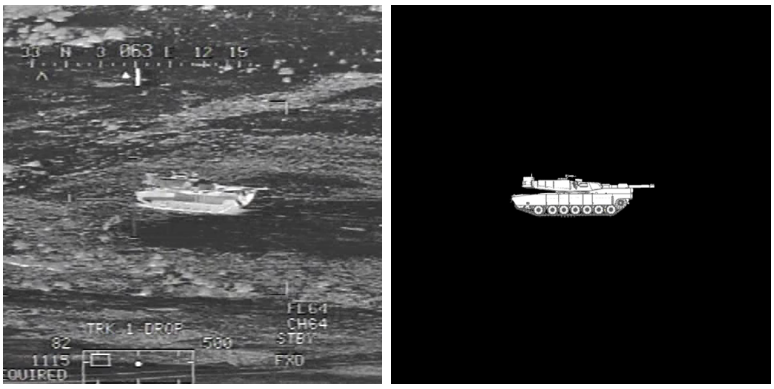

(c)

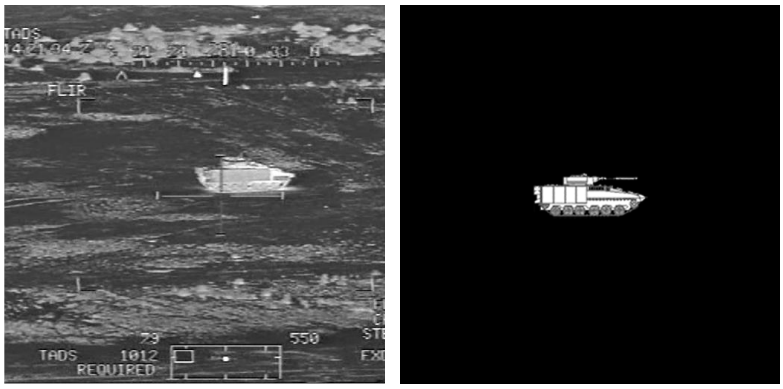

(d)

Figure 3.1 Input and training image samples used for the OT-MACH parameter testing: (a), (b) Nissan patrol real and training image; (c) M1A2 real and training image and (d) British warrior real and training image

The initial testing was made with a simple input image as shown in Figure 3.1(a) with only slight clutter in the background. Figure 3.1(b) shows a Nissan patrol, Figure 3.1(c) shows an M1A2 tank and Figure 3.1(d) shows a British warrior armoured vehicle. Tables 1 to 4 show the result of the PSR results recorded when changing each OT-MACH parameter in turn while the other two are kept at a value of unity for the test images shown in Figure 3.1

α β = γ = 1	α PSR	β α = γ = 1	β PSR	γ β = α = 1	γ PSR
0.00001	49.63	0.00001	17.59	0.00001	79.70
0.0001	49.68	0.0001	17.65	0.0001	76.70
0.001	49.85	0.001	18.19	0.001	76.70
0.01	51.12	0.01	19.87	0.01	76.64
0.1	56.89	0.1	46.17	0.1	76.05
0.2	60.26	0.2	58.56	0.2	75.41
0.3	62.68	0.3	64.80	0.3	74.80
0.4	64.52	0.4	68.21	0.4	74.20
0.5	65.95	0.5	70.10	0.5	73.62
0.6	67.09	0.6	71.09	0.6	73.07
0.7	67.99	0.7	71.50	0.7	72.53
0.8	68.83	0.8	71.55	0.8	72.00
0.9	70.02	0.9	71.36	0.9	71.50
1	71.01	1	71.01	1	71.01

Table 3.1 PSR values obtained as a result of OT-MACH parameter changes for image shown in Figure 3.1(a)

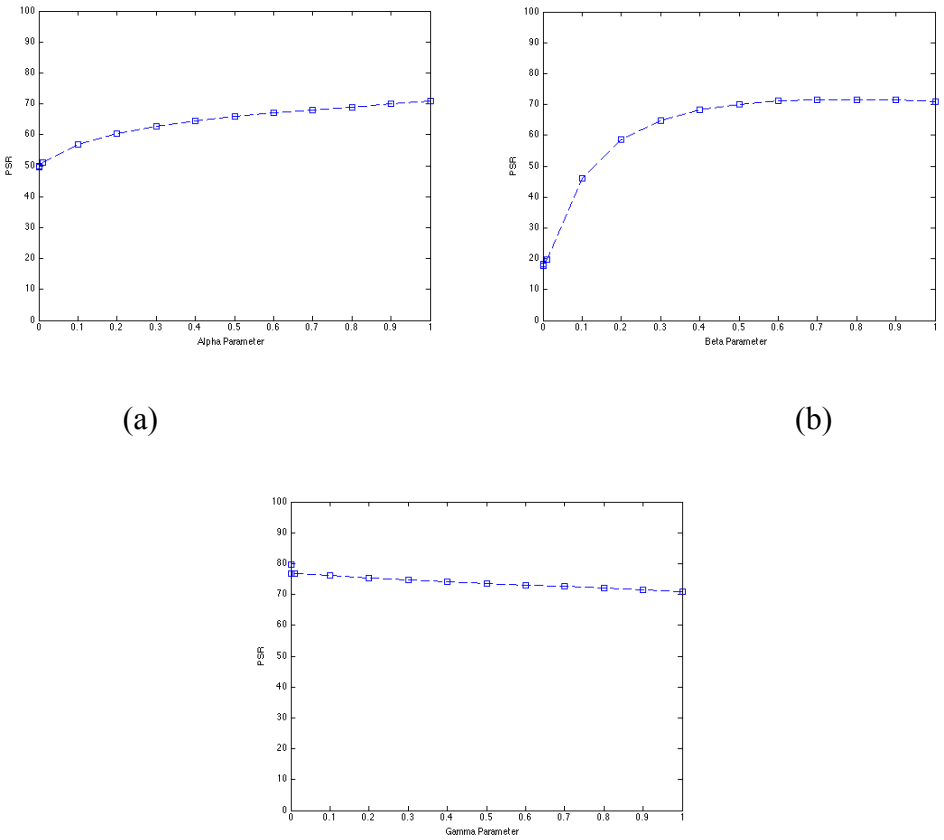

(a) (b)

(c)

Figure 3.2 PSR results for Nissan patrol image shown in Figure 3.1(a) for OT-MACH parameter changes: (a) PSR versus alpha parameter change; (b) PSR versus beta parameter change and (c) PSR versus gamma parameter change

α β = γ = 1	α PSR	β α = γ = 1	β PSR	γ β = α = 1	γ PSR
0.00001	0	0.00001	10.21	0.00001	94.32
0.0001	0	0.0001	0	0.0001	94.32
0.001	0	0.001	19.01	0.001	94.32
0.01	99.4	0.01	47.93	0.01	94.33
0.1	98.64	0.1	75.97	0.1	94.37
0.2	97.84	0.2	82.42	0.2	94.37
0.3	97.16	0.3	85.79	0.3	94.34
0.4	96.55	0.4	88	0.4	94.3
0.5	95.99	0.5	89.58	0.5	94.23
0.6	95.48	0.6	90.79	0.6	94.15
0.7	95	0.7	91.74	0.7	94.05
0.8	94.55	0.8	92.52	0.8	93.95
0.9	94.13	0.9	93.17	0.9	93.84
1	93.72	1	93.72	1	93.72

Table 3.2 PSR values obtained as a result of OT-MACH parameter changes for the image shown in Figure 3.1(b)

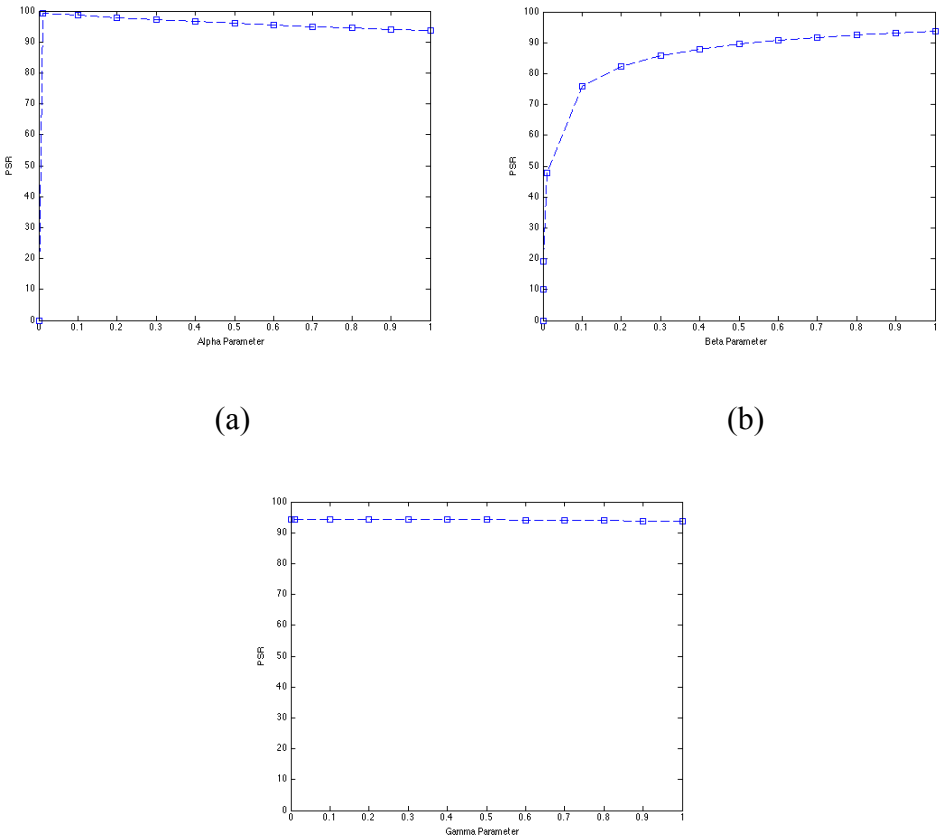

(a) (b)

(c)

Figure 3.3 PSR results for Nissan patrol image shown in Figure 3.1(b) for OT-MACH parameter changes: (a) PSR versus alpha parameter change; (b) PSR versus beta parameter change and (c) PSR versus gamma parameter change

α β = γ = 1	α PSR	β α = γ = 1	β PSR	γ β = α = 1	γ PSR
0.00001	17.16	0.00001	2.88	0.00001	15.92
0.0001	17.16	0.0001	3.11	0.0001	15.92
0.001	17.15	0.001	5.20	0.001	15.92
0.01	17.05	0.01	14.36	0.01	15.91
0.1	16.15	0.1	16.91	0.1	15.76
0.2	15.43	0.2	17.68	0.2	15.61
0.3	14.86	0.3	17.72	0.3	15.46
0.4	15.17	0.4	17.47	0.4	15.13
0.5	15.43	0.5	17.14	0.5	15.41
0.6	15.63	0.6	16.82	0.6	15.55
0.7	15.77	0.7	16.52	0.7	15.68
0.8	15.88	0.8	16.28	0.8	15.80
0.9	15.96	0.9	16.15	0.9	15.68
1	16.01	1	16.01	1	16.01

Table 3.3 PSR values obtained as a result of OT-MACH parameter changes for image shown in Figure 3.1(c)

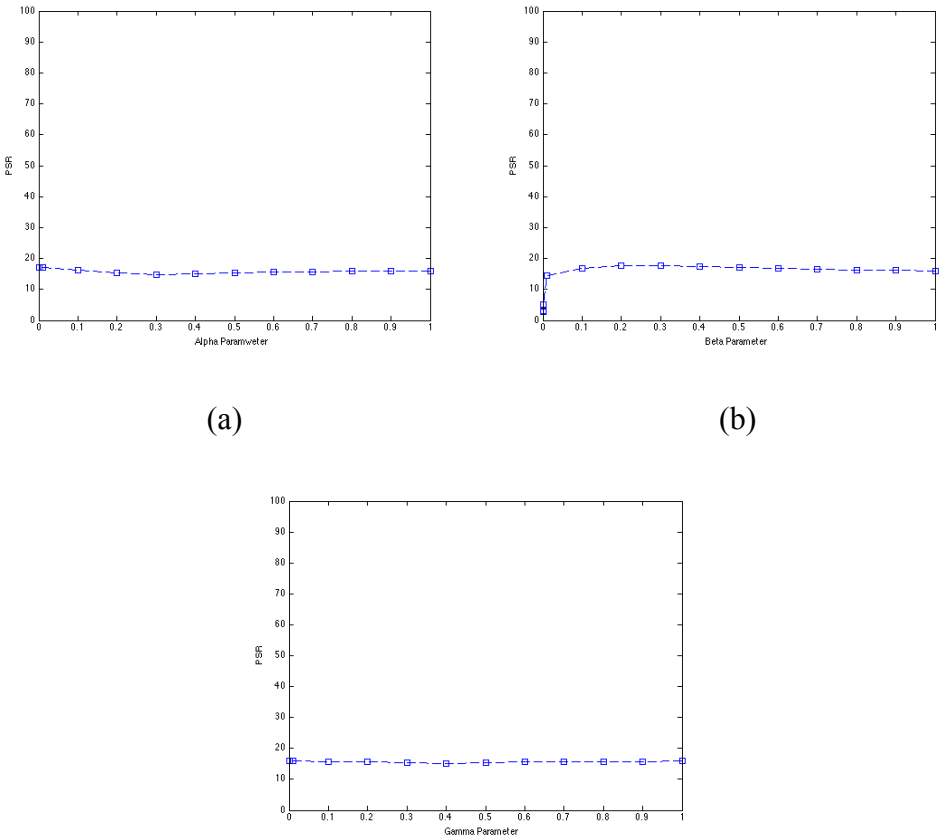

(a) (b)

(c)

Figure 3.4 PSR results for M1A2 tank image shown in Figure 3.1(c) for OT-MACH parameter changes: (a) PSR versus alpha parameter change; (b) PSR versus beta parameter change and (c) PSR versus gamma parameter change

α β = γ = 1	α PSR	β α = γ = 1	β PSR	γ β = α = 1	γ PSR
0.00001	24.09	0.00001	3.05	0.00001	20.08
0.0001	24.09	0.0001	3.20	0.0001	20.08
0.001	24.10	0.001	4.55	0.001	20.09
0.01	24.18	0.01	21.33	0.01	20.10
0.1	24.16	0.1	24.30	0.1	20.25
0.2	23.48	0.2	24.82	0.2	20.42
0.3	22.62	0.3	24.70	0.3	20.57
0.4	21.73	0.4	24.31	0.4	20.71
0.5	20.84	0.5	23.82	0.5	20.85
0.6	20.01	0.6	23.31	0.6	20.98
0.7	20.44	0.7	22.80	0.7	21.11
0.8	20.81	0.8	22.32	0.8	21.23
0.9	21.15	0.9	21.32	0.9	21.35
1	21.46	1	21.46	1	21.46

Table 3.4 PSR values obtained as a result of OT-MACH parameter changes for image shown in Figure 3.1(d)

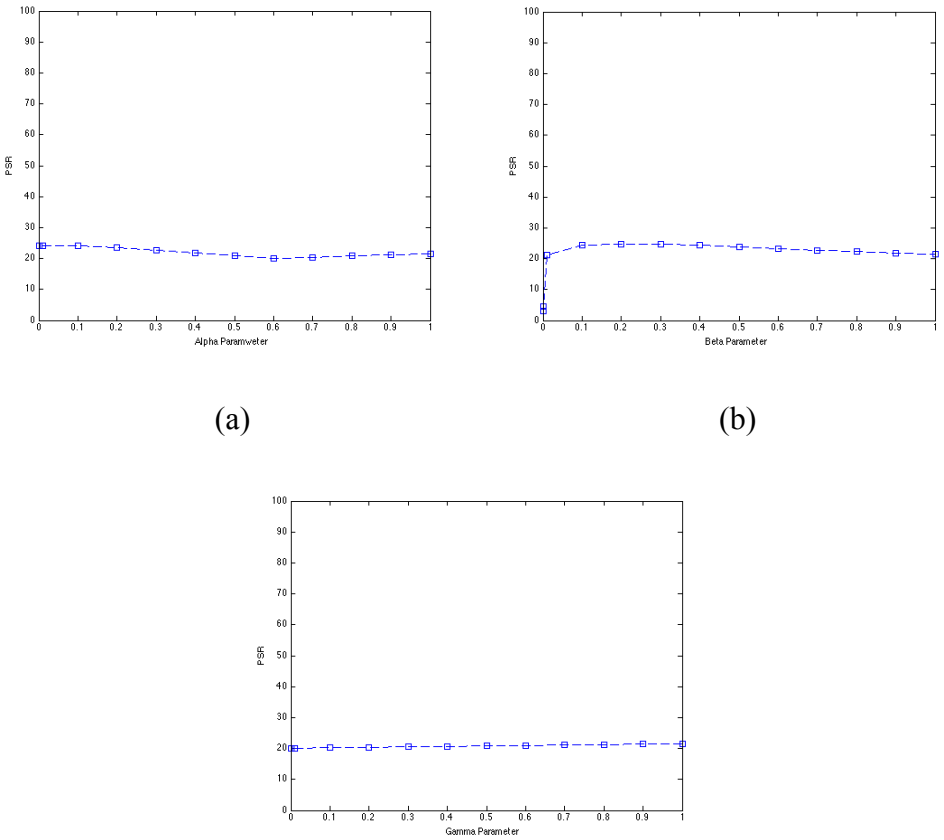

(a) (b)

(c)

Figure 3.5 PSR results for British Warrior image shown in Figure 3.1(d) for OT-MACH parameter changes: (a) PSR versus alpha parameter change; (b) PSR versus beta parameter change and (c) PSR versus gamma parameter change

By looking at the above results, shown in Figures 3.2 to 3.5, it is noticeable that variation of the parameter γ does not affect the PSR values to any great extent. It is also observed that the α and β parameters have a prominent effect on the resultant PSR.

It can be observed that when the input image contains a target in a less cluttered background we obtain a gradually increasing PSR response followed by a relatively steady state region of the PSR response for change in parameter values, whereas for noisy and cluttered background target images the PSR response is limited to a certain

range due to the presence of the high clutter noise which creates side peaks in the correlation plane.

Several conclusions can be drawn from looking at the PSR results for the four tests conducted. The first two tests images, which involves the Nissan patrol vehicle as a target, was acquired in northern Kuwait where the background is almost clutter noise free. The background clutter intensity is minor and does not considerably affect the correlation peak compared to the other test images. In contrast to this, Figure 3.1(c) and 3.1(d) show images obtained with an Apache helicopter mounted FLIR from environments where the background clutter is far stronger. In addition, the sharp edges resulting from the overlay information from the flight computer are also prominent in the images.

The α parameter controls the noise variance or the amount of noise injected to the filter transfer function to help suppress the background clutter [12]. The second parameter investigated was the β parameter. The PSR values show a more or less constant response to changes of the β parameter except at low values less than 0.1. The effect of changing the β parameter is the main drive for the OT-MACH filter behavioural changes. It has a direct effect on the correlation plane result and the detection peak shape. In all the tests that have been conducted, the main control in tuning of the OT-MACH filter response is achieved by varying the β parameter.

That last parameter to look at is the γ parameter. This parameter has a very minimal effect when optimising the performance of the OT-MACH filter and the correlation

result. It can be seen from the results above, that the range of change in the PSR result when changing the γ parameter is very narrow.

3.4 Noise parameter optimisation

Optimisation of the OT-MACH parameters has been investigated in the literature [66], [74]. Since full information for the additive noise value, *C*, is not available at all times [2], [58], several methods have been used to estimate this and set an optimal value of the additive noise input to the filter design. The most common method is the use of the white noise covariant matrix given below [31]:

$$C = \sigma^2 I \qquad \textbf{Eq. 3.1}$$

where σ^2 is the variance about the average input image and *I* is the identity matrix of the same size as the training image. An alternative technique involves use of the current input image statistics to adaptively set the additive noise value in the filter, which allows a continuous up-date of the filter transfer function as and when the input changes.

A model of the power spectral density has also been employed to set the additive noise value [8]. However, to make this work well, a low frequency cut-off has to be predefined to optimise the correlation results.

However, the technique employed in the work presented in this thesis uses the ratio of the input image standard deviation and mean which is then used for the additive noise

term in the filter transfer function, calculated at every frame of a video sequence to generate the statistical value of *C*. Thus the *C* value is given by:

$$C = \frac{\sigma}{\mu} \qquad \textbf{Eq. 3.2}$$

where σ is the current input image standard deviation and μ is the current input image mean. This is known as the coefficient of variation [103]–[105]. The coefficient of variation is a probability measure utilising the input image information variation in order to automatically compute the noise constant. The dynamic calculation of C for every input image allows us to set the parameter α (multiplying the *C* value) to unity [74]. Thus we are only left with the two parameters, β and γ, to optimise in the filter transfer function in order to obtain a useful correlation output.

3.5 Modified OT-MACH evaluation

As discussed in the previous section, the OT-MACH filter can be evaluated by changing the β and γ values whilst keeping the α parameter unity due to the fact that the noise term can be adaptively calculated statistically from the current image [74]. Initially, to build a test benchmark, the tests were carried out with all the OT-MACH parameters set to unity. The OT-MACH parameters β and γ were then changed incrementally between 0 and 1 to obtain the optimal parameter combination. The test involves eight input images from multiple platforms with targets to be detected as shown in Figure 3.6 below.

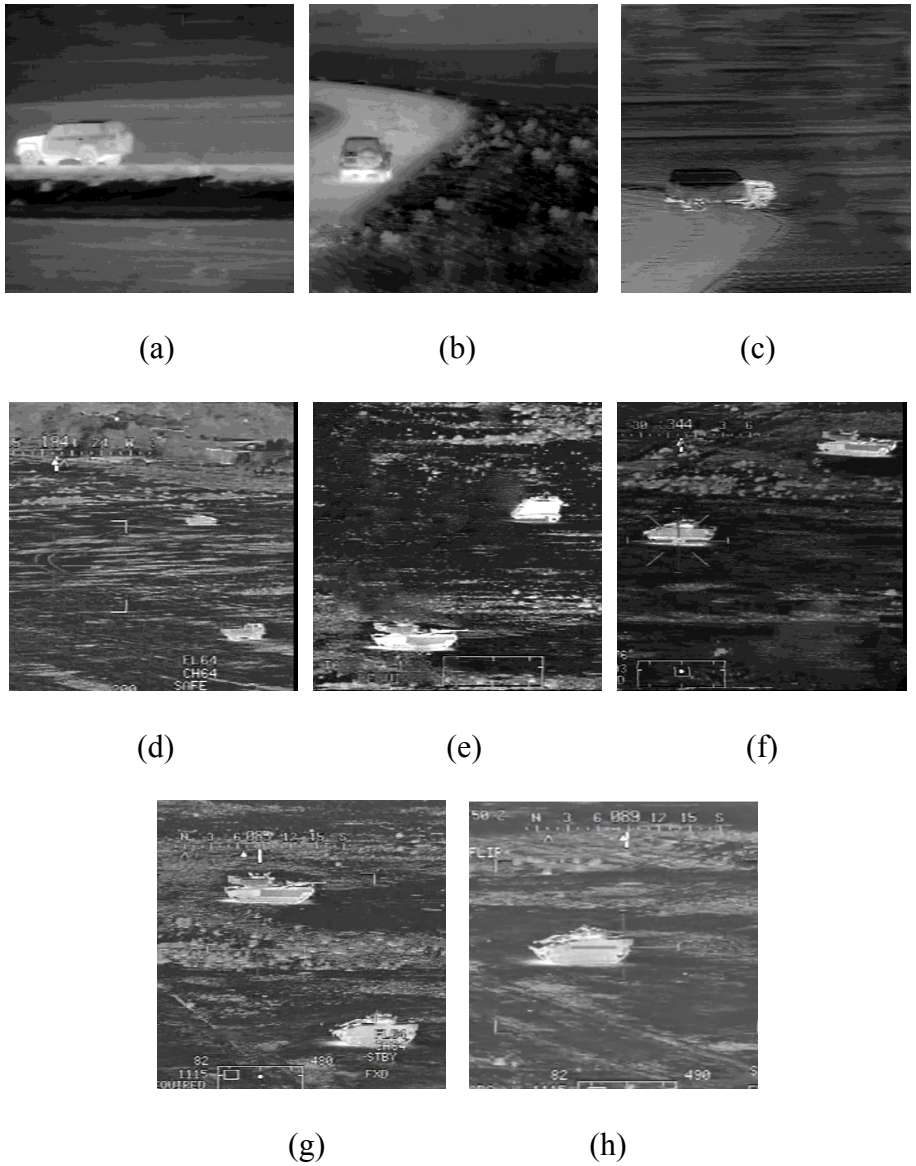

(a) (b) (c)

(d) (e) (f)

(g) (h)

Figure 3.6 Test images used in the OT-MACH evaluation (a), (b) and (c) showing the Nissan Patrol at various times of day and night (d) British warrior armour and military truck (e) M1A2 tank and M113 personal carrier (f) British warrior and M1A2 tank (g) M1A2 tank and British warrior (h) British warrior

Table 3.5 below shows the unity OT-MACH test results for the input images shown in Figure 3.6.

Test images	PSR	TDE
a	93.72	99.48
b	-	100
c	-	100
d	-	100
e	-	100
f	-	100
g	47.01	99.48
h	-	100

Table 3.5 Unity parameter OT-MACH correlation results. The dash indicates false or no detections.

It can be seen clearly that the unity OT-MACH does not perform well when correlated with almost all the test images shown in Figure 3.6.

A next stage of testing was then conducted by changing the OT-MACH parameters β and γ in a range between 0 and 1. The α parameter can be kept set to unity due the adaptive calculation of the statistical value of *C* [74] .The ranges selected for the β and γ parameters are shown in Table 3.6 below.

α	β	γ
1	0.00001	0.00001
1	0.0001	0.0001
1	0.001	0.001
1	0.01	0.01
1	0.1	0.1
1	0.2	0.2
1	0.3	0.3
1	0.4	0.4
1	0.5	0.5
1	0.6	0.6
1	0.7	0.7
1	0.8	0.8
1	0.9	0.9
1	1	1

Table 3.6 Pre-defined beta and gamma OT-MACH parameters

A combination of the two pre-defined parameters (with α kept set to unity) shown in Table 3.6 have been used and the resultant OT-MACH filters have been correlated with the test images shown in Figure 3.6. The process has been repeated 196 times to cover the whole range of combination possibilities of the OT-MACH filter parameters.

Test images	Beta (β)	Gamma (γ)	PSR	TDE
a	1	0.05	94.35	5.61
b	1	0.5	73.62	40.3
c	0.01	0.0025	32.91	94.89
d	0.1	0.025	28.55	81.12
e	$1x10^{-3}$	0.005	22.07	98.97
f	$1x10^{-3}$	0.05	36.46	95.97
g	1	0.05	48.13	55.10
h	0.2	0.9	29.73	75

Table 3.7 OT-MACH optimal parameter values and corresponding PSR and TDE values

In comparison to the results obtained with the OT-MACH filter with the β and γ parameters set to unity, a great improvement has been achieved in the filter PSR and TDE performance as shown in Table 3.7. Sample graphical results are shown below in Figures 3.7 to 3.11.

(a) (b) (c)

Figure 3.7 OT-MACH test result for target (c) in Figure 3.6. (a) Unity parameter OT-MACH correlation result. (b) Test image. (c) Optimal parameter OT-MACH correlation result.

The Nissan patrol test images shown in Figure 3.6(a), 3.6(b) and 3.6(c) have been acquired in different orientations and at different acquisition times. The same car has been imaged in the daytime in Figure 3.6 (a) and (b) and at night time in Figure 3.6(c), which shows less heat emitted from the Nissan Patrol. Figure 3.6(a), acquired in the daytime, shows most of the Nissan Patrol emits heat from its body due the high ambient temperature and also engine heat. All of the Nissan Patrol data set has been acquired in the northern part of Kuwait, where the heat dramatically affects the signature of the car, which then changes the texture of the Nissan Patrol.

Figure 3.8(a) shows the unity parameter OT-MACH filter correlation plane result. The optimal parameter settings computed using the pre-set values between 0 and 1 are shown in Figure 3.8(c). From Figure 3.8(a) and Figure 3.8(c) it can be seen when comparing the results for the test images that there is a high similarity between the correlation results for unity and optimal parameter correlation plane respectively. This is due to the low interference from the relatively uniform background clutter contained in the test image shown in Figure 3.8(b). But it should also be noted that although the detection peak heights are very similar, there are slight peak height difference between the two correlation planes results.

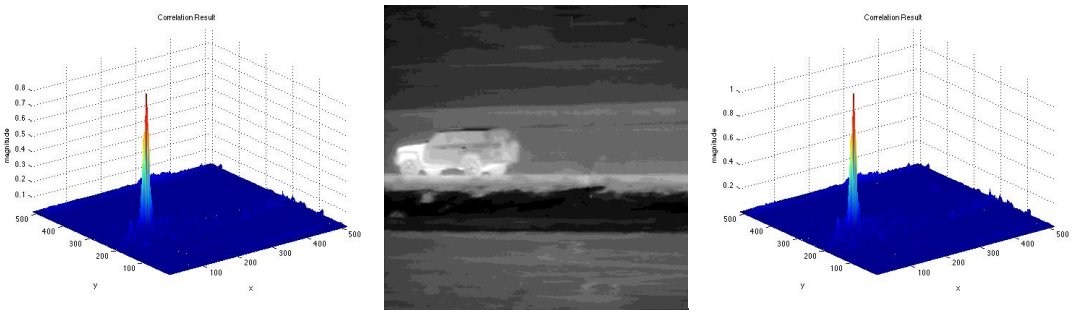

(a) (b) (c)

Figure 3.8 OT-MACH test result for target (a) in Figure 3.6. (a) Unity OT-MACH correlation result (b) test image (c) Optimal parameter OT-MACH correlation result.

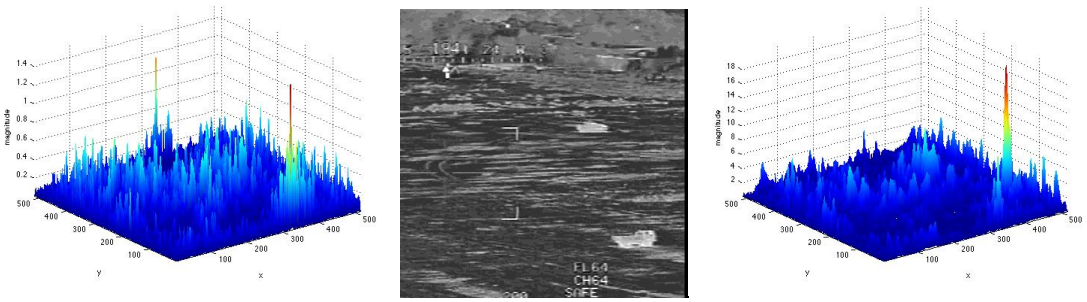

(a) (b) (c)

Figure 3.9 OT-MACH test result for target (d) in Figure 3.6. (a) Unity parameter OT-MACH correlation result. (b) Test image. (c) Optimal parameter OT-MACH correlation result.

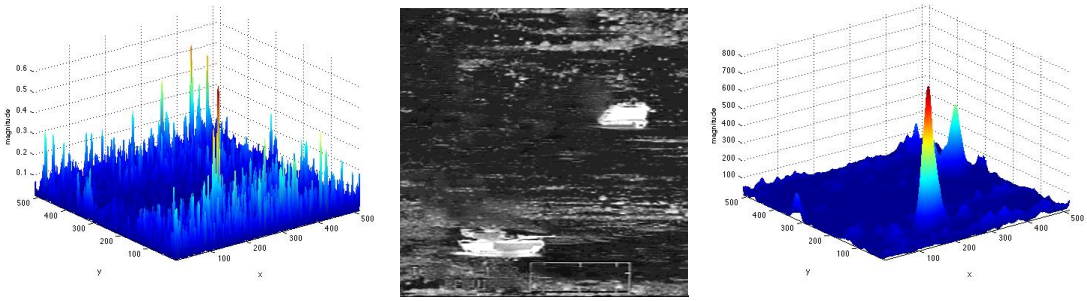

(a) (b) (c)

Figure 3.10 OT-MACH test result for target (e) in Figure 3.6. (a) Unity parameter OT-MACH correlation result.(b) Test image. (c) Optimal parameter OT-MACH correlation result.

(a) (b) (c)

Figure 3.11 OT-MACH test result for target (f) in Figure 3.6. (a) Unity parameter OT-MACH correlation result. (b) Test image. (c) Optimal parameter OT-MACH correlation result.

The results shown in Figures 3.9 to 3.11 shows great improvement to the overall correlation plane and the detected peak after altering the OT-MACH parameters from unity to obtain the optimal parameters. The unity parameter OT-MACH achieves no detection with 100% TDE as shown in Table 3.5, whereas the optimal parameter OT-MACH achieves a PSR value of 73.62 with a TDE of only 40.3, as summarised in Table 3.7.

These test images have highly cluttered backgrounds and contain the flight overlay at the top and bottom of the images. The flight data overlay effects the correlation performance due to its sharp edges, which generate multiple false detection peaks in the correlation plane. However, by choosing the right balance of the OT-MACH optimal parameters the performance of the filter can be improved and the high clutter noise can be overcome.

3.6 Summary

In this chapter, the OT-MACH filter parameter variations have been examined and their effect on achievable PSR correlation values determined for three different types of target object in various degrees of background clutter. These tests were conducted to try and arrive at near optimal relative settings of these parameters for good performance of the OT-MACH filter. From the tests conducted it was determined that the β parameter is the main drive for the overall OT-MACH filter behaviour. On the other hand, γ parameter has the minimal effect on the filter resultant behaviour.

The noise parameter in the OT-MACH transfer function denominator has been considered and it was concluded that it is possible to automatically compute the noise parameter value using the available statistics of the input image intensities. Thus the additive noise can be computed using the ratio of the standard deviation and mean of the input image intensity values whilst maintaining a setting of the α parameter to unity. This simplifies that the filter design and decreases the computational requirements in deriving the ideal OT-MACH filter transfer function by setting two, rather than three, parameters. In order to justify this conclusion, several results have been presented and discussed.

In Chapter 4, further enhancements have been applied to the OT-MACH filter by using a bandpass Difference of Gaussian (DoG) filter. The resulting improvements in performance are discussed in detail.

Chapter 4

The Difference of Gaussian modified OT-MACH (D-MACH) filter performance assessment

Chapter 4 The Difference of Gaussian modified OT-MACH (D-MACH) filter performance assessment

4.1 Chapter organisation

The chapter begins with brief introduction to the difference of Gaussian modified OT-MACH (D-MACH) filter. The Difference of Gaussian filter theory along with the discussions of its transfer function are presented in section 4.3. Section 4.3 also presents a novel method of using the DoG filter as a pre-processing bandpass filter with the OT-MACH filter. The evaluation of the D-MACH is discussed with various result tabulations and graphs in section 4.4. A unique method of automatic adjustment of the DoG filter is detailed in 4.5. The effect of the DoG pre-processing filter on the correlation result also described in section 4.5. Section 4.6 summarises and concludes the chapter.

4.2 Introduction

In the previous chapters the effort was focused towards the optimisation the OT-MACH filter parameters in order to achieve better target detection. In this chapter, the focus is on selecting the required spatial frequencies for filtering using a band pass pre-processing filter. The use of a band bass filter prior to the OT-MACH filter is described in this chapter named the Different of Gaussian modified OT-MACH filter (D-MACH). Several real time images have been tested using the D-MACH filter and the results compared with the OT-MACH filter. Further enhancement has been achieved by choosing the appropriate band pass of the DoG filter determined by analysing the set of

training images used in the OT-MACH filter. The chapter concludes with an overall performance plot showing that the D-MACH filter achieves less false detection peaks in the correlation plane.

4.3 Difference of Gaussian (DoG) filter

Band pass filtering, as the name suggests, allows a set of frequencies in the selected band to pass through in the filtering process. It can be used in pattern recognition where the required band of spatial frequencies in the image being filtered is known. In order to help explain the effect of a band pass filter on target images, Figure 4.1(a) and 4.1(b) show an image and its spatial frequency domain representation along with the frequency band region of interest that contains most of the image information required for effective matched filtering.

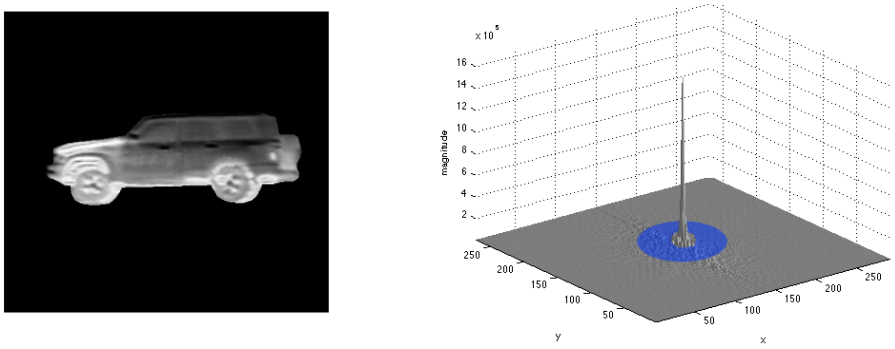

(a) (b)

Figure 4.1 (a) Spatial domain representation of Nissan Patrol (b) Frequency domain magnitude plot of Nissan Patrol spatial frequency spectrum showing bandpass useful in pattern recognition

The Difference of Gaussian (DoG) filter is implemented in the spatial frequency domain of the target as a band pass filter. It can be calculated as a convenient approximation to a scale normalised Laplacian of Gaussian (LoG) filter [106],[48]. The spatial domain numerical approximation of a Laplacian of a Gaussian filter has a high tendency to have a ringing effect that is avoided if the filter is generated with a higher numerical accuracy in the spatial frequency domain. The ringing effect results in the appearance of spurious or ring like edges near the sharp transitions of the OT-MACH filter impulse response. Thus, the frequency domain implementation of the DoG filter is preferred since it avoids these deleterious effects [106].

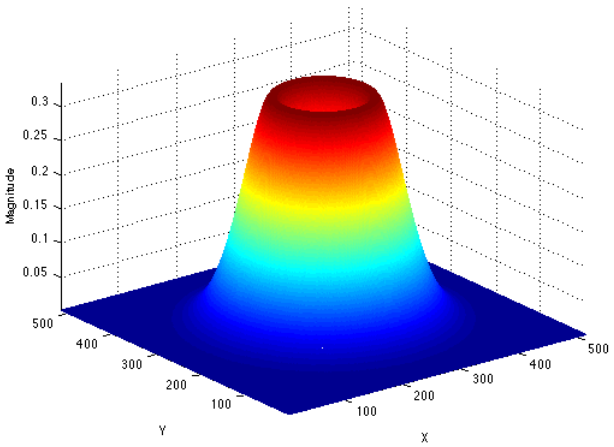

Figure 4.2 Band pass function generated by DoG filter

The DoG function is defined as the difference of two differently scaled Gaussian functions with different standard deviation values. The DoG filter can thus be expressed, in the frequency domain, as:

$$D(u,v) = \frac{1}{2\pi\sigma_2^2}.e^{\left[-\frac{u^2+v^2}{2\pi\sigma_2^2}\right]} - \frac{1}{2\pi\sigma_1^2}.e^{\left[-\frac{u^2+v^2}{2\pi\sigma_1^2}\right]} \qquad \textbf{Eq. 4.1}$$

where the σ_1 and σ_2 represent the different standard deviations of the two Gaussian functions comprising the filter. The ratio between the two sigma values, $\sigma_r = \sigma_2/\sigma_1$, is maintained at 1.6 as this will generate the closest approximationof the DoG filter to a Laplacian of a Gaussian filter and so result in an optimal performance as a band-pass filter [106].

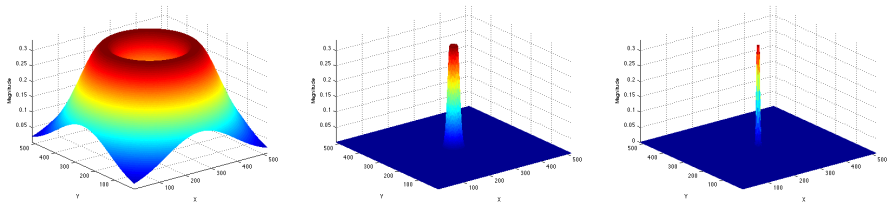

Figure 4.3 DoG based band pass filters for different standard deviation values σ_r (a) σ_r = 0.5 pixels (b) σ_r = 6 pixels and (c) σ_r = 20 pixels

Figure 4.3 shows 2D plots of the DoG filter as applied to the OT-MACH filter, for the values of σ_r indicated i.e. the centre of the array is the zero frequency point and the edges of the array represent the maximal spatial frequencies calculated. The standard deviation value ranges between 0.5 and 20 pixels.

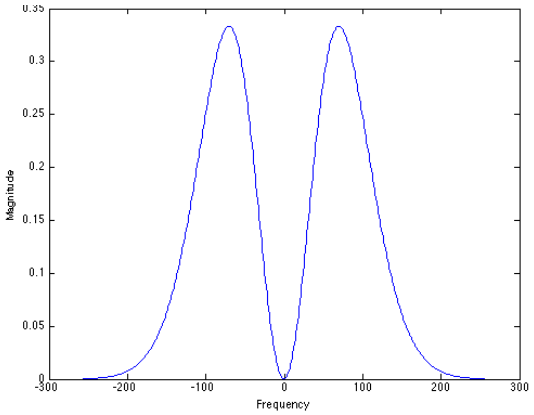

Figure 4.4 DoG filter cross section in the spatial frequency domain

A cross sectional central frequency magnitude plot of the DoG filter is shown in Figure 4.4 with the ratio σ_r being 1.6. It is to be noted that the standard deviation ratio is maintained at 1.6 pixels for optimal performance, as this results in a null zero frequency response [104]. A two stage test has been conducted to evaluate the performance of the OT-MACH filter when modified by a difference of Gaussian (DoG) band pass filter acting as a pre-processing function. Initially, a test benchmark for the OT-MACH filter is established to see the effect of changing the parameters on the filter performance. The DoG filter is then applied to the OT-MACH filter, as illustrated in Figure 4.5 below, and the modified performance evaluated.

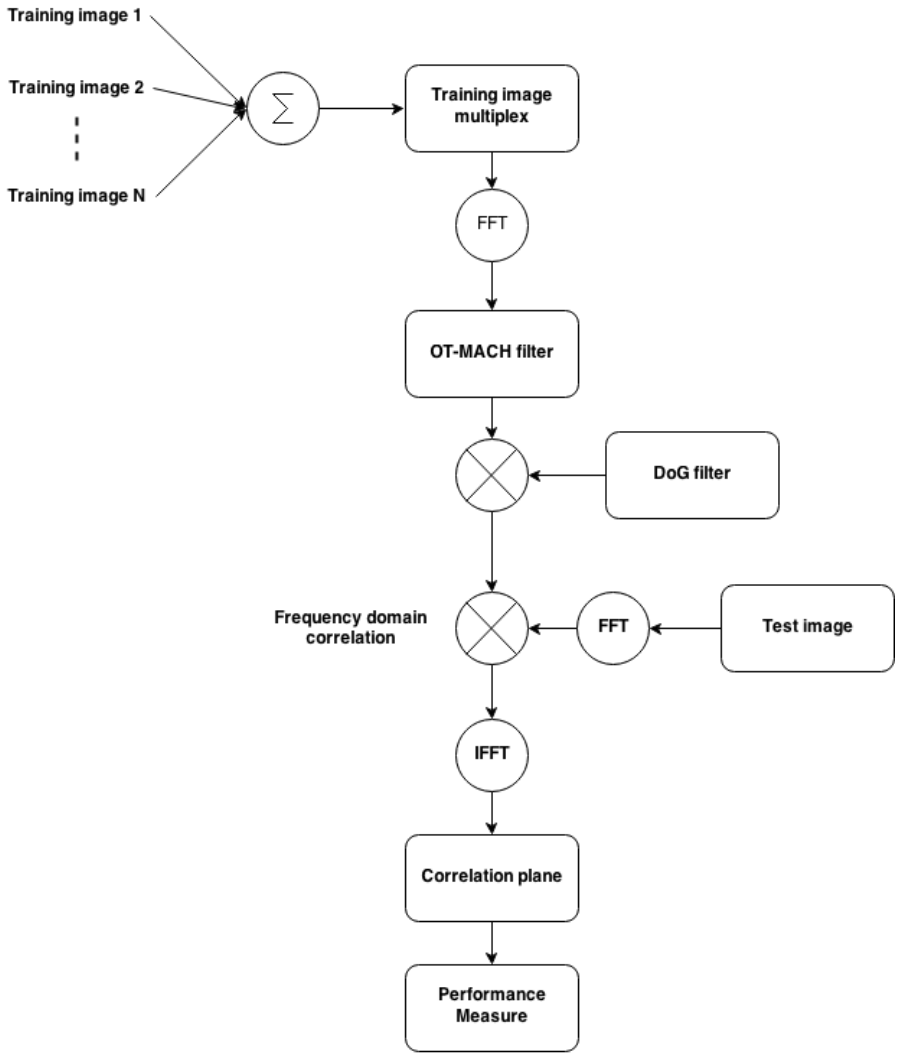

Figure 4.5 Testing process for the D-MACH filter

A double precision addition of several training images is performed to compute a rotationally multiplexed reference image. The reference image obtained after the addition is divided by *N,* the total number of training images to produce a multiplexed reference image which is used in fabricating the OT-MACH filter.

A fast Fourier transform (FFT) is applied to the multiplexed image to obtain a frequency domain representation of the training set. The FFT image is centered by shifting the zero component of the fast Fourier tranform to the center of the spectrum. This is done by swapping the first quadrant with the third quadrant and second quadrant with the fourth quadrant,thus obtaining a shifted FFT training spectrum with which to design the OT-MACH filter.

The OT-MACH filter is designed and computed according the Equation 2.20 to obtain *h*, the OT-MACH filter function. The Difference of Gaussian filter is then applied to the filter function to obtain the bandpass filtered filter function which is then utilised to perform frequency domain multiplication between the test image conjugate spectrum. This is then inverse Fourier transformed to a correlation plane which is then subjected to the set threshold and performance measurement criteria to decide whether the test image contains an in-class or out-of-class target object. The tests conducted involve eight input images from multiple platforms with targets to be detected as shown in Figure 4.6 below.

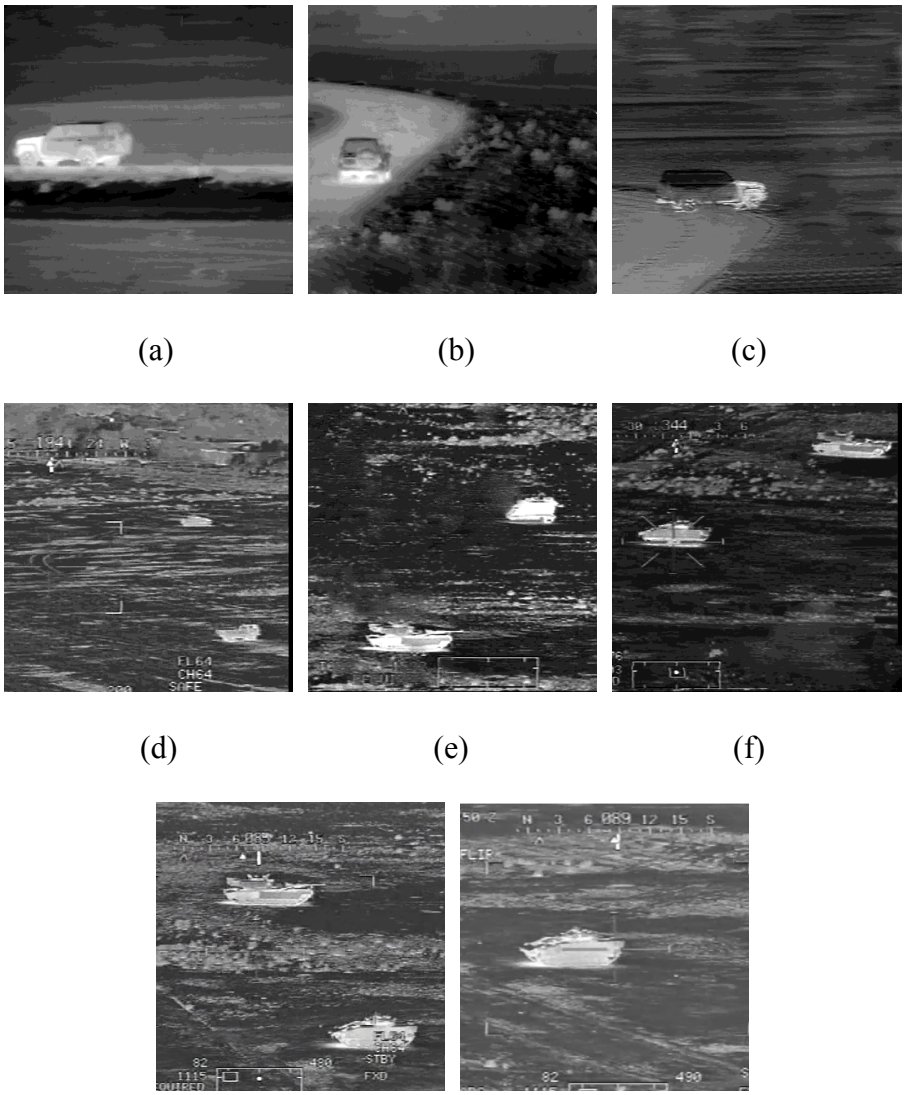

(a) (b) (c)

(d) (e) (f)

(g) (h)

Figure 4.6 Test images used in the D-MACH evaluation (a) Nissan Patrol daytime (b) Nissan Patrol from rear (c) Nissan Patrol night time (d) warrior armour and a truck (e) M1A2 tank and M113 personal carrier (f) and (g) British warrior and M1A2 tank (h) British warrior armour.

4.4 D-MACH filter evaluation

The addition of the difference of Gaussian filter to the OT-MACH filter (which we designate as the D-MACH filter) improves the overall OT-MACH filter performance. Target discrimination ability, overall noise suppression and higher PSR values are produced when the DoG pre-processing filter is employed. The overall correlation plane is improved with less side peaks and so false detection peaks. The evaluations have been carried out with the OT-MACH α parameter set to unity and the noise matrix *C* automatically calculated from the input image as described in Chapter 3 [74]. The β and γ parameters are varied between 0.00001 and 1. A comparison of the frequency domain responses between the OT-MACH filter as shown in Figure 4.7(a) and D-MACH filter as shown in Figure and 4.7(b). The β and γ parameters are kept at unity for this comparison and the DoG filter σ_r ratio is set to 1.6.

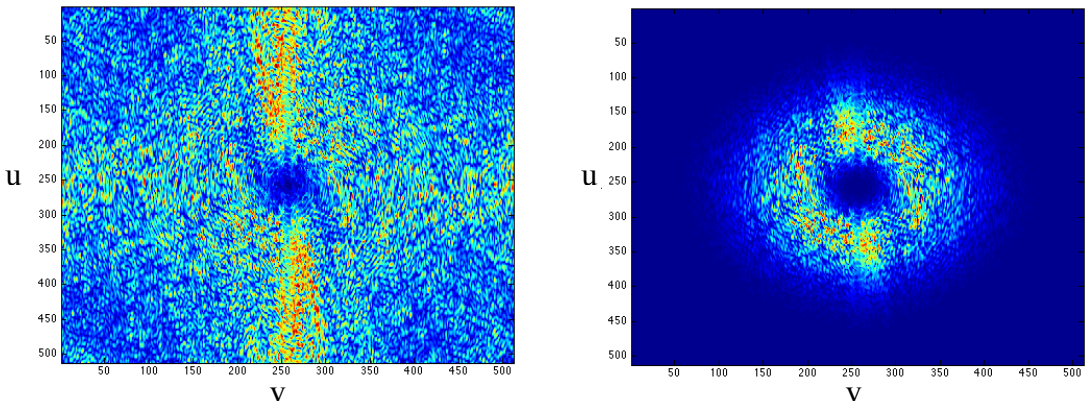

(a) (b)

Figure 4.7 (a) 2D plot of OT-MACH spectral amplitude and (b) 2D plot of D-MACH spectral amplitude

Test image	OT-MACH Beta	OT-MACH Gamma	OT-MACH PSR	OT-MACH TDE	D-MACH Beta	D-MACH Gamma	DoG filter sigma	D-MACH PSR	D-MACH TDE
a	1	0.05	94.35	5.61	0.5	0.025	1	93.01	0
b	1	0.5	73.62	40.3	0.4	0.0025	3	65.78	3.57
c	0.01	0.0025	32.91	94.89	1	0.25	7	25.16	16.83
d	0.1	0.0025	28.55	81.12	1	0.5	9	18.56	1.53
e	0.001	0.025	22.07	98.97	$1x10^{-4}$	0.01	5	26.46	94.9
f	0.001	0.05	36.46	95.91	0.01	0.25	5	42.8	91.82
g	1	0.5	48.13	55.1	1	0.5	3	49.62	36.32
h	0.2	0.9	29.73	75	1	0.05	6	31.65	1.53

Table 4.1 OT-MACH and D-MACH performance comparison

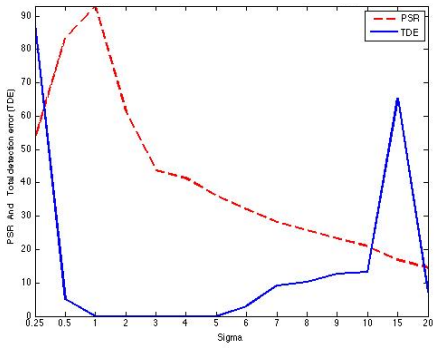

(a)

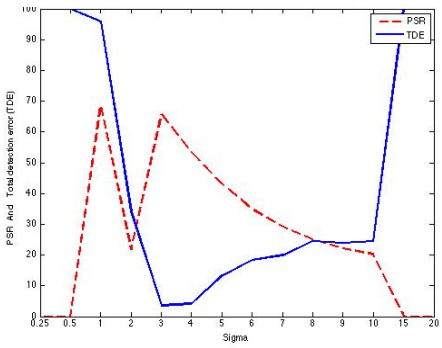

(b)

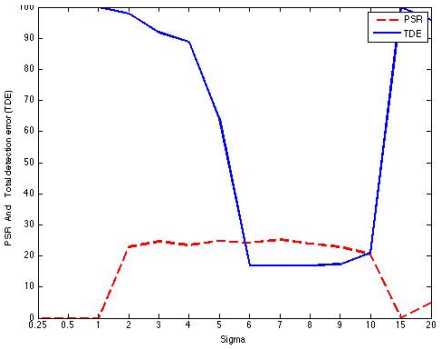

(c)

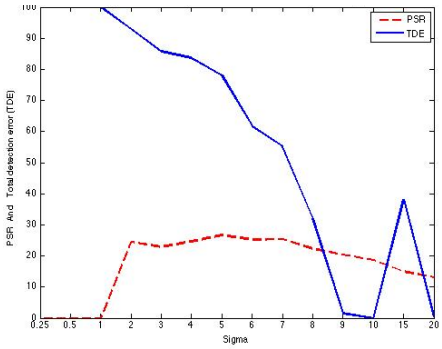

(d)

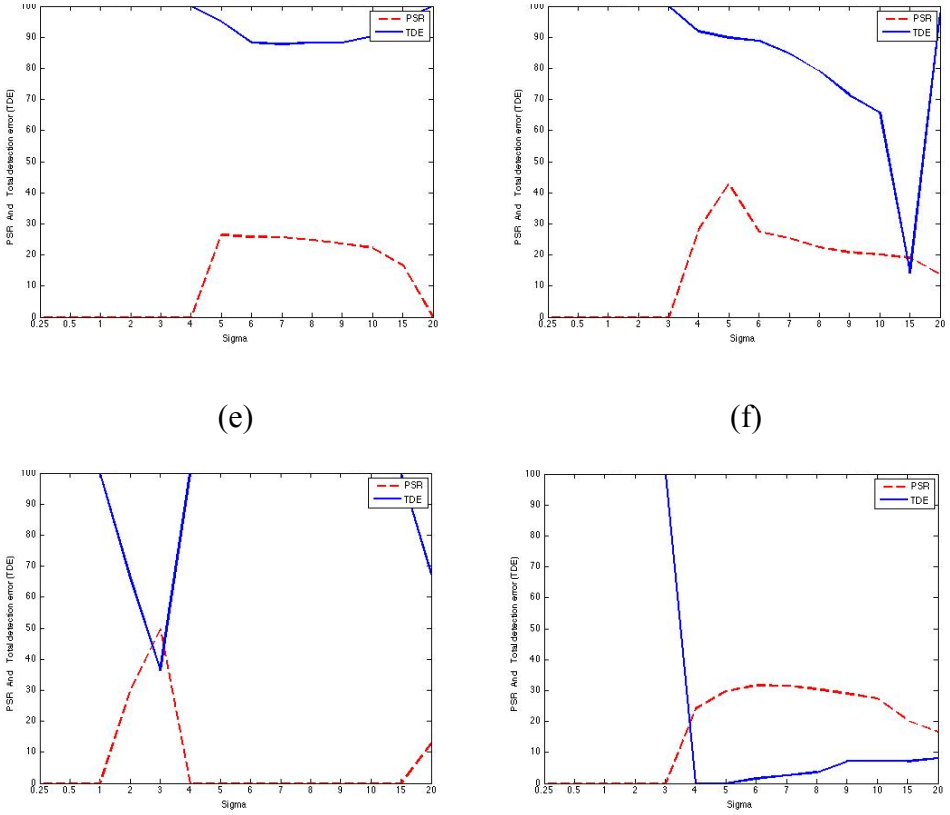

Figure 4.8 D-MACH correlation performance results with varying DoG filter σ_r values as shown in the x-axis (a) Test image 4.6(a) PSR & TDE result, (b) Test image 4.6(b) PSR & TDE result, (c) Test image 4.6(c) PSR & TDE result, (d) Test image 4.6(d) PSR & TDE result, (e) Test image 4.6(e) PSR & TDE result, (f) Test image 4.6(f) PSR & TDE result, (g) Test image 4.6(g) PSR & TDE result and (h) Test image 4.6(h) PSR & TDE result

Figure 4.8 illustrates the overall effect of adding the DoG pre-processing filter to the OT-MACH filter. It shows two measurements: PSR, which indicates the correlation peak quality; and TDE, which reflects the overall correlation plane behaviour in terms of the number of false peaks. The optimal range is clearly in a region where a high PSR and low TDE can be simultaneously obtained.

It can be observed from the comparison Table 4.1 that the D-MACH filter performance is better than the OT-MACH filter with respect to the PSR values obtained and the corresponding TDE values for each test image evaluated. It can be ascertained that the TDE obtained for the D-MACH filter is far better when it comes to finding targets with less false alarms in various test conditions. Particularly, the test image in Figure 4.6(d) shows a TDE result of 1.53% of error for the D-MACH filter whereas the TDE for the same test image when evaluated with the OT-MACH filter was 81.12%. Thus the D-MACH filter shows greater robustness in its response to the different test images.

Test image Figure 4.6	Sigma (σ_{min}) in pixels	Sigma (σ_{max}) in pixels
(a)	2	9
(b)	3	8
(c)	2	10
(d)	8	15
(e)	5	10
(f)	4	10
(g)	2-2	20-20
(h)	4	15

Table 4.2 D-MACH optimal regions

It can be observed from Figure 4.8 that there is an optimal region for each test image where PSR is high and the corresponding TDE is low. This observation for the D-

MACH filter gives a minimum and maximum σ_r value in which the optimal region lies, as shown in Table 4.2. It can be seen that for test images 4.6 (a), (b) and (c) the range of the optimal regions is very similar. The structure of the background clutter is similar in these images, which then leads to the similarity in the extent of the optimal ranges of σ_r. Test result graphed in Figure 4.8(g) shows two very narrow optimal regions. Thus it indicates two limited detection windows within the whole range. This is due to the very cluttered background and object similarity in these images.

4.5 Automatic adjustment of the Difference of Gaussian band pass filter

The Difference of Gaussian filter has been used in conjunction with the OT-MACH filter by other researchers who achieved a noticeable improvement in overall filter performance [77], [99]. In this work, the DoG filter parameters have to be manually set by choosing appropriate values of the standard deviation parameters σ_1 and σ_2 that control the band pass location of the filter. These parameters are application dependent and affect the correlation output result in different ways depending on the complexity of the input image. Having such restrictions on the requirement to select the right value for the band pass of the DoG filter manually rules out the use of such a filter in a real time application where the input image changes rapidly.

4.5.1 DoG Filter parameter automatic adjustment

There is clearly a need for the automation of selection of the DoG filter standard deviation due to the number of parameters that must be correctly set in both the OT-

MACH and DoG filters to obtain useful results [75]. Consideration is now given to the correct setting of these parameters.

The two-dimensional projected views of the 3-D CAD model of a given reference object are combined to form a single multiplexed reference template image to represent the target vehicle at different in-plane rotations. The 2-D discrete Fourier transform of the multiplexed template image will represent the spatial frequencies of the template only without any disruption from additional spatial frequency content arising from noise or clutter which will be present in a typical input training image. The high magnitude of the lower spatial frequency terms contained in the template spectrum are used to determine the correlation response diameter in the frequency domain which is multiplied by two to compute the value of the σ_1 parameter of the DoG filter. The value of the σ_2 parameter of the DoG filter is then computed by multiplying σ_1 by 1.6 in order to obtain the ideal shape of the DoG filter, as discussed previously [106] [100].

Since the spatial frequency spectrum of the input image contains spatial frequency content originating from the background clutter as well as the reference template, the Difference of Gaussian filter band pass location is set according to the high amplitude central spatial frequency of the multiplexed reference image spectrum so as to exclude the higher spatial frequency terms largely generated by the background clutter present in the input scenes. Figure 4.9 shows the multiplexed reference training image in the spatial domain and its corresponding spatial frequency power spectrum.

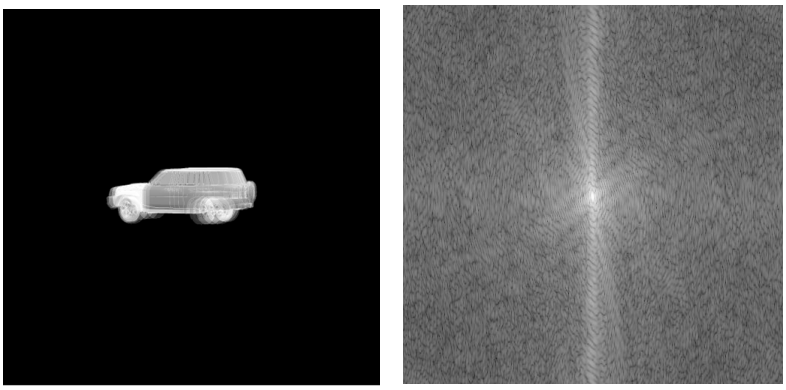

(a) (b)

Figure 4.9 Multiplexed training image shown in: (a) the spatial domain and (b) the spatial frequency power spectrum of the image

The DoG filter parameters σ_1 and σ_2 are set keeping a ratio between them of 1.6 so a correctly formed DoG function is produced using the measured diameter information using the relations shown in Equations 4.2 and 4.3 below:

$$D_{spec} = \sqrt{\frac{4.spec\_area}{\pi}} \qquad \textbf{Eq. 4.2}$$

$$\sigma_1 = 2D_{spec} \qquad \textbf{Eq. 4.3}$$

When applied the to the OT-MACH filter, the DoG pre-processing filter will be limited to a relatively narrow bandwidth the transmitted spatial frequencies, as shown in Figure 4.10 below.

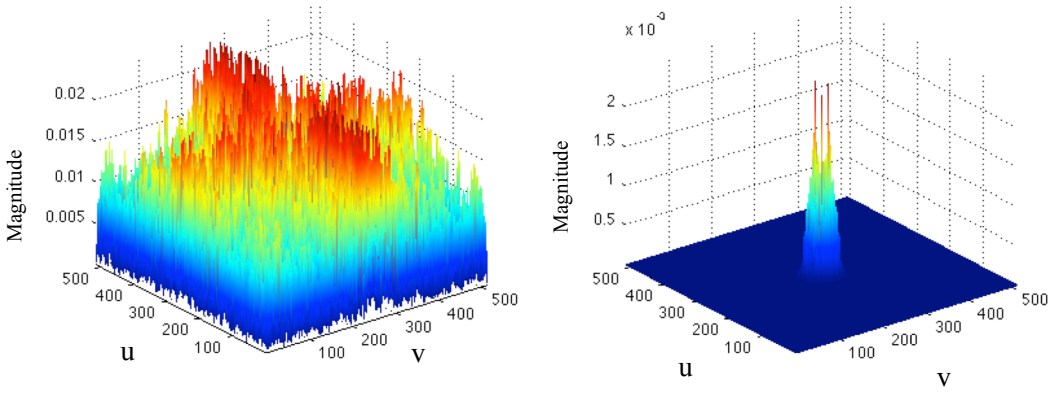

(a) (b)

Figure 4.10 (a) OT-MACH spatial frequency domain magnitude and (b) OT-MACH after applying the DoG pre-processing filter

The DoG filter is applied to an OT-MACH filter with the α, β and γ parameters kept fixed at unity and kept unchanged throughout the whole set of tests conducted to evaluate D-MACH, with the results shown in Figure 4.11. Detection has been achieved with test images in several scenarios, detectable output correlation peaks being produced in each case.

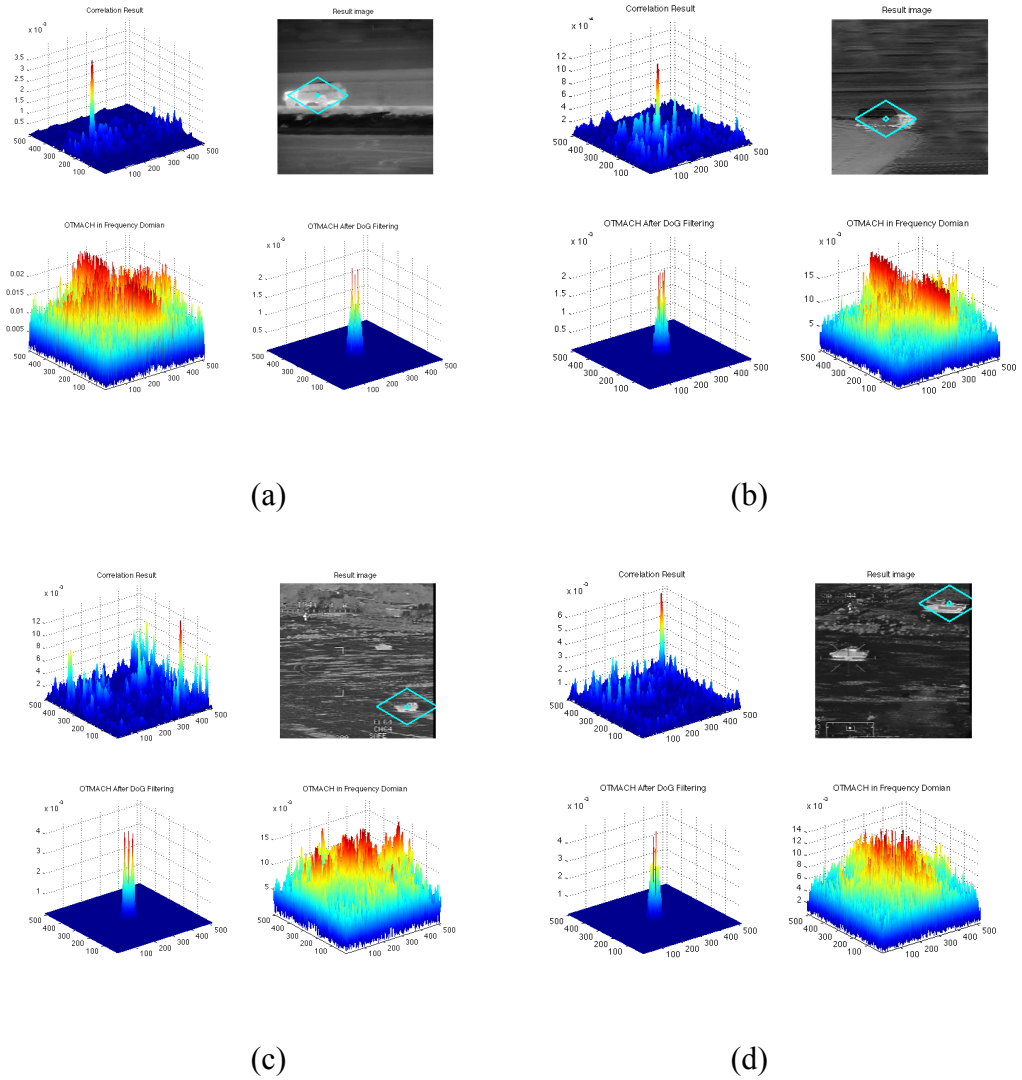

Figure 4.11 Comparison of correlation results using the OT-MACH and D-MACH filters on indicated test images: (a) test image 4.6(a), (b) test image 4.6(c), (c) test image 4.6(d), (d) test image 4.6(f)

Figure 4.11 shows the correlation results for the four input images from the two different platforms employed. Each result shows the OT-MACH and D-MACH magnitude spectra and the correlation results from each filter as mesh plot representations. The result consist of four diagrams, top-right show the input image with the target detection diamond, top-left shows the resultant correlation peak, bottom-right

shows the OT-MACH mesh plot and bottom-left shows the OT-MACH result after DoG filtering.

4.5.2 The effect of the DoG pre-processing filter on the correlation results

Applying the DoG pre-processing filter to the OT-MACH filter improves the correlation results, as can be seen by the results presented in Table 4.1 and Figure 4.11 with β the and γ parameters kept fixed at unity, as discussed in the previous sections. However, the method can also be used to reduce the number of false peaks present in the correlation plane when changes to the OT-MACH β and γ parameter values between 0 and 1 are made. Figure 4.12 shows two surface plots derived from the correlation planes obtained from test image 4.6(c), firstly without a DoG pre-processing filter, and then with the filter applied.

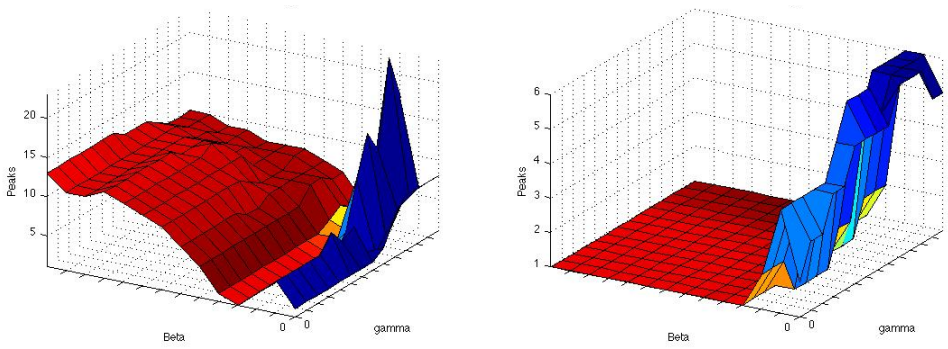

(a) (b)

Figure 4.12 Surface plot, generated from test image 4.6(c) of the number of correlation peaks above half the maximum peak height for varying beta and gamma values between 0 and 1: (a) without the DoG pre-processing filter, (b) with the DoG pre-processing filter

From the surface plots shown in Figure 4.12, it is clear that by applying the DoG pre-processing filter there is a considerable improvement in the single peak detection over

most of the ranges of the β and γ parameter values. Even at the extremes of the graph range, where β is less than 0.3 and γ is greater than 0.7, the number of peaks present in the correlation plane that are more than half that maximum peak height drops significantly from 20 peaks to only 6 by using D-MACH filter. Thus the addition of the DoG pre-processing filter produces a significant improvement in the performance of the OT-MACH filter when applied to difficult detection problems with high background clutter.

4.6 Summary

Chapter 4 introduces the Difference of Gaussian (DoG) band pass filter in combination with the OT-MACH filter. The DoG filter acts as a pre-processor to the OT-MACH filter prior the correlation with the test input image. Initially, as described in Chapter 3, the OT-MACH filter was evaluated by changing the α, β and γ parameters in the transfer function of the filter. With all these parameters set to unity, the OT-MACH filter does not produce a useable result when used with images containing high cluttered backgrounds since the β and γ OT-MACH filter parameters are incorrectly set to reject such clutter. Tests were presented in Chapter 3 to find the optimal values of the OT-MACH parameters by the changing the β and γ parameters whilst keeping the α value set to unity and using an adaptive input image noise model [74].

In this chapter, the Difference of Gaussian (DoG) filter has been added to the OT-MACH filter as pre-processing filter and the resulting performance enhancements evaluated. The results have been quantified by two measurements, notably the PSR and TDE values obtained from the correlation planes generated by the filters.

The D-MACH filter has multiple parameters that need to be adjusted i.e. the β and γ parameters of the OT-MACH filter and also the DoG pre-processing filter standard deviation setting to control its band pass location. Automation of the setting of the DoG pre-processing filter standard deviation has been proposed in this chapter and the resulting encouraging performance improvement of the D-MACH filter over the unmodified OT-MACH filter has been discussed, particularly when dealing with difficult images containing a high clutter background. The correlation peaks generated are sharper and a more stable overall correlation plan is produced with fewer false peaks.

Chapter 5 proposes and then assesses an alternative improvement method to the OT-MACH filter, which uses a Rayleigh distribution filter as a pre-processing filter in place of the DoG filter. Both pre-processing filters are evaluated and compared with the aim of producing a better correlation result than when using the OT-MACH filter alone.

Chapter 5

OT-MACH performance improvement with Rayleigh distribution pre-processing filter

Chapter 5 OT-MACH performance improvement with Rayleigh distribution pre-processing filter

5.1 Chapter Organisation

The chapter begins with an introduction to the Rayleigh distribution based band pass filter and presents a motivation to use the filter with an OT-MACH filter for detection and identification purposes. Section 5.3 introduces the test data set used for the Rayleigh distribution pre-processed OT-MACH filter (named the R-MACH filter) evaluation. Section 5.4 discusses the Rayleigh distribution filter in detail along with a description of the filter transfer function. A comparison study between the Difference of Gaussian and Rayleigh distribution band pass filter based OT-MACH filters have been conducted in detail in section 5.5. Section 5.6 addresses a novel method of utilising the R-MACH filter for human detection in FLIR camera sequences. A two stage approach for identification of targets using the R-MACH filter is introduced in section 5.7 followed by section 5.8 which details the need for identification in security and surveillance situations in real-world applications. Section 5.9 presents the two stage approach of identification in detail along with an explanation of each stage involved. Finally, the two stage R-MACH identification results involving various targets is presented and analysed to validate the proposed identification process. The chapter concludes with a summary and conclusions in section 5.11.

5.2 Introduction

A Rayleigh distribution filter assisted Optimal Trade-off Maximum Average Correlation Height (OT-MACH) filter for target recognition in FLIR imagery is proposed in this chapter. The Rayleigh distribution filter is applied to the OT-MACH filter in order to eliminate high frequency noise and to enhance the performance of the filter for recognising targets in highly cluttered scenes. The performance enhancement obtained by using the Rayleigh distribution filter with the OT-MACH filter, which we name the R-MACH filer, is evaluated and compared with the D-MACH filter described in the previous chapter i.e. the OT-MACH filter employing the Difference of Gaussian (DoG) band pass filter. In this chapter, the Rayleigh distribution filter is compared to Difference of Gaussian filter and shown to make further improvement to the OT-MACH filter performance. The effect of the standard deviation setting on both the Rayleigh distribution filter and the Difference of Gaussian filter applied to the OT-MACH filter is also presented and assessed with several examples in order to determine the enhancements given by the Rayleigh filter in comparison to the DoG filter for robust target recognition.

5.3 FLIR test data set for R-MACH evaluation

FLIR videos have been acquired in both day and night conditions to simulate the effect of solar heating on the target vehicles. Five target vehicles have been tested with the correlation filters being assessed, as listed below:

a. M1A2 Abrams tank
b. British Warrior armoured vehicle
c. M113 armoured personnel carrier
d. Military truck
e. Nissan patrol vehicle

Screenshots of the acquired videos are shown in Figures 5.1 and 5.2, from which the nature of the background clutter is clear. The aim of the proposed technique is to discriminate a pre-defined target object from the highly cluttered background, which includes the information overlay as shown in the FLIR images in Figure 5.2 and also other test images without and screen overlays as shown in Figure 5.1.

(a) Target 1 (b) Target 2 (c) Target 3

Figure 5.1 Example FLIR images of Nissan patrol vehicle showing different heat signatures and orientations (a) Nissan patrol in day time (b) and (c) Nissan patrol at night time

The first set of FLIR images, shown in figure 5.1, contains a Nissan patrol vehicle. The images have been acquired by a FLIR Ranger HRC imager with a 640x480 focal plane array operating in a wavelength range 3-5 μm, which is used for border security in

Northern Kuwait. The IR video sequences from this sensor have been recorded at various times of the day and night, which affects the car heat signature, as illustrated by the example frames shown in Figure 5.1.

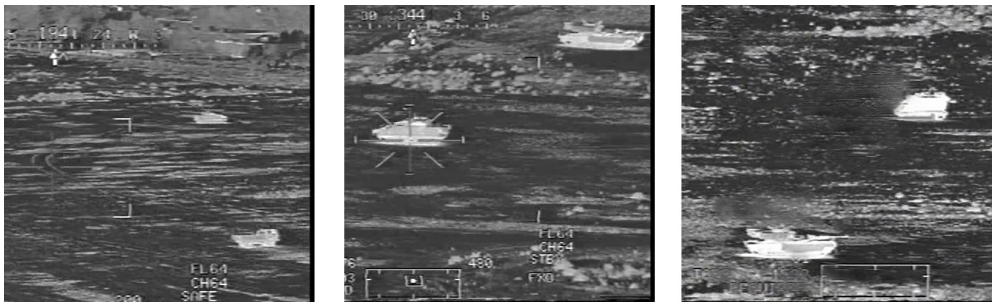

(a) Target 4 (b) Target 5 (c) Target 6

Figure 5.2 Example FLIR images of multiple targets acquired by the Apache helicopter FLIR sensor (a) British warrior armour and military truck (b) M1A2 tank and British warrior and (c) M1A2 tank and M113 personal carrier

5.4 Rayleigh distribution filter

A correlation filter design has to make a compromise between tolerance to intra-class distortions of the target object, such as changes in orientation angle, and resistance to similar non-target objects and clutter in the input scene. The OT-MACH filter allows this compromise to be made by appropriate adjustment of the α, β and γ parameters to set relative weighting between the three terms in the filter transfer function. In Chapter 3, only the OT-MACH β and γ parameters needed to be set to achieve the desired filter behaviour as the noise matrix was adaptively calculated from the current input image which allowed the α parameter to be kept fixed a unity [74].

The filter then will be band pass in nature; however, the work presented in Chapter 4 has shown that by explicitly forcing a band pass structure on the filter to ensure, in particular, that the high amplitude low frequency spectral components are fully suppressed, can enhance further the performance of the OT-MACH filter. To accomplish this, a difference of Gaussian (DoG) pre-processing filter has been introduced, as described in Chapter 4.

In this chapter an alternative band pass filter constructed using a Rayleigh filter function is introduced and its performance compared with the DoG filter. The Rayleigh filter is described by the Rayleigh probability density function:

$$f(r,\sigma) = \frac{r}{\sigma^2} e^{\frac{-r^2}{2\sigma^2}}, \quad r \geq 0 \qquad \textbf{Eq. 5.1}$$

where a radial co-ordinate, *r*, is used to produce an isotropic, circularly symmetric 2-D distribution and σ is the standard deviation parameter that controls the filter width. The Rayleigh filter is applied to the OT-MACH filter transfer function as a pre-processing filter in place of a DoG filter.

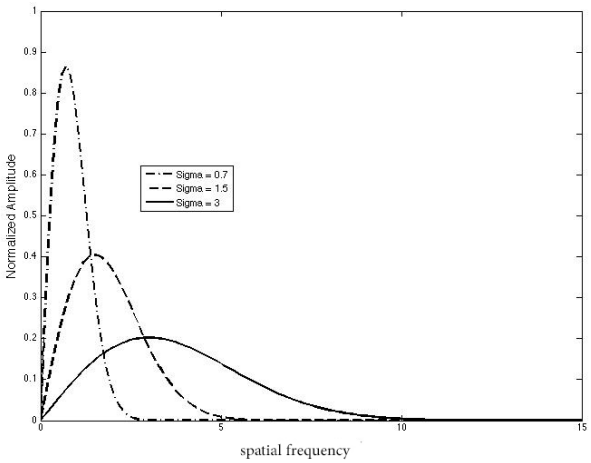

Figure 5.3 Rayleigh probability density function plot at σ values of 0.7, 1.5 and 3

In pixels showing the sharp cut-off at low spatial frequencies

As illustrated in Figure 5.3, the Rayleigh distribution has the characteristic of a sharp fall-off at the centre of the (circularly symmetric) distribution which when applied in the frequency domain will remove the zero and low spatial frequency content of the filter transfer function. The filter falls smoothly towards higher spatial frequencies and so acts as a band pass pre-processing filter to the OT-MACH filter.

Justification for using the Rayleigh probability density function is that it describes the distribution of the magnitude of a complex number when the real and imaginary components are uncorrelated and normally distributed with equal variance. Since the complex Fourier spectral components of a natural image may be expected, at least approximately, to possess these statistics it seems reasonable to employ the Rayleigh distribution in the Fourier domain to ensure the band pass nature of the pattern recognition filter.

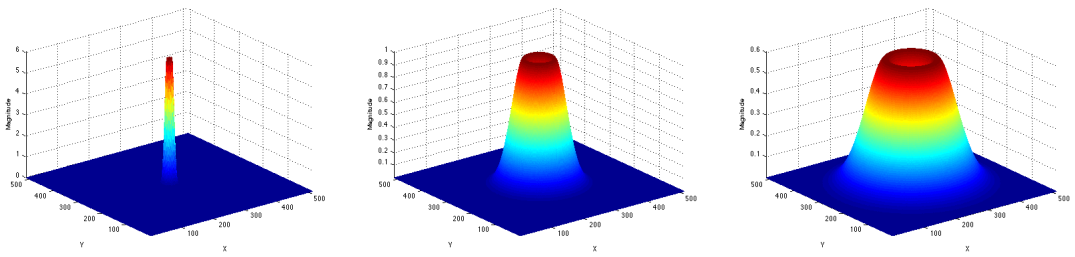

(a) $\sigma = 0.1$ (b) $\sigma = 0.6$ (c) $\sigma = 1$

Figure 5.4 Rayleigh filter function mesh plots with different values of the standard deviation, σ (a) σ = 0.1 , σ = 0.6 and (c) σ = 1

It can be seen from Figure 5.4, increasing the standard deviation value of the Rayleigh filter increases its band pass. In this Chapter, the effect of using the Rayleigh filter with different σ values ranging between 0 and 1 is examined. It is evident that a minor

change to the standard deviation value generates a large effect on the output. The Rayleigh filter is very sensitive to changes of σ, but the fact that only a single parameter requires alteration minimises the computation needed to obtain an optimum band pass for the filter.

5.5 Test results and comparisons between filter responses

In this section a comparison of the results achieved by pre-processing the OT-MACH filter with the Rayleigh filter and the DoG filter is made. A sample result for the Nissan Patrol target vehicle is shown in Figure 5.5, where the OT-MACH transfer function, correlation plane and the correlated target image with a detection dot to verify the target location, are also shown. The tests have been carried out with different standard deviation ranges for both the Rayleigh and DoG filters. Table 5.1 below shows the standard deviation values employed.

Rayleigh filter σ	0.07	0.08	0.09	0.1	0.2	0.3	0.4	0.5	0.6	0.7	0.8	0.9	1
DoG filter σ	0.5	1	2	3	4	5	6	7	8	9	10	15	20

Table 5.1 The standard deviation range for both Rayleigh and DoG filters

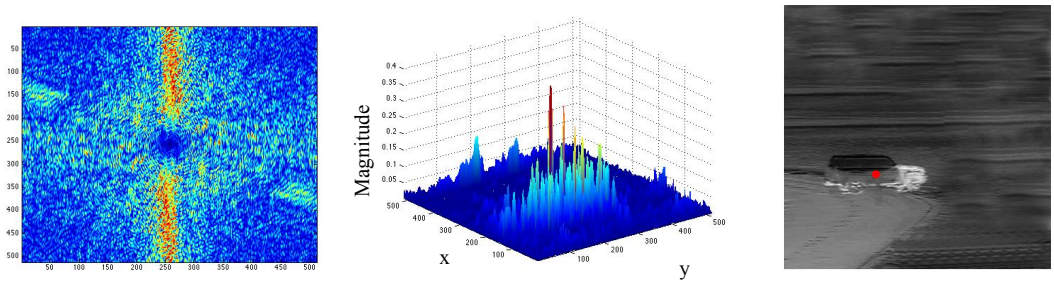

(a) (b) (c)

Figure 5.5 Target 3 sample result, (a) OT-MACH filter transfer function power spectrum, (b) correlation plane, (c) target detection

Figure 5.5(a) shows the OT-MACH filter power spectrum. It can be observed that it contains some high spatial frequency components, which have not been sufficiently attenuated by the transfer function. This makes the filter less tolerant to the clutter background present in the FLIR test images. Figure 5.5(b) displays the mesh plot of the correlation plane obtained for the target object shown in Figure 5.5(c).

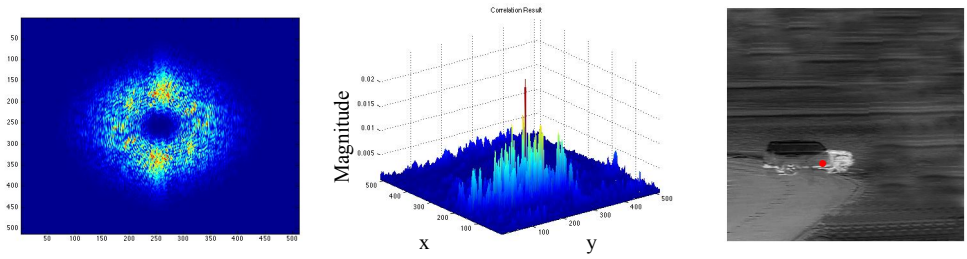

(a)

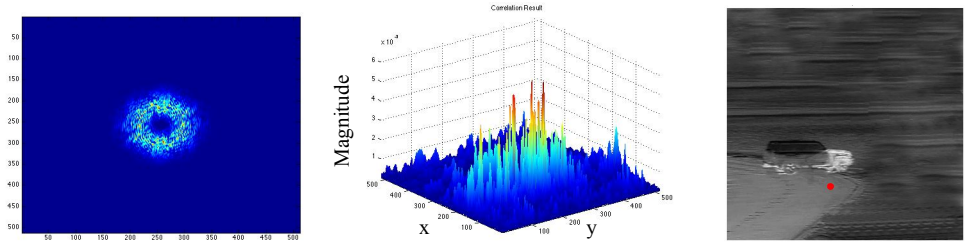

(b)

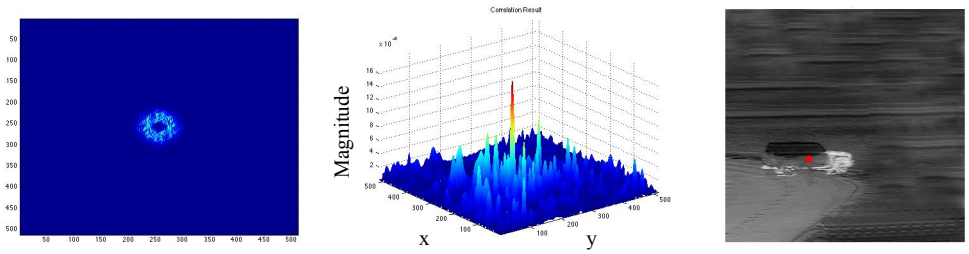

(c)

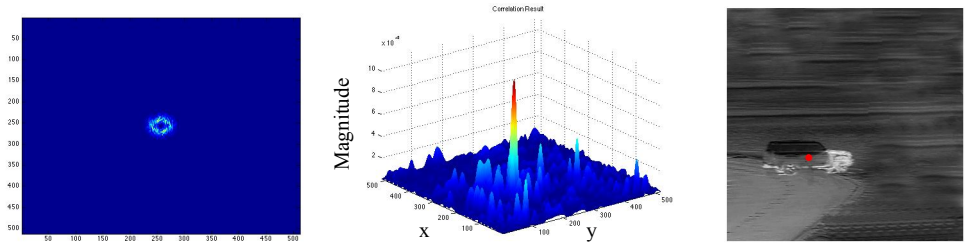

(d)

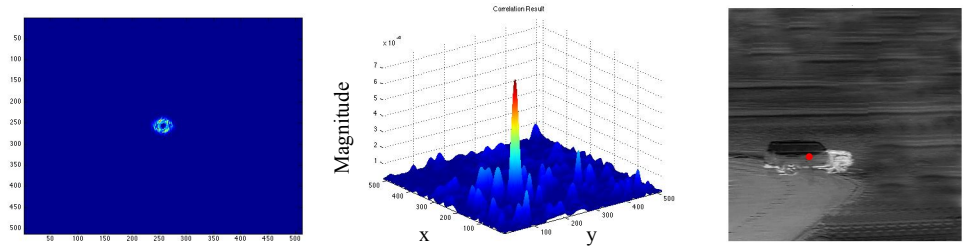

(e)

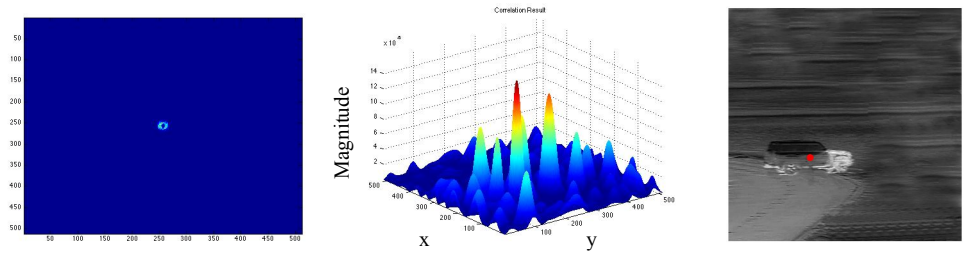

(f)

Figure 5.6 DoG filtered OT-MACH transfer functions, correlation plane plots and the target detected for the range of standard deviation values indicated for Target 3 using the following σ_r values: (a) $\sigma_r = 1$ (b) $\sigma_r = 2$ (c) $\sigma_r = 4$ (d) $\sigma_r = 6$ (e) $\sigma_r = 8$ (f) $\sigma_r = 10$

It can be seen from the results shown in Figure 5.6, that the standard deviation value change required to obtain an effective band pass for robust target detection in the case of D-MACH is very large. Figure 5.6 (a) using σ_r = 1 shows a poor performance due to the presence of many side lobes or false detection peaks, thus making it difficult to obtain a sustained detection when the target is moving in a video sequence. At the higher value of σ_r = 4, the detection peaks observed in the correlation plane exhibit much less side lobe structure. When the σ_r value increases the detection peak gradually gets better as seen in Figure 5.6 (d) and 5.6(e), until it reaches a point where σ_r = 10 as shown in Figure 5.6 (f) where the peak loses its sharpness and also the side lobe false detection increases due to the smaller band pass of the DoG filter which rejects most of the needed frequencies to match the target. This makes the application of appropriate standard deviation selection for the DoG filter difficult for accurate target detection from highly cluttered scenes.

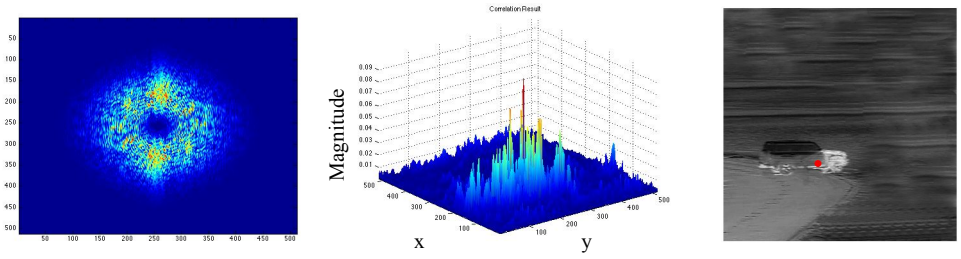

(a)

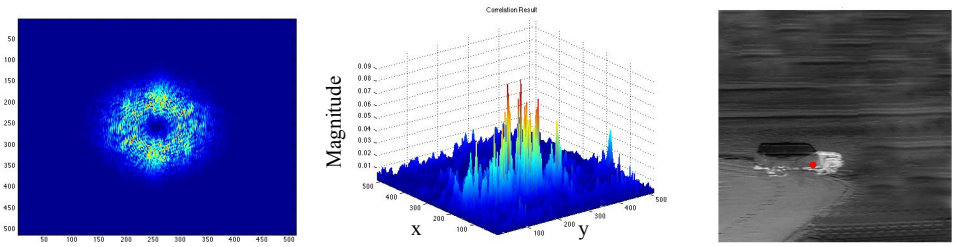

(b)

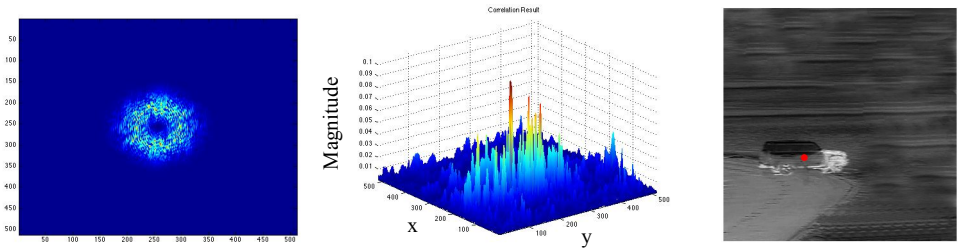

(c)

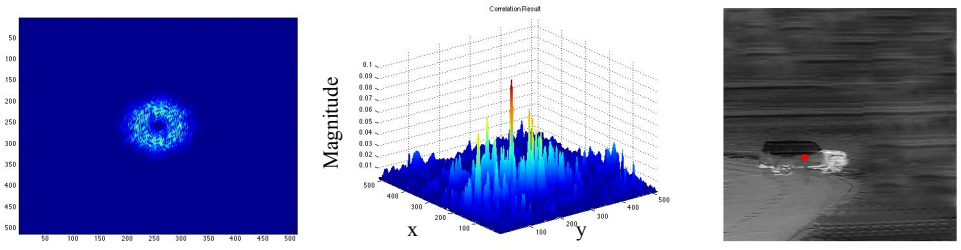

(d)

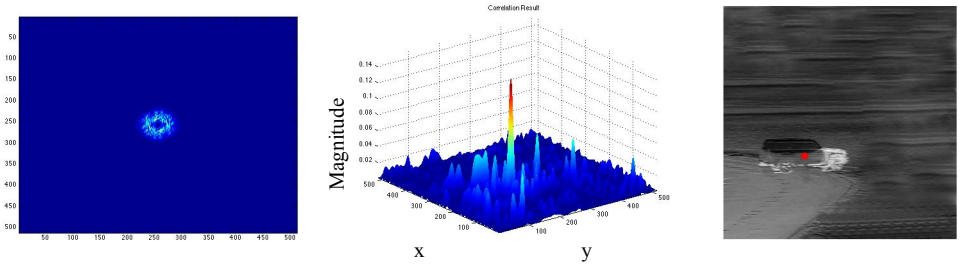

(e)

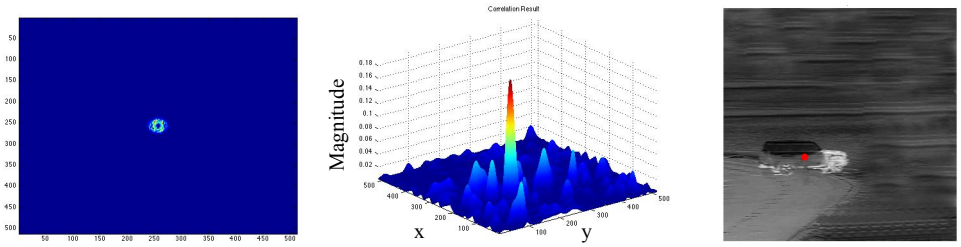

(f)

Figure 5.7 R-MACH filter transfer functions, correlation plane plots and the targets detected for the range of standard deviation for Target 3 using the following σ values: (a) σ = 0.09 (b) σ = 0.2 (c) σ = 0.4 (d) σ = 0.6 (e) σ = 0.8 (f) σ = 1

It can be seen from Figure 5.7 that the standard deviation value change required to obtain an optimal band pass filter for robust target detection in the case of the R-MACH

filter is less sensitive and ranges between 0 and 1. This makes the application of the standard deviation appropriate selection for the Rayleigh filter easier for accurate target detection in cluttered FLIR scenes.

It can be observed in Figure 5.7(a), where σ = 0.09, that the band pass of the Rayleigh filter is broader thus allowing a wide frequency response but still allows matching of the target. However, the correlation plane contains many side lobes which could confuse the target detection. In Figure 5.7 (c), where σ = 0.4, it can be observed that the band pass obtained for the Rayleigh filter is much more limited and this results in a correlation plane with a clearly detectable peak for the target and the side lobes which could result in false detection are suppressed. As the σ goes higher and approaches unity it can be observed that the side lobes suppression improves still further and a sharper peak is obtained at the target location in the correlation plane as shown in Figure 5.7 (d) and 5.7(e). When the σ value for the Rayleigh filter is equal to 1, as shown in Figure 5.7 (f), it can be observed that the detection peak becomes broader but the side lobes remain suppressed, thus validating the assertion that the R-MACH filter σ value is tolerant in tuneability for accurate detections. This in turn makes the σ value selection easier when compared to correct selection of σ_r for the DoG filter based OT-MACH (D-MACH) filter.

The tests have been carried out on different target images with the addition of the Rayleigh filter and the DoG filter. The standard deviation of the pre-processing filters has been altered and the performance enhancement to the OT-MACH filter assessed as a result. The detection criterion used for a true positive is that only a single correlation peak is produced by the filter with no other peaks in the correlation plane exceeding half

of the maximum detection peak. If the correlation plane has one or more peaks exceeding half the maximum peak height, it will be regarded as a false positive detection.

Detection window Range				
Target	RAY		DoG	
	σ_{min}	σ_{max}	σ_{min}	σ_{max}
1	0.07	1	0.5	20
2	0.07	1	0.5	20
3	0.07	1	6	15
4	0.07	0.3	4	20
5	0.07	0.2	6	20
6	0.2	1	1	7

Table 5.2 True positive detection range when changing the standard deviation values for the Rayleigh and DoG pre-processing filters.

It can be seen from Table 5.2, a wider range of standard deviation values is required by the DoG pre-filtered OT-MACH to achieve a successful performance level for target detection compared to the Rayleigh filter. These results indicate that the Rayleigh filter may be preferable to the DoG filter as a pre-processor to the OT-MACH in order to improve its detection capability.

The performance measures PSR and PCE are plotted in Figure 5.8 versus standard deviation for both the Rayleigh and DoG pre-processed OT-MACH filter for the three target images shown in Figure 5.1.

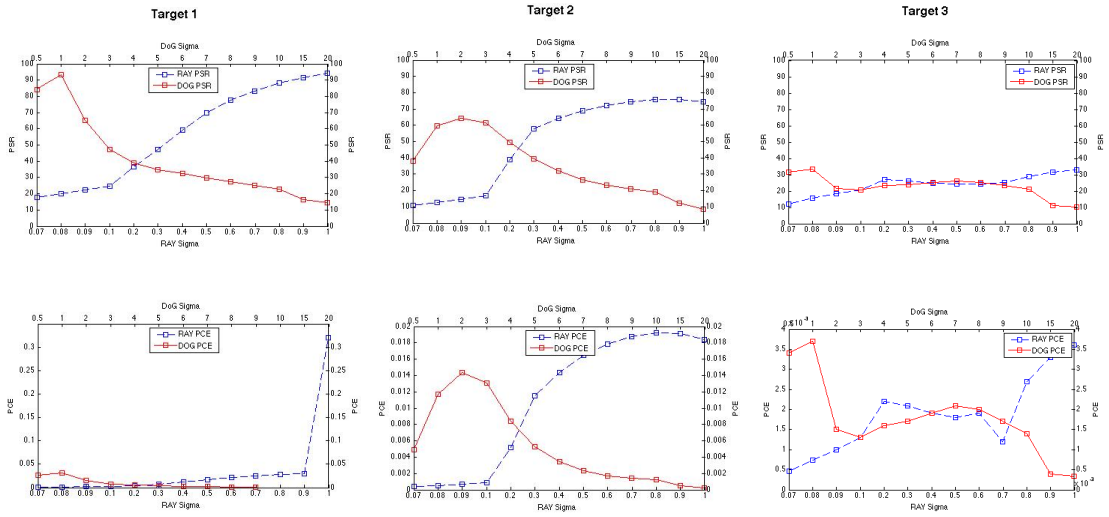

(a) (b) (c)

Figure 5.8 Correlation performance measure plots containing ideal detection regions for the R-MACH and DoG pre-filtered OT-MACH filters for: (a) Target 1 (b) Target 2 and (c) Target 3

In Figure 5.8,the red line in the graphs indicates the DoG filtered OT-MACH PSR or PCE values and the blue dotted line indicates the R-MACH filter PSR or PCE values for different standard deviation settings of the pre-processing filters. The plots show four axes: the top *x*-axis depicts the DoG filter standard deviation variation; the bottom *x*-axis depicts the Rayleigh filter standard deviation variation; the left *y*-axis shows the performance measure of the Rayleigh filter and the right *y*-axis shows the performance measure of the DoG filter. The ideal detection region for each target is highlighted based on high PSR and high PCE correlation performance measures as tabulated in the Table 5.3 below.

Ideal performance measures in the detection region						
Filter	RAY			DoG		
Target	1	2	3	1	2	3
σ	1	0.9	1	1	0.09	0.5
PSR	94.05	75.62	33.09	93.11	64.47	26.09
PCE	0.321	0.0191	0.0036	0.0314	0.0144	0.0018

Table 5.3 For Target 1, 2 and 3 in Figure 5.1, ideal performance measures in the detection region

Table 5.3 indicates that the overall composite filter performance is better when using the Rayleigh filter rather than the DoG filter as the OT-MACH pre-processing filter for Targets 1, 2 and 3 (shown in Figure 5.1) with higher PSR and PCE values being produced by the Rayleigh pre-processing filter.

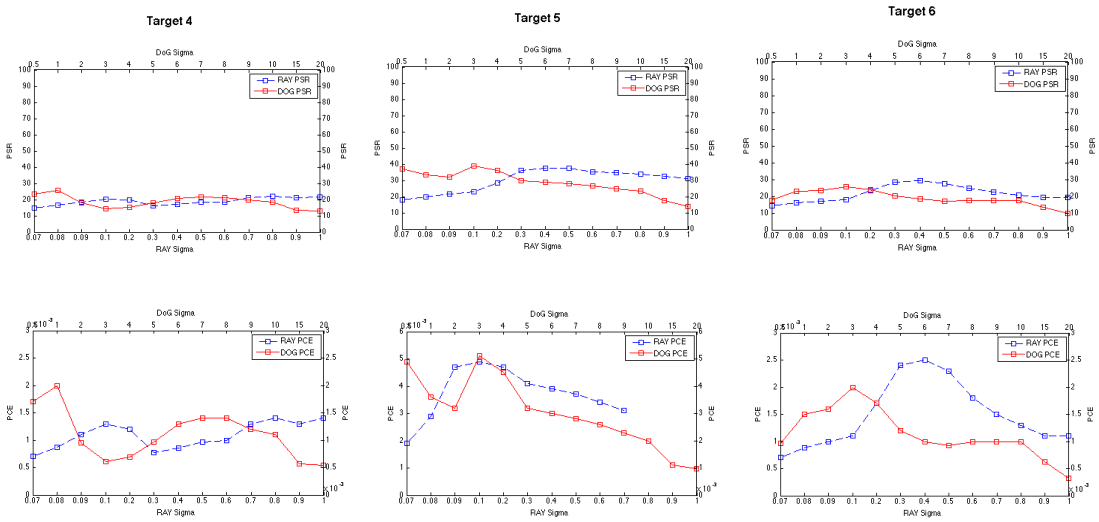

(a) (b) (c)

Figure 5.9 Correlation performance measure plots showing the ideal detection regions for the R-MACH and DoG pre-filtered OT-MACH filters for: (a) Target 4 (b) Target 5 and (c) Target 6

Ideal performance measures in the detection region						
Filter	RAY			DoG		
Target	4	5	6	4	5	6
σ	0.1	0.2	0.4	7	6	0.1
PSR	21.42	23.43	37.58	20.075	18.19	38.68
PCE	0.0014	0.0017	0.0039	0.0013	0.001	0.0051

Table 5.4 Target 4, 5 and 6 ideal performance measures in the detection region for each filter.

Table 5.4 shows that the performance measures are also improved when using the Rayleigh pre-processing filter as compared to the DoG pre-processing filter with higher PSR and higher PCE being obtained for targets 4 and 5. However, for Target 6 (shown in Figure 5.2) the PSR and PCE values obtained using the DoG pre-processing filter are better.

It can be seen from Tables 4 and 5 that the R-MACH filter performance is sufficient for robust target detection for most of the images tested in contrast to that obtained using the DoG pre-filtered OT-MACH filter. It is evident from the FLIR dataset on which the tests were conducted that the optimal Rayleigh standard deviation parameter value may be selected based on the combination of higher PSR and PCE values.

5.6 Human detection using the R-MACH filter

The importance of Human detection in computer vision has lead researchers to focus on the topic for many years due to the threat caused by human intervention in secure environments [6], [95], [107]–[111]. An improvement to the Optimal Trade-off Maximum Average Correlation Height (OT-MACH) filter with the addition of a Rayleigh distribution filter has been used to detect humans in FLIR imagery scenes. The Rayleigh distribution filter is applied to the OT-MACH filter to provide a sharper low frequency cut-off which improves the OT-MACH filter performance in terms of target discrimination. The OT-MACH filter has been trained using a Computer Aided Design (CAD) model of the target object and tested on the corresponding real target object in high clutter environments acquired from a FLIR sensor. Evaluation of the performance of the Rayleigh modified OT-MACH filter is reported in this section for the recognition of humans present within a FLIR image data set.

5.6.1 Human FLIR imagery

Some examples of the data used to test the OT-MACH filter's ability to discriminate and detect a pre-defined human from a cluttered background scene are shown in Figure 5.10 below.

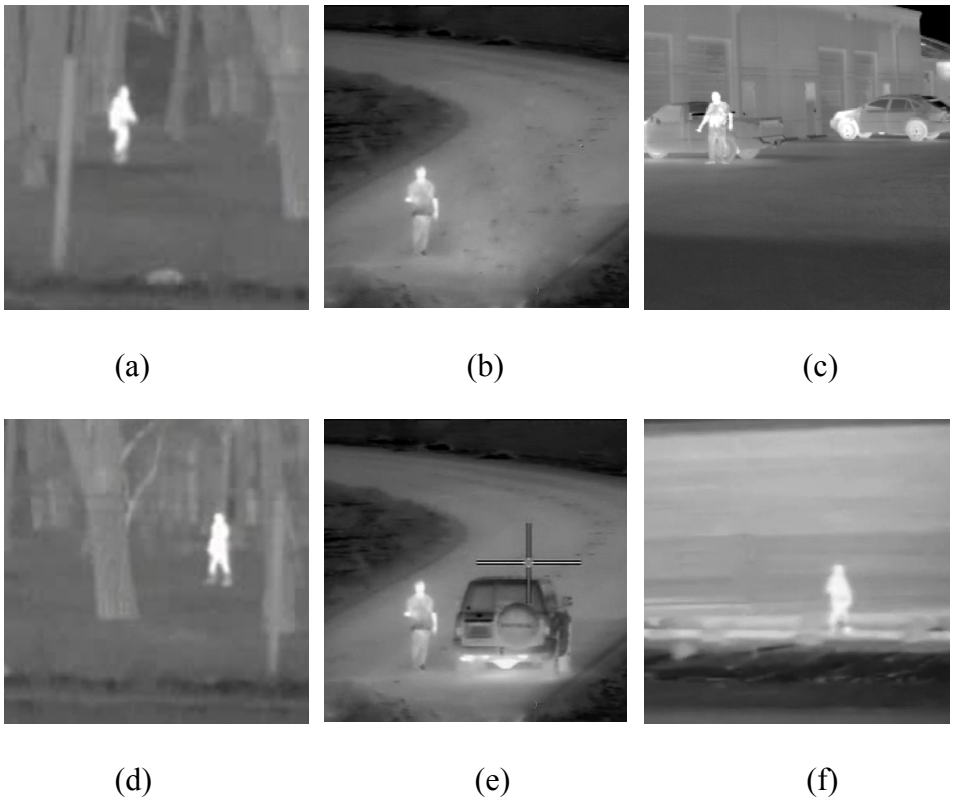

(a) (b) (c)

(d) (e) (f)

Figure 5.10 FLIR imagery from multiple sensors showing human activity: (a) walking man in a wood (b) walking man on a road(c) a man together with two cars (d) a man in a wood (e) a man with a single car (f) walking man in the desert

The filter has been tested with real data sets from different platforms and application scenarios. The Nissan patrol data was acquired by the Ranger HRC FLIR imager with a 640x480 focal plane array operating between 3-5 μm wavelengths and is used for border security in Northern Kuwait. The test images in Figure 5.10 show grayscale level indicating the temperature of the object with white the hottest and black the coolest.

The OT-MACH filter was trained with two-dimensional views derived from rendered CAD models of a human. Several out-of-plane rotations (0° to 360°) of the selected humans have been used. Figure 5.11 shows a few examples of the training set images.

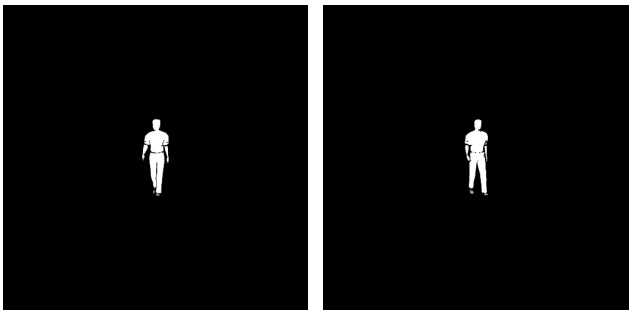

Figure 5.11 Example training images - 3D CAD models of human

The advantage of using FLIR images over visible band images is the ability to discriminate the humans from the background due to their thermal difference. The use of two-dimensional projected views (derived from CAD models) as the training images enables the OT-MACH filter to efficiently detect humans in the scenes and is due to the presence of enhanced and complete edges in the training set as compared to the actual target data set. The rendering of the CAD models to match the FLIR signature of the target allows them to be more effectively correlated against the FLIR data. The ultimate solution will be the capability to design and render 3D models of any target description, which can then be used in any desired detection scenario.

5.6.2 Results demonstrating Human detection in varying clutter backgrounds

Detecting humans in cluttered backgrounds is a demanding task, especially when using FLIR imagery in which the heat signature of the object is the main means of detection. The Rayleigh distribution modified OT-MACH filter has been used for human detection in this research. Combining the two filters has the advantage of improving the OT-MACH filter performance, as previously demonstrated for vehicle recognition.

Tests have been conducted on the test FLIR images both with, and without, the use of the Rayleigh distribution filter. Much work has been conducted to optimise the OT-MACH parameters α, β and γ in order to improve the filter discrimination ability [36],[38]. For the current application the OT-MACH parameters β and γ have been fixed to a value of 0.001 and the α parameter is set automatically using the statistical information of the input target image, as previously described [58]. The β and γ parameter values settings have been found in the testing performed to be near optimal for all the test images. Although it is possible to get better discrimination ability by adjusting the parameters between tests, for this comparison both filters are fixed with the same parameter values to unify the benchmark setting for both filters. Initially, the FLIR images were tested without the addition of the Rayleigh distribution filter and then the same tests were conducted with the use of the Rayleigh distribution filter as a pre-processing stage to the OT-MACH filter to yield the results presented below.

5.6.3 Human detection test result

Multiple tests were conducted on the sample images, with example correlation plots and PSR results shown in the figures and tables below.

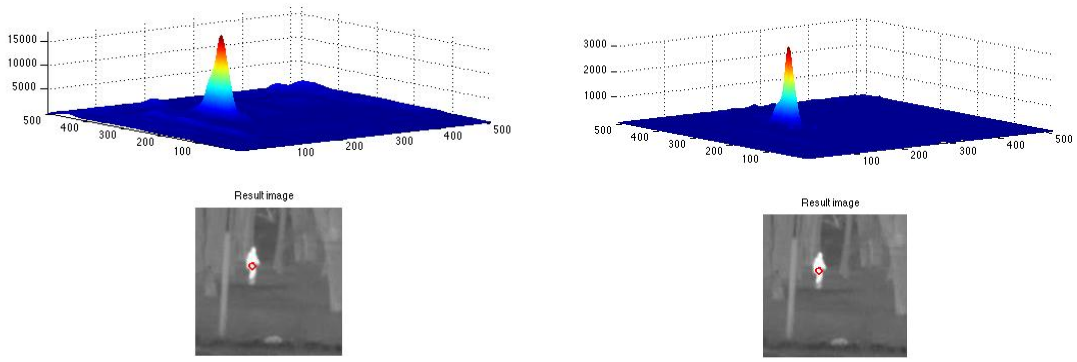

(a) (b)

Figure 5.12 Detection result for Human figure shown in 5.10(a): (a) is the OT-MACH correlation plane and (b) is the OT-MACH Rayleigh modified filter correlation plane

Image	β	γ	OT-MACH PSR	R-MACH PSR
5.10 (a)	0.001	0.001	24.93	39.45

Table 5.5 PSR result for image 5.10(a)

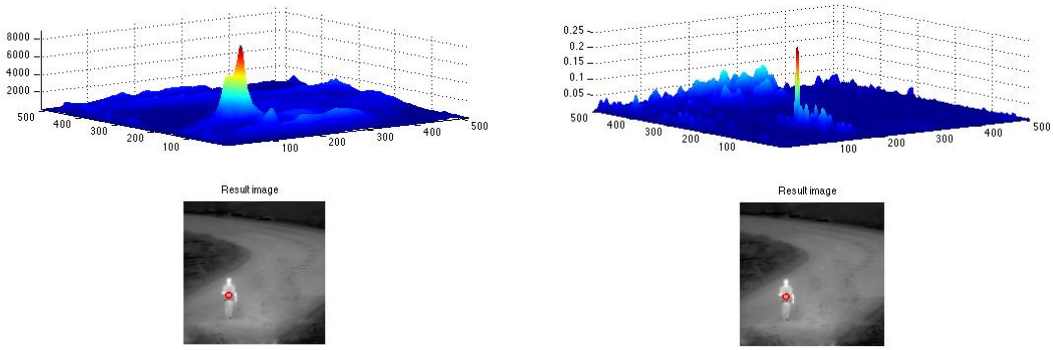

(a) (b)

Figure 5.13 Detection result for Human figure shown in 5.10(b): (a) is the OT-MACH correlation plane and (b) is the OT-MACH Rayleigh modified filter correlation plane

Image	β	γ	OT-MACH PSR	R-MACH PSR
b	0.001	0.001	24.93	31.88

Table 5.6 PSR result for image 5.10(b)

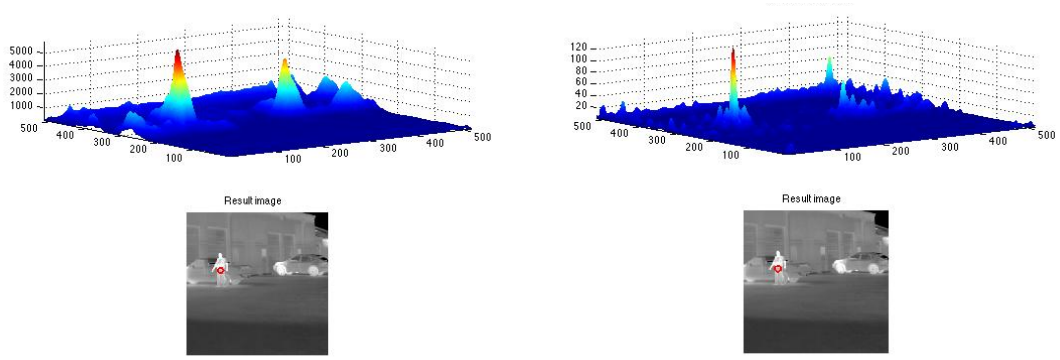

(a) (b)

Figure 5.14 Detection result for Human figure shown in 5.10(c): (a) is the OT-MACH correlation plane and (b) is the OT-MACH Rayleigh modified filter correlation plane

Image	β	γ	OT-MACH PSR	R-MACH PSR
c	0.001	0.001	-	28.44

Table 5.7 PSR result for image 5.10(c)

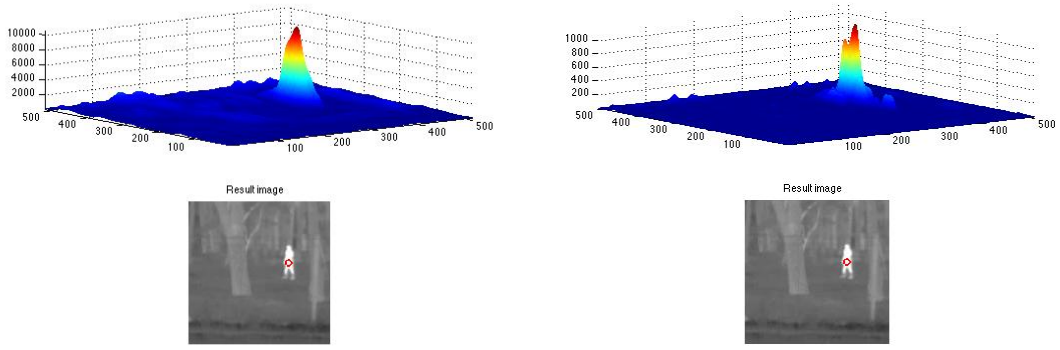

(a) (b)

Figure 5.15 Detection result for Human figure shown in 5.10(d): (a) is the OT-MACH correlation plane and (b) is the OT-MACH Rayleigh modified filter correlation plane

Image	β	γ	OTMACH PSR	R-MACH PSR
d	0.001	0.001	18.04	26.16

Table 5.8 PSR result for image 5.10(d)

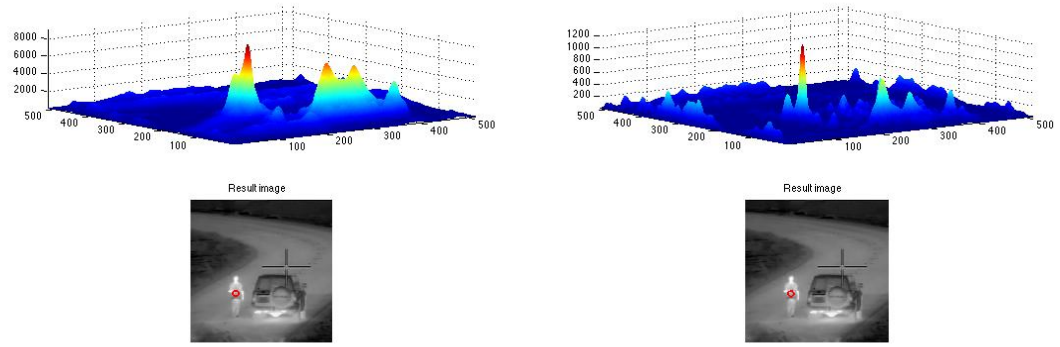

(a) (b)

Figure 5.16 Detection result for Human figure shown in 5.10(e): (a) is the OT-MACH correlation plane and (b) is the OT-MACH Rayleigh modified filter correlation plane

Image	β	γ	OT-MACH PSR	R-MACH PSR
e	0.001	0.001	-	25.24

Table 5.9 PSR result for image 5.10(e)

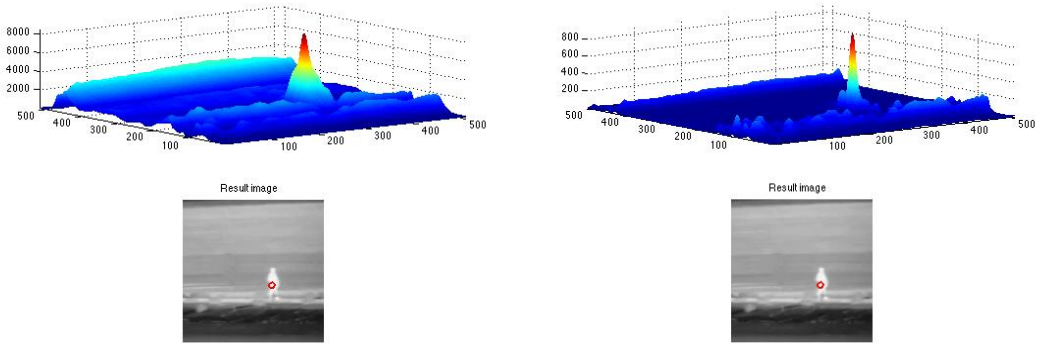

(a) (b)

Figure 5.17 Detection result for Human figure shown in 5.10(f): (a) is the OT-MACH correlation plane and (b) is the OT-MACH Rayleigh modified filter correlation

Image	β	γ	OT-MACH PSR	R-MACH PSR
f	0.001	0.001	10.05	24.7

Table 5.10 PSR result for image 5.10(f)

The above results clearly show how the addition of the Rayleigh distribution filter improves the OT-MACH overall performance. It can be observed that the PSR result is higher with the addition of the Rayleigh distribution filter. It can be seen from Figure

5.14 and 5.16 shown above that the OT-MACH filter did not manage to suppress the background clutter enough, which resulted in high false peaks exceeding half of the detection peak, which therefore affected the PSR result. The addition of the Rayleigh distribution filter can also be seen to have produced a sharper correlation peak and a much more stable correlation plane that makes the detection of the human in the scene more reliable. Thus the addition of the Rayleigh filter to the OT-MACH filter has produced a noticeable improvement to the PSR results achieved for the task of human detection in cluttered FLIR imagery reported in this section.

It can thus be concluded that humans can thus be detected in cluttered FLIR imagery. The OT-MACH filter parameters have been modified to find the optimal settings that were determined to be 0.001 for both the β and γ parameters. The frequency domain application of the Rayleigh filter to the OT-MACH filter function was employed to enhance the discrimination capability of the filter design, leading to a reduction in the number of peaks present in the correlation plane by tuning the filter to an appropriate band pass to provide a suitable compromise in filter response between distortion tolerance and resistance to clutter. The overall results obtained have shown a significant improvement to the correlation plane and subsequent target detection over use of the unmodified OT-MACH filter alone. The proposed technique thus allows a good starting point for the further optimisation of the R-MACH filter to allow better detection and recognition of human targets in highly cluttered FLIR scenes.

5.7 Identification in defence and security applications

5.7.1 Target identification using two stage R-MACH

Several identification methods have been researched in the literature to help the decision cycle in defence and security applications [1], [112]–[117]. The Rayleigh enhanced OT-MACH filter (R-MACH) can be efficiently used for ascertaining the target classification thereby giving a feasibility of identification. In this section a novel two-stage process of utilising the R-MACH filter is discussed to arrive at some conclusions on target identification. In the previous sections it has been determined that an R-MACH filter has improved performance when compared to a normal OT-MACH or D-MACH filter for real time target detection scenarios. The normal two stage correlation process, as detailed in section 5.7.5 below, that requires intensive computing is moderated because of the use of simplified tuning of the standard deviation of the Rayleigh filter. The following sections introduce an important application utilising the R-MACH filter in real-time identification of various targets together with a brief description of the use of two-dimensional cross sections of 3D models of the targets for training of the filter.

In defence and security applications, gathering quality information about an object or a target of interest gives the operator information that leads to identifying the target so the right action can be taken accordingly in real time situations. There are multiple systems used in operational fields that give the identity of a plane, ship or other vehicle targets, collectively called Identification Friend or Foe (IFF) systems. The IFF system is pre-fed with the information related to the vehicles, ships or planes and exchanged, for instance,

among the authorities' private Air Traffic Control line (ATC) to keep track of the plane with positive identification information. Such systems are used in the defence world where they help the operator to accurately characterise the target to be either friendly, enemy, natural or possibly unknown and so assists in making a successful tactical decision [118]–[120]. The drawback of such systems is that they uses a radio signal which is an active process and so could be jammed, hidden or changed during the operation.

In the following section, a decision support system concept that helps the operator to identify the target is proposed using an image processing technique. There are multiple advantages when using an image based identification system in defence and security applications since it is a passive system and so cannot be detected or interrupted which gives the operator a solid advantage in real time operation.

5.7.2 Two stage target identification process

As an illustrative example of the proposed two-stage R-MACH identification process use is made of 3D model snapshots as training images and a video sequence acquired by an Apache helicopter of multiple targets in a high clutter background.

5.7.3 Training images used in the identification process

The OT-MACH filter was trained with two-dimensional projected views of the 3D models of the target objects. Several out-of-plane rotations (0° to 360°) of the selected

targets have been used. Figure 5.18 shows an example projection from the training data set.

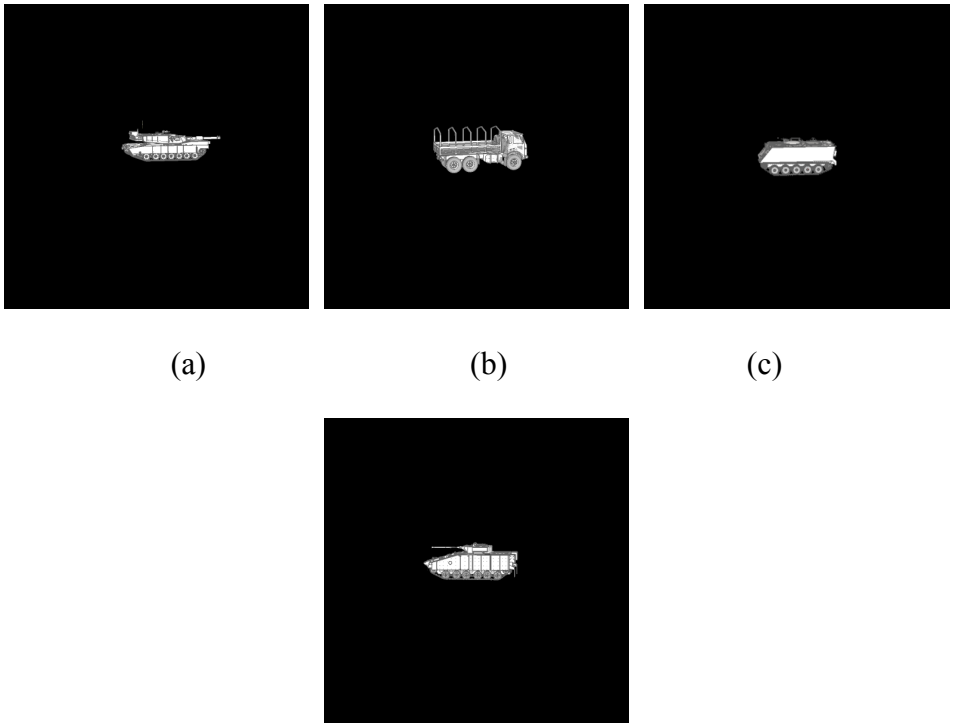

(a) (b) (c)

(d)

Figure 5.18 2-D Training images: (a) M1A2 tank (b) military truck (c) M113 personal carrier (d) British Warrior armour

5.7.4 Test images used for identification evaluation

Intensive tests have been carried out on 15 real world FLIR images acquired by an Apache helicopter for several targets. The images contain single and multiple targets in the scene. Examples of the target types that have been tested with the proposed techniques are shown in Figure 5.19.

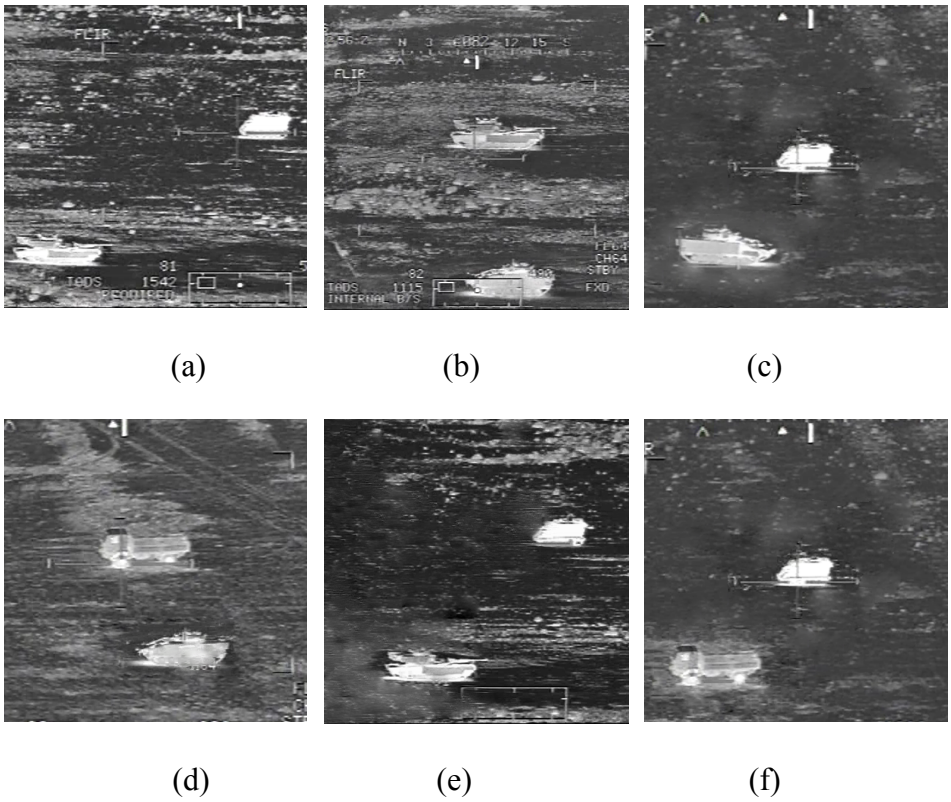

Figure 5.19 FLIR test images showing different targets: (a) M113 personal carrier and M1A2 tank (b) M1A2 tank and British warrior armour (c) British warrior armour and M113 personal carrier (d) British warrior armour and military truck (e) M113 personal carrier and M1A2 tank (f) M113 personal carrier and military truck

5.7.5 Two stage R-MACH identification methodology

The identification process utilises a two stage R-MACH correlation as shown in Figure 5.21 and 5.22. The first stage of the identification process involve creating a rotational multiplexed training image by adding and dividing the resultant image by the total number of the training images summed together in the space domain. This step is considered as a training image preparation step for the OT-MACH filter design. The filter is designed as given in equation (2.19) after performing a fast Fourier transform on the multiplexed image. The computed OT-MACH filter function h is then

appropriately bandpass filtered using the Rayleigh filter as a pre-processing filter in order to improve the performance of the OT-MACH filter in detecting the trained target in a test image. A further fast Fourier transform is then performed on the spatial domain input test image and complex multiplied with the R-MACH transfer function in the frequency domain and then inverse fast Fourier transformed to obtain a correlation plane output. The region of interest (ROI) is located in the resultant correlation plane using threshold statistics. The target image is then passed on to a segmentation module that isolates the target out from the background using background segmentation and morphological operations.

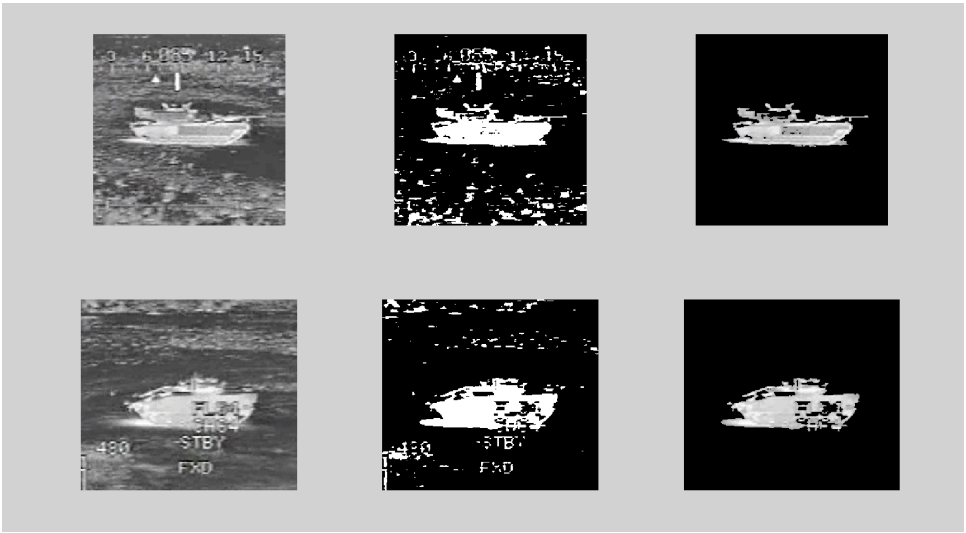

(a) (b) (c)

Figure 5.20 Target segmentation using morphological operations: (a) Region of interest sliced image (b) Segmented image (c) Masked image

Figure 5.20(a) shows a selected region of interest image that results from the first stage correlation. The image then further segmented and the cluttered background removed to reduce the false peak generation prior to the second stage correlation as shown in Figure

5.20(b). The mask in which the target is located in the target image is created as shown in Figure 5.20(c). Several morphological operations have been applied to obtain the output as shown in the flow chart in Figure 5.21. The three-stage method of morphologically processing and re-imposing the detected target is carried out as shown in Figure 5.20. The actual texture of the target from the input image is then re-imposed to the centre of a blank training template image thus creating a training image for the Stage 2 of the identification process as shown in Figure 5.21.

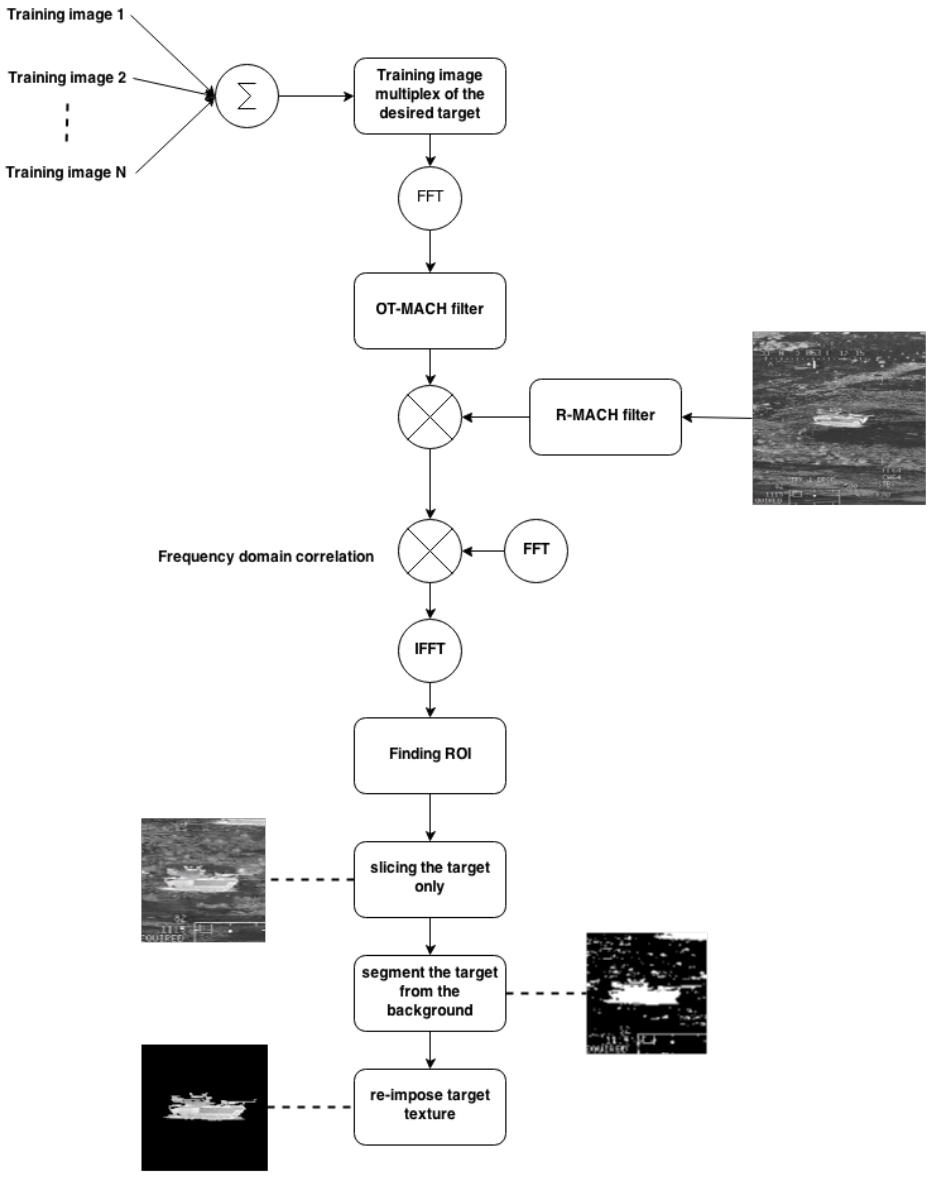

Figure 5.21 Stage 1 of the R-MACH identification process

In Stage 2 of the identification process the background-removed centred target image is used to ascertain the identity of the detected target from amongst a bank of various OT-MACH filter functions of several possible targets, namely: the Warrior, M1A2, HUMVEE, M113 and military truck. Each of these possible targets are used to create a bank of OT-MACH filters which is Rayleigh filtered using a set of Rayleigh standard deviation parameters as shown in the flow chart in Figure 5.22. In this way, a bank of R-MACH filters for each possible target is formulated in order to identify the target obtained from the test image in Stage 1. Each of the R-MACH filter transfer functions of the possible targets are cross-correlated with the target image obtained in the Stage 1 to obtain a number of correlation planes for each set of Rayleigh parameters. The final step of the Stage 2 identification process involves measuring the PSR for each of the correlation planes obtained. The PSR values obtained in each parameter iteration are then used to plot analytic graphs. In an optimal region of the best PSR measurements the target identity can be confirmed, thus concluding the Stage 2 of the target identification process.

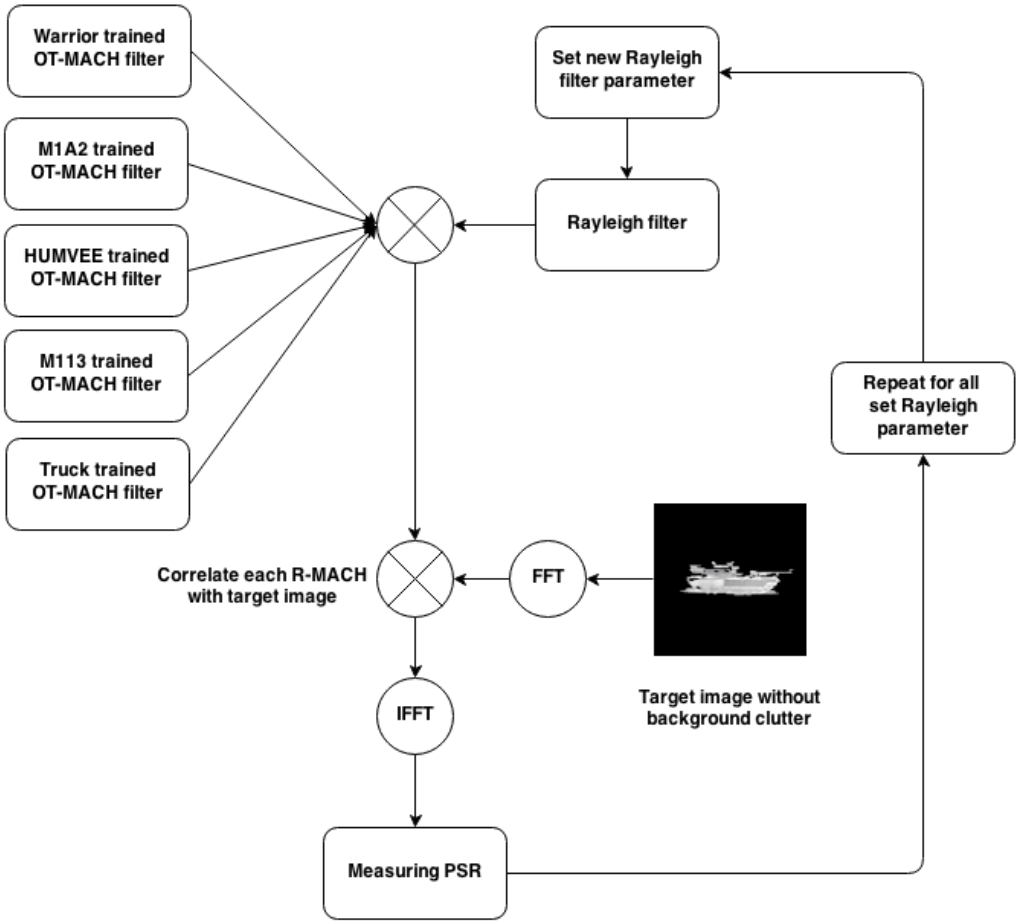

Figure 5.22 Stage 2 of the R-MACH identification process

5.8 R-MACH identification study result

Several R-MACH based identification results are presented in this section to help assess the functionality, accuracy and validation of the identification technique using the two stage process presented in the previous section.

The following results are presented as combined plots of PSR versus sigma order to perform target identification. The observations show that there is always a true detection range in sigma for a *particular* target in the presence of the target and/or non-targets. However, it must be emphasised that the σ_r ranges must be adjusted for a particular reference object since the ranges vary between reference objects. It can also be observed that there is a high similarity in the behaviour of the plot for each target when compared with the plots of several non-targets. As an example, it can be seen that the target M113 PSR plots shown in Figure 5.23(b), 5.25(b), 5.27(c) and 5.28(b) have a similar pattern.

In the Figure 5.23(a), an M113 personal carrier and an M1A2 tank are used as test images for the two-stage R-MACH process. The targets are detected using the first R-MACH filter, to be then passed into a segmentation and morphological module to slice out the target texture into a zero background test image prior to subsequent identification in Stage 2 using the optimised parameter R-MACH filter.

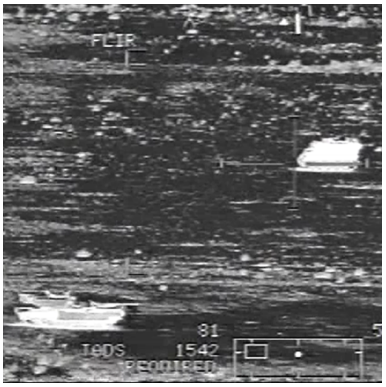

(a)

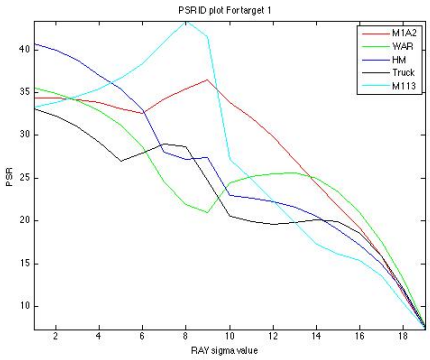

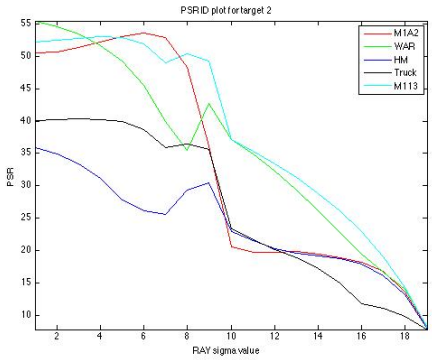

(b) (c)

Figure 5.23 Target identification result for image shown in Figure 5.19(a): (a) Test image with M113 personal carrier and M1A2 tank (b) PSR result for R-MACH trained with M1A2 training set (c) PSR result for R-MACH trained with M113 personal carrier training set

Figures 5.23(b) and (c) present graphs of PSR against sigma values, from which it is possible to ascertain the target identity. This is done by plotting the PSR obtained for the same test image using different R-MACH filters designed for the M1A2 tank, Warrior, Humvee, Truck and M113 personal carrier target objects, respectively. The plots suggest that target 1, which is the M1A2 in the test image, shows a prominent PSR with sigma values between 10 and 14 on the *x*-axis of the graph, whereas when target 2

is correlated, which is M113 personal carrier, the PSR shows highest values for sigma values less than 6, which is nearer the ideal sigma ranges of the Rayleigh filter. From the graphs it can be observed that the two stages R-MACH identification process identifies the M113 and M1A2 for the respective target inputs, the PSR showing high values over wide ranges of the sigma values of the R-MACH filter. Thus a relatively simple decision making process can be used to ascertain the presence of the target and its identity utilising the comparison of each PSR result produced from the R-MACH filter for each target object over a range of sigma values.

Similarly, a British warrior armour vehicle and the M1A2 tank are present in the same test image shown in Figure 5.24(a) and are used to test the identification the targets separately using the two stage process. It can be observed that even though the British warrior armour contains a lot of clutter in its foreground and background due to the presence of overlays and text, the graphs presented in Figure 5.24(b) and (c) show promising identification results.

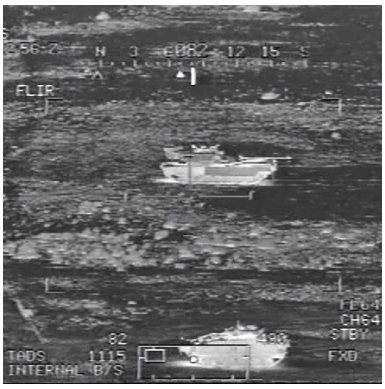

(a)

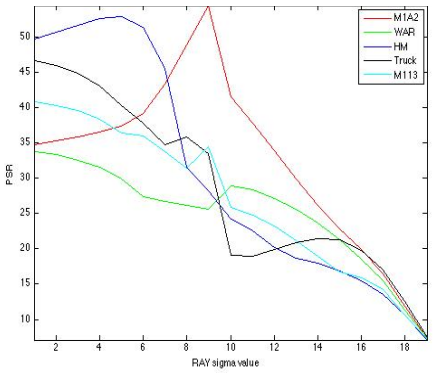

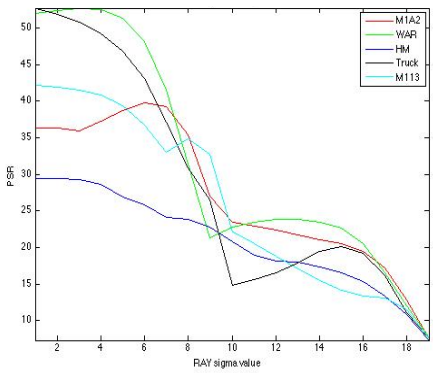

(b) (c)

Figure 5.24 Target identification result for image shown in Figure 5.19(b): (a) Test image with British warrior armour and M1A2 tank (b) PSR result for R-MACH trained with M1A2 training set (c) PSR result for R-MACH trained with British warrior armour training set

Figure 5.24(b) and (c) show the PSR behaviour for each target separately when correlated with R-MACH filters trained on different targets. From the graphs presented it can be seen that the M1A2 based PSR shows prominence in the ideal Rayleigh sigma regions, then diminishes and merges with the PSR obtained for the British warrior armour vehicle as well as those for the other targets being considered. A similar result can be observed in the Figure 5.24(c) for the British warrior armour vehicle PSR values compared with all other target PSRs obtained using the British warrior as a target.

Furthermore, a different view of a test image containing the M113 and M1A2 targets is used as a test case to evaluate the two-stage R-MACH identification process as shown in Figure 5.25(a). The graphical test results for PSR versus R-MACH sigma values for the M1A2 and M113 are presented in Figure 5.25(b) and (c), respectively.

Figure 5.25(a) shows the test image containing the M113 personal carrier and the British warrior armour vehicle. The PSR comparison results against correlation of the M113 and British warrior armour target with the bank of R-MACH filters designed for different targets is shown in Figure 5.25(b) and (c), respectively.

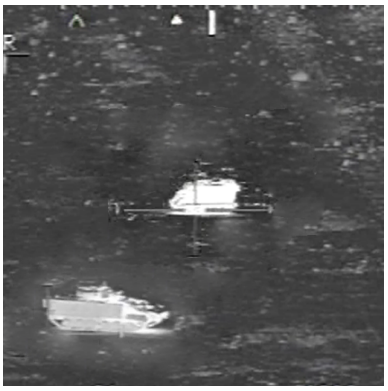

(a)

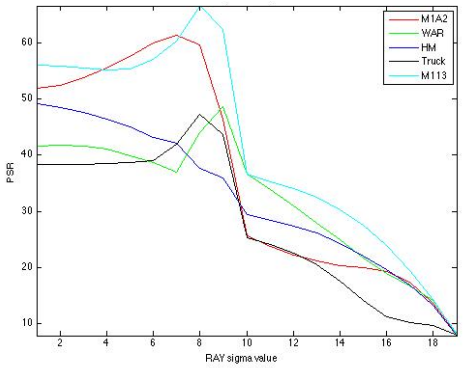

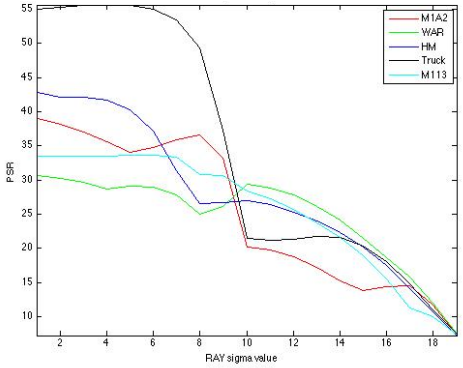

(b) (c)

Figure 5.25 Target identification result for image shown in Figure 5.19(c): (a) Test image with M113 personal carrier and British warrior armour (b) PSR result for R-MACH trained with M113 personal carrier training set (c) PSR result for R-MACH trained with British warrior armour training set

From the graphical results obtained for the M113 and British warrior targets in Figure 5.25(b) and (c), respectively, it can be observed that the good PSR performance is achieved for each in turn when used as a target reference. In order to validate the identification process, Figure 5.26(a) presents a test image containing a military truck and a British warrior armour vehicle. When using the two stage R-MACH filter identification processes, each target obtained separately as a test image in Stage one of the procedure is evaluated by plotting the PSR obtained against R-MACH filters trained for different targets, as shown in Figure 5.26(b) and (c). The results shown in Figure

5.26(b) and (c) can be used to deduce that when the input target is a military truck the PSR obtained is high in the ideal performance sigma region, as shown in Figure 5.26(b). A similar result is obtained when the target used as a template derived from Stage one of the process is a British warrior, as shown in Figure 5.26(c). Further results validating the two stage R-MACH identification process are presented in Figure 5.27, Figure 5.28. Figure 5.28(a) shows a test image with a different view containing the British warrior and a military truck. The results of the PSR versus sigma plots for each target in Figure 5.26(a) are presented in Figure 5.26(b) and (c) for the British warrior and military truck, respectively.

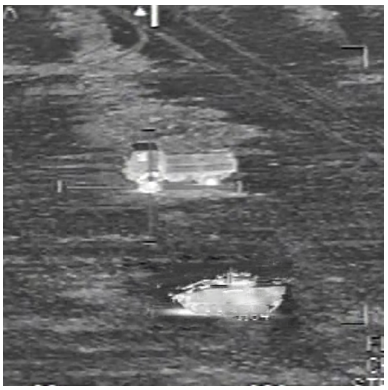

(a)

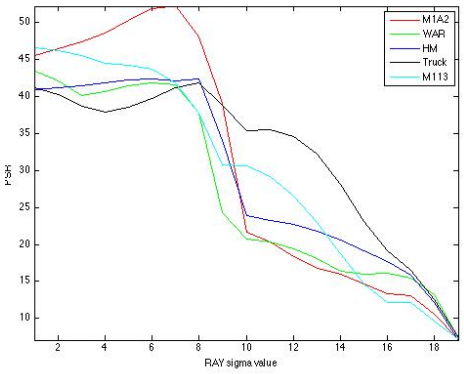

(b)

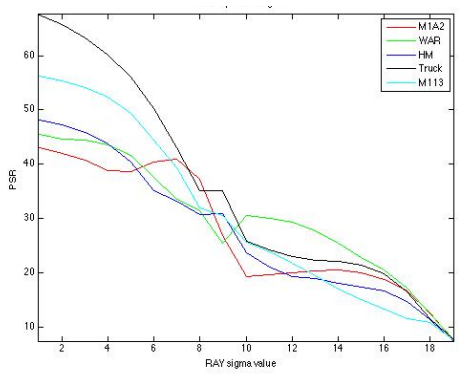

(c)

Figure 5.26 Target identification result for image shown in Figure 5.19(d): (a) Test image with military truck carrier and British warrior armour (b) PSR result for R-MACH trained with

military truck training set (c) PSR result for R-MACH trained with British warrior armour training set

Figure 5.27(a) shows a test image containing an M1A2 tank and an M113 Personnel carrier captured in a different view. Figure 5.27(b) and (c) shows the PSR plots for each of them, considered separately as targets for correlation.

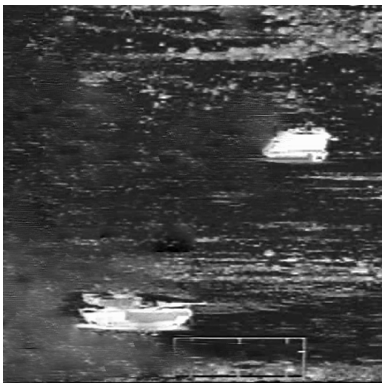

(a)

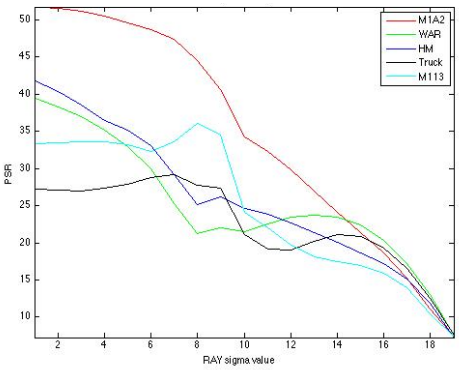

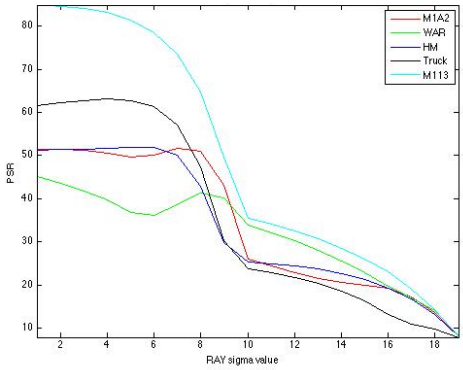

(b) (c)

Figure 5.27 Target identification result for image shown in Figure 5.19(e): (a) Test image with M1A2 tank and M113 personal carrier (b) PSR result for R-MACH trained with M1A2 tank training set (c) PSR result for R-MACH trained with M113 personal carrier training set

Figure 5.28(a) shows a test image containing a military truck and an M113 Personnel carrier in close proximity and Figure 5.28(b) and (c) show the PSR plots for each of them considered separately as targets for correlation.

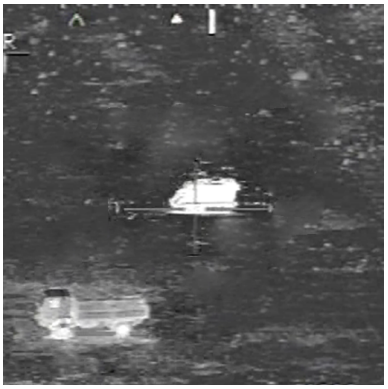

(a)

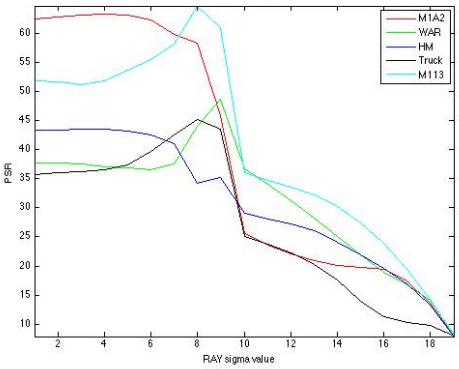

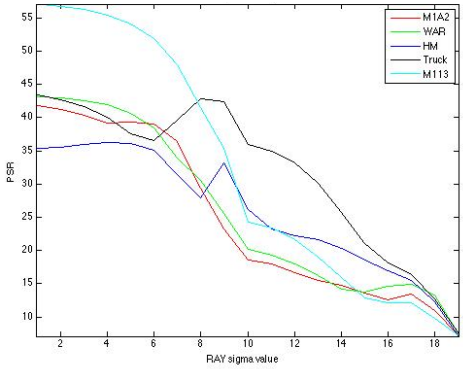

(b) (c)

Figure 5.28 Target identification result for image shown in Figure 5.19(f): (a) Test image with military truck and M113 personal carrier (b) PSR result for R-MACH trained with M113 personal carrier training set (c) PSR result for R-MACH trained with military truck training set

It has been noted that the PSR values obtained for each target is unique for that target test image. A series of tests have been conducted to illustrate and support the idea being presented. Multiple R-MACH filters are trained with several target training sets each in order to find the unique corresponding PSR values. Correlation of the multiple R-MACH filters with the same test image containing the target across various sigma

values have been tested and the PSR values are plotted in the graphs presented in this section for comparison and analysis.

5.9 Summary

In this Chapter, the Rayleigh distribution filter is proposed as a pre-processing filter for the OT-MACH filter. It is concluded that the Rayleigh pre-processing filter gives improved performance over the DoG pre-processing filter when used with the OT-MACH filter in real time target detection scenarios using FLIR imagery. It has been noted that the Rayleigh filter simplifies the tuning of the standard deviation of the pre-processing filter for robust target detection due to its requirement for only a narrow range of variation of this single parameter.

Several comparison results tabulating the PSR and PCE for the FLIR target images with and without overlay clutter have been made. It is concluded that the R-MACH filter results in a better PSR and so demonstrates improved performance when employed as a pre-processing filter for the OT-MACH filter. The additional advantage of using the Rayleigh filter is that it has only one standard deviation term to be controlled as compared to the DoG filter which has two. The standard deviation values of the true positive detection range for the Rayleigh filter are between 0.07 and 1 whereas for the DoG filter the range lies between 0.5 and 20.

The Chapter also introduces Human detection using the R-MACH filter which is compared with an OT-MACH filter for detection accuracy based on the resulting PSR

values produced. It has been shown in this Chapter that the PSR values obtained by using R-MACH are improved over those obtained using an unmodified OT-MACH filter for Human detection. The use of the R-MACH filter thus allows a good starting point for the further optimisation of the OT-MACH filter design to allow better detection and recognition of Human targets from within highly cluttered FLIR imagery. A novel method of detecting Humans in several situational awareness scenarios is presented, to be further enhanced as discussed in the Future work section in Chapter 6.

It has also been established that vision based identification of targets is of the most importance in security and surveillance real-time situations helping to reduce the human error involved in suspect detection and awareness in any covert activity in hostile environments.

The identification of targets is introduced in the final sections of this chapter, where the emphasis is on utilising the R-MACH filter and assessing its feasibility for use as an identification filter which is discussed in detail. A two stage approach for identifying target objects and analysing the PSR result to arrive at a conclusion regarding the identity of the target is evaluated and several test results are presented and discussed. A graphing method which involves plotting the PSR values versus the Rayleigh filter standard deviation value is presented to assess multiple correlation results resulting from R-MACH filters trained for different targets. It has been validated that for a certain ideal sigma range of Rayleigh filter, PSR based identification is possible.

Chapter 6

Conclusions and further work

Chapter 6 Conclusions and further work

6.1 Conclusion

In this thesis, correlation pattern recognition filters have been studied in detail in order to arrive at improvements to the OT-MACH filter, particularly when this is applied to FLIR imagery for defence and security applications. In the first part of the thesis, an introduction to the theory and also the practicalities involved in target detection, recognition and identification used in military and allied domains has been given.

The second chapter of the thesis introduces the optimal trade-off maximum correlation height (OT-MACH) filter and its derivation. The requirement to optimise the filter for target detection in several environmental conditions has been considered in detail. The parameters of the OT-MACH filter have been detailed and utilised in finding a solution to the optimisation problems involved with the filter design. It is clearly identified that the selection of training images to construct the optimal performance filter is an important issue in achieving ideal results. Out-of-plane rotational multiplexing of the training images in order to attain computational efficiency is also discussed, along with conclusions regarding the number of training images possible in a single filter. Illumination effects when using real and 3D training data have been discussed, along with considerations concerning the mapping of FLIR data texture information onto the CAD target model to improve the accuracy of the model and allow improved target detection. Important factors that affect the OT-MACH filter performance, namely the background clutter noise and rotational distortion effects, have been discussed in detail to establish that the performance of the filter can be assessed using various statistical correlation plane parameters. The classical performance metrics for correlation filter

performance assessment such as PSR and PCE are discussed to measure and optimise the filter performance. Furthermore, new performance metrics are also introduced, namely: Area of peak at half-height (AHH); Number of peaks at half maximum height (NPHH) and Total detection error (TDE), which are discussed in detail as additional performance metrics to support quantification of the filter performance.

Chapter 3 of the thesis examines the OT-MACH filter parameter variations and their effect on achievable PSR correlation values determined for various types of targets in simple to challenging background clutter. Further tests are conducted to arrive at near optimal relative settings of these parameters for good performance of the OT-MACH filter. From the tests and results discussed it is concluded that the β parameter is the main drive for the overall OT-MACH filter behaviour and γ has a minimum effect.
The noise parameter in the OT-MACH transfer function denominator has been considered and it has been concluded that it is possible to automatically compute the noise parameter value using the available input image intensity statistics. Thus the additive noise can be computed using the ratio of the standard deviation and mean of the input image intensity values whilst maintaining a setting for the α parameter of unity. The simplification of the filter design and decrease in the computational requirements in deriving the ideal OT-MACH filter transfer function by setting two, rather than three, parameters is the outcome of these considerations. In order to justify this conclusion, several results have been presented.

In Chapter 4 of the thesis, further improvements of the OT-MACH filter performance is achieved by using a bandpass pre-processing filter in conjunction with the OT-MACH filter. The advantages of using the Difference of Gaussian (DoG) filter in this role with

the OT-MACH filter function have been described. The DoG filter is thus used as a pre-processor to the OT-MACH filter prior to the complex multiplication with the test input image spectrum. Evaluation the OT-MACH filter performance with changes of the α, β and γ parameters in the transfer function is carried out for various FLIR imagery based targets. It is concluded that with all the parameters set to unity, the OT-MACH filter does not produce a useable result when used with images containing high cluttered backgrounds since the β and γ OT-MACH filter parameters are incorrectly set to reject such clutter. The Difference of Gaussian (DoG) filter was added to the OT-MACH filter as pre-processing filter (which was named the D-MACH filter) and the resulting performance re-evaluated. The results have been quantified by two measurements, notably the PSR and TDE values obtained from the correlation planes generated by the filters.

The D-MACH filter has multiple parameters that need to be adjusted i.e. the β and γ parameters of the OT-MACH filter and also the DoG pre-processing filter standard deviation setting to control its band pass. Automation of the setting of the DoG pre-processing filter standard deviation has been proposed in this Chapter and the resulting encouraging performance improvement of the D-MACH filter over the OT-MACH filter has been discussed, particularly when dealing with difficult images containing a high clutter background. The correlation peaks generated are sharper and a more stable overall correlation plan is produced with fewer false peaks.

Chapter 5 discusses further improvement to the OT-MACH filter by using the Rayleigh distribution filter as a pre-processer to the OT-MACH filter (which was named as the R-MACH filter). It has been shown that the Rayleigh distribution filter simplifies the problem of the tuning of the standard deviation of the pre-processing filter for robust

target detection due to its requirement for only a narrow range of variation of this single parameter. Several comparison results tabulating the PSR and PCE for the FLIR target images with and without overlay clutter have been analysed. It is further concluded that the R-MACH filter results in a better PSR and demonstrated improved performance when employed as a pre-processing filter for the OT-MACH filter on a target detection test. The standard deviation values of the true positive detection range for the Rayleigh filter are between 0.07 and 1, whereas for the DoG filter the range lies between 0.5 and 20.

Chapter 5 also utilises the R-MACH filter but for Human detection scenarios in FLIR imagery data. It is compared with the OT-MACH filter for detection accuracy based on the resulting PSR values. The PSR values obtained using the R-MACH filter are improved as compared to those obtained using a normal OT-MACH filter for detecting Human targets. It is been established that the use of R-MACH filter promises better detection capability, as an improved version of the OT-MACH filter, for challenging highly cluttered FLIR imagery data.

The overall achievements of this thesis are listed below.

- It has been found that the β parameter is the main drive for the overall OT-MACH filter behaviour and the γ parameter has a minimal effect on the filter transfer function.
- The noise factor C_x in the OT-MACH transfer function can be automatically computed using the statistics of the input image intensities as presented in in Al-Kandri *et al* [74].

- Additional bandpass filtering has been incorporated into the OT-MACH filter based on the Difference of Gaussian (DoG) filter. This additional filter acts as a pre-processor and has been shown to result in improvements in the discrimination ability of the overall composite filter as described in Al-Kandri *et al* [75].

- Further improvement has been suggested for automating selection of the DoG filter standard deviation setting as has been proposed in Al-Kandri *et al* [75].

- An alternative pre-processing filter has been introduced, namely the Rayleigh distribution filter. The incorporation of the Rayleigh filter into the OT-MACH filter resulted better detection accuracy when the filter was applied to highly cluttered backgrounds and difficult target detection scenarios such as human detection in thermal infra-red imagery as described in Al-Kandri *et al* [33], [76].

6.2 Future work

Further to the work conducted in this thesis, several innovative improvements can be attempted. The following two main approaches are outlined as a proposal for intended future work in the area of target detection using correlation pattern recognition filters. These are for improvements in the approach of using training images in designing the filter and the use of the PSR quantification for classification.

An important step in the design of the OT-MACH filter is the selection of training images for a particular target. The thesis has discussed the reasons for the limitation to the number of the training images that can be used in constructing a single multiplexed filter for ideal performance. This limitation forces the construction of a bank of filters to accommodate, for instance, scale and orientation invariant target detection for a single target. A possible approach to solve this limitation is to introduce a different representation of the training image set. An orthographical representation of the 3D model of a target can be used as training set for the OT-MACH filter construction. Figure 6.1 illustrates the orthographical representation example of an M1A2 tank in a particular scale. Using this projection, each view of the orthographical representation of the target is multiplexed to construct the OT-MACH filter reduces a need to develop a bank of filters to cover all orientations of the reference object. Although there are some limitations to this approach, the method could assist in reducing the computational intensity of generating a reference template for target detection for a particular scale.

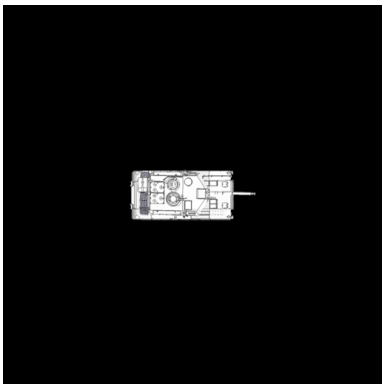

(a)

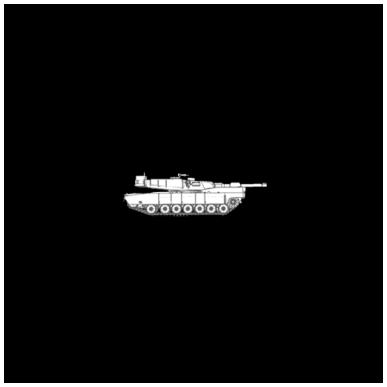

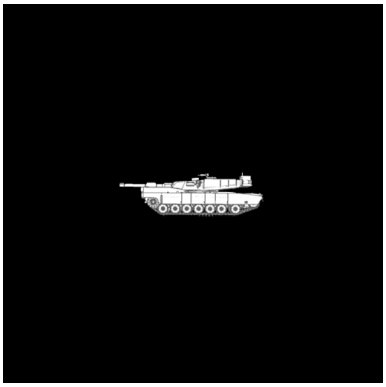

(b) (c)

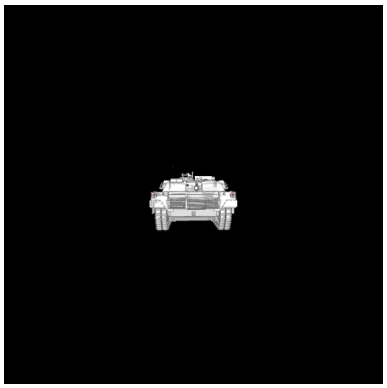

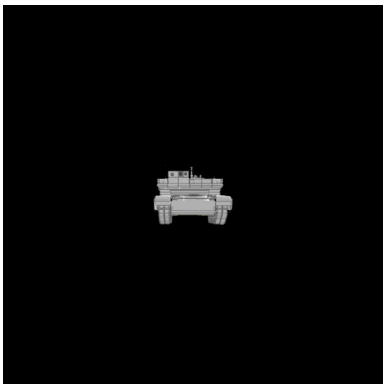

(d) (e)

Figure 6.1 M1A2 orthographical representation: (a) Plan view of M1A2 tank (b) and (c) Side view of the M1A2 tank (d) Front view of the M1A2 tank (e) Back view of the M1A2 tank

A second possible approach to present the training images that could contain maximum information and so minimise the number of training images used, is the unfolding or

UV mapping technique. UV mapping is the process of making a 2D representation out of a 3D model. The letters U and V are used to represent the axes of the 2D projected plane derived from the 3D representation in *x*, *y* and *z* axes as shown in Figure 6.2 [120].

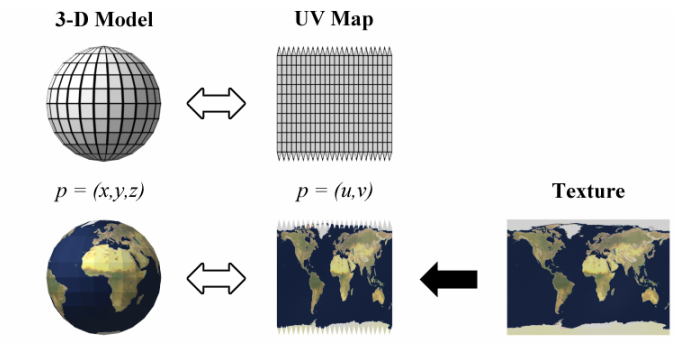

Figure 6.2 UV mapping of 3D model

It can be seen in Figure 6.2 that the 2D representation displays almost all the information contained in the original 3D model [120]. A similar process could be applied to the training images for most of the targets that can be represented as a 3D model, an example being shown in Figure 6.3.

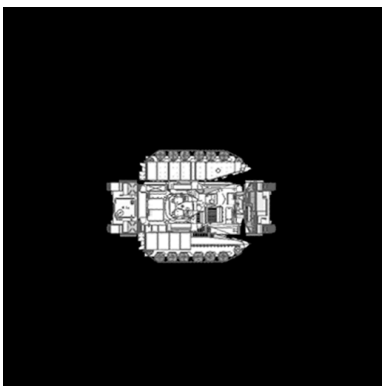

Figure 6.3 British warrior UV mapped

References

[1] M. Klima and C. Republic, “Correlation identification in security applications: discussion,” pp. 2–6.

[2] H. Zhou and T. Chao, “MACH filter synthesizing for detecting targets in cluttered environment for gray-scale optical correlator,” *Proc. SPIE*, vol. 3715, pp. 394–398, 1999.

[3] Y. Li, Z. Wang, and H. Zeng, “Correlation filter: an accurate approach to detect and locate low contrast character strings in complex table environment,” *Pattern Anal. Mach. Intell. IEEE Trans.*, vol. 26, no. 12, pp. 1639–1644, 2004.

[4] Alfalou, C. Brosseau, P. Katz, and M. S. Alam, “Decision optimization for face recognition based on an alternate correlation plane quantification metric.,” *Opt. Lett.*, vol. 37, no. 9, pp. 1562–4, May 2012.

[5] L. Novak, G. Owirka, and C. Netishen, “Radar target identification using spatial matched filters,” *Pattern Recognit.*, no. 2, 1994.

[6] S. Ali and S. Lucey, “Are Correlation Filters Useful for Human Action Recognition?,” *2010 20th Int. Conf. Pattern Recognit.*, pp. 2608–2611, Aug. 2010.

[7] M. Alder, “An Introduction to Pattern Recognition.”

[8] S. Tan, R. C. D. Young, and C. R. Chatwin, “Markovian and autoregressive clutter-noise models for a pattern-recognition Wiener filter.,” *Appl. Opt.*, vol. 41, no. 32, pp. 6858–66, Nov. 2002.

[9] D. Casasent and D. Psaltis, “Position, rotation, and scale invariant optical correlation.,” *Appl. Opt.*, vol. 15, no. 7, pp. 1795–9, Jul. 1976.

[10] A. Gardezi, “Pattern recognition employing spatially variant unconstrained correlation filters,” 2013.

[11] J. Shang, C. Chen, and W. Wang, “Recognition of distorted target based on Mexican hat optimum trade-off maximum average correlation height algorithm,” vol. 8193, p. 81933E–81933E–7, Jun. 2011.

[12] B. Kumar, A. Mahalanobis, and R. Juday, *Correlation pattern recognition*. 2005.

[13] monique Pavel, *fundamentals of pattern recognition*. .

[14] *Pattern Recognition And Image Preprocessing*. .

[15] M. Nixon and A. Aguado, *Feature extraction and image processing*. 2008.

[16] W. Chao, “Introduction to pattern recognition,” *Natl. Taiwan Univ. Taiwan*, 2009.

[17] K. L. Grauman, *Visual object recognition*. .

[18] W. Pratt and J. Wiley, *Digital image processing: PIKS inside*. 2001.

[19] C. Chen, L. Pau, and P. Wang, *Handbook of Pattern Recognition and Computer Vision*. 2010.

[20] E. R. Davies, *Computer and machine vision: theory, algorithms, practicalities*. .

[21] G. Blanchet and M. Charbit, *Digital Signal and Image Processing Using MATLAB (Digital Signal and Image Processing series)*. 2006.

[22] N. Mohamed, "Digital Filters Design for Signal and Image Processing (Digital Signal and Image Processing series)," *portal.acm.org*, Jan. 2006.

[23] A. Bovik, "Handbook of Image and Video Processing," pp. 1–974, Mar. 2004.

[24] R. Gonzalez, R. Woods, and S. Eddins, *Digital image processing using MATLAB*, vol. 624. 2004.

[25] A. Bovik, *The essential guide to Image Processing*. 2009.

[26] T. Acharya, *Image Processing Principles and Applications*. 2005, pp. 1–451.

[27] "Adaptive Filtering Primer with MATLAB - Poularikas and Ramadan.pdf." .

[28] S. Karris, *Signals and systems with MATLAB applications*. 2003.

[29] A. Lugt, "Signal detection by complex spatial filtering," *Inf. Theory, IEEE Trans.*, vol. 10, no. 2, pp. 139–145, 2002.

[30] B. Li, "Experimental Evaluation of FLIR ATR Approaches—A Comparative Study," *Comput. Vis. Image Underst.*, vol. 84, no. 1, pp. 5–24, Oct. 2001.

[31] A. Yilmaz, K. Shafique, and N. Lobo, “Target-tracking in FLIR imagery using mean-shift and global motion compensation,” *IEEE Work. ...*, 2001.

[32] A. Yilmaz, K. Shafique, and M. Shah, “Target tracking in airborne forward looking infrared imagery,” *Image Vis. Comput.*, vol. 21, no. 7, pp. 623–635, Jul. 2003.

[33] A. Alkandri and N. Bangalore, “Human detection using OT-MACH filter in cluttered FLIR imagery,” *... 2013 Proc. ...*, 2013.

[34] B. Schachter, “A survey and evaluation of FLIR target detection/segmentation algorithms,” 1982.

[35] S. Der, C. Dwan, A. Chan, H. Kwon, and N. Nasrabadi, “Scale-insensitive detection algorithm for FLIR imagery,” no. February, 2001.

[36] M. M. Mouthaan, S. P. van den Broek, and E. A. Hendriks…, “Region descriptors for automatic classification of small sea targets in infrared video (Journal Paper),” *Opt. Eng.*, Jan. 2011.

[37] C. R. del-Blanco, F. Jaureguizar, L. Salgado, and N. Garcia, “Target Detection Through Robust Motion Segmentation and Tracking Restrictions in Aerial Flir Images,” *2007 IEEE Int. Conf. Image Process.*, vol. 5, 2007.

[38] A. Yilmaz, “Target tracking in airborne forward looking infrared imagery,” *Image Vis. Comput.*, vol. 21, no. 7, pp. 623–635, Jul. 2003.

[39] H. Parry, A. Marshall, and K. Markham, “Region template correlatino for flir target tracking,” *BMVC*, 1996.

[40] B. Bhanu and R. D. Holben, “Model-based segmentation of FLIR images,” *IEEE Trans. Aerosp. Electron. Syst.*, vol. 26, 1990.

[41] C. R. del-Blanco, F. Jaureguizar, L. Salgado, and N. Garcia, “Target Detection Through Robust Motion Segmentation and Tracking Restrictions in Aerial Flir Images,” *2007 IEEE Int. Conf. Image Process.*, vol. 5, 2007.

[42] J. Xu, J. Chen, L. Dou, and Z. Liu, “Moving Target Detection and Tracking in FLIR Image Sequences Based on Thermal Target Modeling,” in *2010 International Conference on Measuring Technology and Mechatronics Automation*, 2010, pp. 715–720.

[43] L. A. Chan, S. Z. Der, and N. M. Nasrabadi, “Dual-band FLIR fusion for target detection,” in *Applications of Artificial Neural Networks in Image Processing VII*, 2002, vol. SPIE-4668, pp. 108–118.

[44] C. Wei and S. Jiang, “Automatic Target Detection and Tracking in FLIR Image Sequences Using Morphological Connected Operator,” in *Intelligent Information Hiding and Multimedia Signal Processing, 2008. IIHMSP ’08 International Conference on*, 2008, pp. 414–417.

[45] J. Johnson, “Analysis of Image Forming Systems.”

[46] C. Hester and D. Casasent, “Multivariant technique for multiclass pattern recognition,” *Appl. Opt.*, vol. 19, no. 11, pp. 1758–1761, 1980.

[47] B. Kumar, D. Carlson, and A. Mahalanobis, “Optimal trade-off synthetic discriminant function filters for arbitrary devices,” *Opt. Lett.*, vol. 19, no. 19, pp. 1556–1558, 1994.

[48] D. Casasent, “Unified synthetic discriminant function computational formulation.,” *Appl. Opt.*, vol. 23, no. 10, p. 1620, May 1984.

[49] D. P. Casasent and W. a Rozzi, “Computer-generated and phase-only synthetic discriminant function filters.,” *Appl. Opt.*, vol. 25, no. 20, p. 3767, Oct. 1986.

[50] P. Refregier, “Optimal trade-off filters for noise robustness, sharpness of the correlation peak, and Horner efficiency.,” *Opt. Lett.*, vol. 16, no. 11, pp. 829–31, Jun. 1991.

[51] S. Martínez-Díaz and V. Kober, “Nonlinear synthetic discriminant function filters for illumination-invariant pattern recognition,” *Opt. Eng.*, vol. 47, p. 67201, 2008.

[52] R. K. Wang, C. R. Chatwin, and M. Y. Huang, “Modified filter synthetic discriminant functions for improved optical correlator performance.,” *Appl. Opt.*, vol. 33, pp. 7646–7654, 1994.

[53] B. V. Kumar and J. Brasher, “SYNTHETIC DISCRIMINANT FUNCTIONS FOR RECOGNITION OF IMAGES ON THE BOUNDARY OF THE CONVEX HULL OF THE TRAINING SET,” *Pattern Recognit.*, vol. 27, no. 4, pp. 543–548, 1994.

[54] B. Kumar, “Tutorial survey of composite filter designs for optical correlators,” *Appl. Opt.*, vol. 31, no. 23, pp. 4773–4801, 1992.

[55] B. V. K. V. Kumar, “Minimum-variance synthetic discriminant functions,” *JOSA*, pp. 1579–1584, 1986.

[56] A. Mahalanobis, B. V Kumar, and D. Casasent, “Minimum average correlation energy filters.,” *Appl. Opt.*, vol. 26, pp. 3633–3640, 1987.

[57] A. Mahalanobis and D. Casasent, “Performance evaluation of minimum average correlation energy filters,” *Appl. Opt.*, vol. 30, no. 5, pp. 561–572, 1991.

[58] A. Mahalanobis, B. Vijaya Kumar, S. Song, S. Sims, and J. Epperson, “Unconstrained correlation filters,” *Appl. Opt.*, vol. 33, no. 17, pp. 3751–3759, 1994.

[59] A. Mahalanobis and B. Kumar, “Optimality of the maximum average correlation height filter for detection of targets in noise,” *Opt. Eng.*, vol. 36, p. 2642, 1997.

[60] J. Liu, J. Luo, and M. Shah, “Action recognition in unconstrained amateur videos,” *Acoust. Speech Signal Process. 2009. ICASSP 2009. IEEE Int. Conf.*, pp. 3549–3552, 2009.

[61] S. Bhuiyan, M. Alam, and M. Alkanhal, “New two-stage correlation-based approach for target detection and tracking in forward-looking infrared imagery using filters based on extended maximum average correlation height and polynomial distance classifier correlation,” *Opt. Eng.*, vol. 46, p. 86401, 2007.

[62] S. Bhuiyan, M. Alam, and S. Sims, “Target detection, classification, and tracking using a maximum average correlation height and polynomial distance classification correlation filter combination,” *Opt. Eng.*, vol. 45, p. 116401, 2006.

[63] M. Alkanhal, B. Kumar, and A. Mahalanobis, “Improving the false alarm capabilities of the maximum average correlation height correlation filter,” *Opt. Eng.*, vol. 39, p. 1133, 2000.

[64] A. Gardezi, A. Alkandri, P. Birch, and R. Young…, “A space variant Maximum Average Correlation Height (MACH) filter for object recognition in real time thermal images for security applications,” *Soc. Photo-Optical ...*, Jan. 2010.

[65] S. Goyal, N. Nishchal, V. Beri, and A. Gupta, “Wavelet-modified maximum average correlation height filter for out-of-plane rotation invariance,” *Opt. J. Light Electron Opt.*, vol. 120, no. 2, pp. 62–67, 2009.

[66] O. C. Johnson, W. Edens, T. T. Lu, and T.-H. Chao, “Optimization of OT-MACH filter generation for target recognition,” 2009, vol. 7340, no. 818, pp. 734008–734008–9.

[67] P. K. Banerjee, J. K. Chandra, and A. K. Datta, “Feature based optimal trade-off parameter selection of frequency domain correlation filter for real time face authentication,” in *Proceedings of the 2011 International Conference on Communication, Computing & Security*, 2011, pp. 295–300.

[68] E. Cheng, “Automatic Target Recognition (ATR) for Submarine Periscope Systems,” pp. 1–6, Jul. 2008.

[69] P. Bone, I. Kypraios, R. Young, and C. Chatwin, “Fully invariant object recognition in cluttered scenes,” *Inf. Technol. 2004, Proc. SPIE (Edited by Veacheslav V. Perju Andrei M. Andriesh*, vol. 5822, pp. 1–12, 2005.

[70] A. Gardezi, P. Birch, I. Kypraios, and R. Young…, “Implementation of the Maximum Average Correlation Height (MACH) filter in the spatial domain for object recognition from clutter backgrounds,” *Proc. SPIE*, Jan. 2010.

[71] A. Gardezi, A. Alkandri, P. Birch, and T. Qureshi…, “An implementation and performance evaluation of a space variant OT-MACH filter for a security detection application using FLIR sensor,” …, Jan. 2010.

[72] A. Gardezi, A. Al-Kandri, P. Birch, and R. Young…, “Enhancement of the speed of space-variant correlation filter implementations by using low-pass pre-filtering for kernel placement and applications to real-time security …,” *Proc. ...*, Jan. 2011.

[73] and C. C. Gardezi, Akber, Nagachetan Bangalore, Ahmed Al-Kandri, Philip Birch, Rupert Young, “Application of speed-enhanced spatial domain correlation filters for real-time security monitoring,” *SPIE Secur. Defence, pp. 81890R-81890R*.

[74] A. Alkandri, A. Gardezi, P. Birch, and R. Young…, “Parameter optimization of the optimal trade-off maximum average correlation height filter (OT-MACH) for FLIR imaging in high clutter environments,” in *Proceedings of SPIE*, 2011.

[75] A. Alkandri, A. Gardezi, N. Bangalore, P. Birch, R. Young, and C. Chatwin, “Automatic parameter adjustment of difference of Gaussian (DoG) filter to

improve OT-MACH filter performance for target recognition applications," in *Proceedings of SPIE*, 2011, vol. 8185, no. 1, p. 81850M–81850M–8.

[76] A. Alkandri, N. Bangalore, A. Gardezi, P. Birch, and R. Young, "Improving OT-MACH filter performance for target recognition applications with the use of a Rayleigh distribution filter School of Engineering and Informatics," no. 2.

[77] B. Mitra, W. Hassan, N. Bangalore, P. Birch, R. Young, and C. Chatwin, "Tracking illegally parked vehicles using correlation of multi-scale difference of Gaussian filtered patches," 2011, pp. 805503–805503–9.

[78] F. Sadjadi and A. Mahalanobis, "Target-adaptive polarimetric synthetic aperture radar target discrimination using maximum average correlation height filters," *Appl. Opt.*, vol. 45, no. 13, pp. 3063–3070, 2006.

[79] R. Kerekes, "Integrating correlation filtering and tracking for better target detection," *spie.org*, pp. 2–4.

[80] R. K. Singh, "Advance correlation filter for multi-class synthetic Aperture radar detection and classification," 2002.

[81] J. Shang, Y. Zhang, Q. Zhang, and W. Wang, "Distorted target recognition based on canny operator enhancing OT-MACH filter," vol. 8559, p. 85590N–85590N–7, Nov. 2012.

[82] C. Ng, M. Savvides, and P. Khosla, "Real-time face verification system on a cell-phone using advanced correlation filters," 2005.

[83] J. S. X. T. Z. Mao, “Ship target detection and tracking in cluttered infrared imagery,” pp. 1–13, May 2011.

[84] W. Kun, Z. Yongqiang, P. Quan, and Z. Hongcai, “IR Target Detection Based on Kernel PCA and Quadratic Correlation Filters,” pp. 448–452, Aug. 2007.

[85] B. Bhanu, “Automatic Target Recognition: State of the Art Survey,” *IEEE Trans. Aerosp. Electron. Syst.*, vol. AES-22, no. 4, pp. 364–379, Jul. 1986.

[86] A. Rodriguez, “AUTOMATIC TARGET RECOGNITION OF MULTIPLE TARGETS FROMTWO CLASSES WITH VARYING VELOCITIES USING CORRELATION FILTERS,” *Image Process. (ICIP), 2010*, pp. 2781–2784, 2010.

[87] R. Kallman, “Construction of low noise optical correlation filters,” *Appl. Opt.*, vol. 25, p. 1032, 1986.

[88] G. Schils and D. Sweeney, “Iterative technique for the synthesis of distortion-invariant optical correlation filters,” *Opt. Lett.*, vol. 12, no. 5, pp. 307–309, 1987.

[89] G. Ravichandran and D. Casasent, “Advanced in-plane rotation-invariant correlation filters,” *IEEE Trans. Pattern Anal. Mach. Intell.*, pp. 415–420, 1994.

[90] G. Ravichandran and D. Casasent, “Minimum noise and correlation energy optical correlation filter,” *Appl. Opt.*, vol. 31, no. 11, pp. 1823–1833, 1992.

[91] O. Gualdrón and H. H. Arsenault, “Optimum rotation-invariant filter for disjoint-noise scenes.,” *Appl. Opt.*, vol. 35, no. 14, pp. 2507–13, May 1996.

[92] S. Tan, R. Young, D. Budgett, J. Richardson, and C. Chatwin, "A pattern recognition Weiner filter for realistic clutter backgrounds," *Opt. Commun.*, vol. 172, no. 1–6, pp. 193–202, 1999.

[93] P. Bone, R. Young, and C. Chatwin, "Position-, rotation-, scale-, and orientation-invariant multiple object recognition from cluttered scenes," *Opt. Eng.*, vol. 45, p. 77203, 2006.

[94] M. Rodriguez, J. Ahmed, and M. Shah, "Action mach a spatio-temporal maximum average correlation height filter for action recognition," *Comput. Vis. Pattern Recognition, 2008. CVPR 2008. IEEE Conf.*, pp. 1–8, 2008.

[95] W. Hassan, B. Mitra, N. Bangalore, P. Birch, R. Young, and C. Chatwin, "Robust human intrusion detection technique using hue-saturation histograms," p. 80550J–80550J–12, 2011.

[96] S. Winger, T. Lu, and T.-H. Chao, "Optimization of nonlinear kernel PCA feature extraction algorithms for automatic target recognition," vol. 8055, no. 818, p. 80550E–80550E–11, Apr. 2011.

[97] P. Bone, "Fully invariant object recognition and tracking from cluttered scenes," no. October, pp. 1–159, 2007.

[98] B. V. K. VijayaKumar, "Correlation Filters With Controlled Scale Response," *IEEE Trans. Image Process.*, Jan. 2006.

[99] P. Birch, B. Mitra, N. M. Bangalore, S. Rehman, R. Young, and C. Chatwin, "Approximate bandpass and frequency response models of the difference of Gaussian filter," *Opt. Commun.*, vol. 283, no. 24, pp. 4942–4948, Dec. 2010.

[100] P. Birch, B. Mitra, N. M. Bangalore, S. Rehman, R. Young, and C. Chatwin, "Approximate bandpass and frequency response models of the difference of Gaussian filter," *Opt. Commun.*, vol. 283, no. 24, pp. 4942–4948, Dec. 2010.

[101] B. Kumar and L. Hassebrook, "Performance measures for correlation filters," *Appl. Opt.*, vol. 29, no. 20, pp. 2997–3006, 1990.

[102] R. Kerekes and B. Kumar, "Selecting a composite correlation filter design: a survey and comparative study," *Opt. Eng.*, vol. 47, p. 67202, 2008.

[103] K. Kelley, "Sample size planning for the coefficient of variation from the accuracy in parameter estimation approach.," *Behav. Res. Methods*, vol. 39, no. 4, pp. 755–66, Nov. 2007.

[104] B. Y. L. H. K. D. B. Owenf and J. I. Rosenblattft, "Confidence intervals for the coefficient of variation for the normal and log normal distributions," pp. 25–32, 1964.

[105] J. Forkman, "Estimator and Tests for Common Coe ± cients of Variation in Normal Distributions," pp. 233–251, 2009.

[106] D. Marr and E. Hildreth, "Theory of edge detection," *Proc. R. Soc. London. Ser. B, Biol. Sci.*, pp. 187–217, 1980.

[107] V. Reilly, B. Solmaz, and M. Shah, “Geometric Constraints for Human Detection in Aerial Imagery,” pp. 1–14.

[108] K. Mikolajczyk, C. Schmid, and A. Zisserman, “Human detection based on a probabilistic assembly of robust part detectors,” in *Proc. European Conference on Computer Vision (ECCV)*, 2004, vol. 3021, pp. 69–82.

[109] N. Dalal and B. Triggs, “Histograms of oriented gradients for human detection,” *2005 IEEE Comput. Soc. Conf. Comput. Vis. Pattern Recognit.*, vol. 1, 2005.

[110] O. Tuzel, F. Porikli, and P. Meer, “Human Detection via Classification on Riemannian Manifolds,” *2007 IEEE Conf. Comput. Vis. Pattern Recognit.*, pp. 1–8, 2007.

[111] C. Beleznai and H. Bischof, “Fast human detection in crowded scenes by contour integration and local shape estimation,” *2009 IEEE Conf. Comput. Vis. Pattern Recognit.*, 2009.

[112] C. E. Baum, “Signature-based target identification and pattern recognition,” *IEEE Antennas Propag. Mag.*, vol. 36, no. 3, pp. 44–51, Jun. 1994.

[113] S. Billings and S. Fakhouri, “Identification of a class of nonlinear systems using correlation analysis,” *Electr. Eng. Proc. ...*, vol. 125, no. 7, pp. 691–697, 1978.

[114] A. Sha’meri, A. Zabidi, and M. Muhammad, “Embedded vision systems for ship recognition,” *TENCON 2009 - 2009 IEEE Reg. 10 Conf.*, pp. 1–5, Nov. 2009.

[115] T. Teng, J. Patra, and E. Ang, “Identification and tracking of dim moving targets in FLIR using artificial neural networks,” *Signal Process. Its ...*, pp. 223–226, 2003.

[116] S. Sun, J. Park, and Y. Park, “Identification of military ground vehicles by feature information fusion in FUR images,” *Image Signal Process. ...*, vol. 2, pp. 871–876, 2003.

[117] P. Withagen, “Automatic classification of ships from infrared (FLIR) images,” …, vol. 3720, 1999.

[118] R. D’Amico, “joint fires coordination: service specialties and bounary challenges,” 1997.

[119] J. Horner, “Fire Support Coordination Measures by the Numbers,” 1999.

[120] R. Veit, “Joint Targeting: Improving the Playbook, Communications, and Teamwork.,” 1996.